

Interference Management and QoS Enhancement in 5G NOMA Networks

Sumita Majhi

Interference Management and QoS Enhancement in 5G NOMA Networks

*Synopsis Report submitted
of the requirements for the degree of*

Doctor of Philosophy

in

COMPUTER SCIENCE AND ENGINEERING

by

Sumita Majhi

Under the supervision of

Dr. Pinaki Mitra



DEPARTMENT OF COMPUTER SCIENCE AND ENGINEERING
INDIAN INSTITUTE OF TECHNOLOGY GUWAHATI

July 2025

Copyright © Sumita Majhi, 2025. All Rights Reserved.

This thesis is dedicated to my Parents
- whose blessings, inspriation, unconditional love and support made my path of sucess.

DECLARATION

I hereby certify that

- a. The work contained in this thesis is original and has been done by myself and the general supervision of my supervisor.
- b. The work has not been submitted to any other Institute for any degree or diploma.
- c. Whenever I have used materials (data, theoretical analysis, results) from other sources, I have given due credit by citing them in the text of the thesis and giving their details in the references. Elaborate sentences used verbatim from published work have been clearly identified and quoted.
- d. No part of this thesis can be considered plagiarism to the best of my knowledge and understanding and take complete responsibility if any complaint arises.

Date : 11____/09____/2024____

Sumita Majhi

Place: Guwahati, India



Department of Computer Science and Engineering
Indian Institute of Technology Guwahati
Guwahati - 781039, Assam, India

Dr. Pinaki Mitra
Associate Professor

Ph: +91-361-2582352
Email: pinaki@iitg.ac.in

CERTIFICATE

This is to certify that the thesis entitled “**Interference Management and QoS Enhancement in 5G NOMA Networks**” being submitted by **Sumita Majhi** to the Department of Computer Science and Engineering, Indian Institute of Technology Guwahati, is a record of bonafide research work carried out by her under my supervision and is worthy of consideration for the award of the degree of Doctor of Philosophy of the Institute.

To the best of my knowledge, no part of the work reported in this thesis has been presented for the award of any degree at any other institution.

Date : 11____/09____/2024____

Place: Guwahati, India

Dr. Pinaki Mitra
(Thesis Supervisor)

ACKNOWLEDGMENTS

“No one who achieves success does so without acknowledging the help of others. The wise and confident acknowledge this help with gratitude.”

I am thankful to everyone who played a role in my academic journey and the completion of this thesis. I extend my heartfelt appreciation to my supervisor, Dr. Pinaki Mitra, for his invaluable guidance and unwavering support. Dr. Mitra’s calm and composed demeanor has always been a source of inspiration, allowing me to navigate through challenging phases with confidence. His encouragement and belief in my abilities have motivated me to push boundaries and explore unconventional perspectives. I consider myself truly fortunate to have had the privilege of working under his supervision.

Additionally, I extend my appreciation to the members of the Doctoral Committee: The DC chair, Prof. Pradip K. Das, Dr. Hanumant Singh Shekhawat, and Dr. Moumita Patra, for their insightful guidance and expertise throughout my research. I am grateful to the Department of Computer Science and Engineering at IIT Guwahati for providing me with the necessary resources and opportunities to pursue my studies.

I would also like to express my sincere gratitude to Dr. Shankar Kumar Ghosh from Shiv Nadar Institution of Eminence, Delhi NCR, for his invaluable contributions. His expertise and guidance were instrumental in the successful completion of this work.

Special thanks go to my friends and family for their constant support, love, and encouragement throughout the ups and downs of this journey. Without all of you, this work would not have been possible. Thank you.

Guwahati, September 2024

Sumita Majhi

ABSTRACT

With their ultra-high data speeds, minimal latency, and huge connection, fifth-generation (5G) wireless networks hope to transform mobile communication completely. It is challenging to accommodate a wide range of user needs within the constrained spectrum resources, such as low-power sensor data transmission and high-bandwidth video streaming. In this case, typical Orthogonal Multiple Access (OMA) approaches employed in previous generations have drawbacks that might be addressed by Non-Orthogonal Multiple Access (NOMA), a promising technology that has emerged as a crucial information-theoretic method, especially in 5G and beyond. Specifically, this paper explores the area of power-domain NOMA, which is known for its more flexible resource distribution than code-domain NOMA networks. NOMA lets numerous users share the same resources, but OMA allocates specialized resources to each user, resulting in inefficient spectrum usage when user requirements differ dramatically.

However, the introduction of several optimization issues by the growth of user equipment inside 5G has prompted the investigation of multi-objective optimization (MOO) in NOMA networks. This work uniquely tackles the trade-off between spectral efficiency (SE) and energy efficiency (EE), whereas previous studies mainly concentrated on single or dual objectives that suffer from local minimization problems. NOMA technology is a viable way to improve spectral efficiency because of its distinct power-domain approach. This eventually forces us to investigate the use of NOMA in multiuser MIMO communications, highlighting the possible improvements in system throughput overall. Although there are obstacles like intra-cluster interference, adding device-to-device (D2D) connectivity to 5G networks lowers power consumption while simultaneously increasing spectral efficiency and system throughput. NOMA uses successive interference cancellation (SIC) technique at the receiving end which solely depends on perfect channel state information (CSI). Perfect CSI in real scenario is not possible due to dynamic nature of the environment. A very few work has been done in this direction to take partially decoded data as an addition to traditional CSI to predict channel status. Existing study evaluates conventional Data-Aided Channel Estimation techniques in the search for more effective channel estimation in NOMA networks, highlighting their shortcomings in dynamic and interference-prone situations. The following sections explore the complexities of these suggested approaches, highlighting the importance of trade-offs in network optimization and reducing the local minimization problem due to the use of existing multi-objective optimization (MOO) solutions. In Contribution 1, we work on the collaboration between reinforcement learning (RL) and multi-objective optimization genetic algorithms (MOGA) to minimize the local minimization problem. Integrating RL algorithms with MOGA provides a dynamic way to optimize long-term decision-making

inside networks. In order to reduce intra-cluster interference due to the reason for using the SIC technique at the receiver and enhance the performance of MIMO-NOMA networks, the research in contribution 2 suggests using Multiple Interference Cancellation (MIC) techniques. The SIC technique solely depends on perfect CSI, which is not possible in wireless 5G networks. In contribution 3, we researched a unique channel estimation technique for a dynamic and fast-changing environment to overcome the challenges of imperfect CSI. Recurrent neural networks (RNNs) and long short-term memory (LSTM) networks are used as a channel estimation technique that highlights the need for data-driven and adaptable solutions in a dynamic environment. Utilizing machine learning to forecast future channel values effectively replaces iterative approaches and tackles issues related to imprecise channel state information. In Contribution 4, we propose a viable resolution to the inherent user separation difficulties seen in NOMA systems. This study examines the performance of Gold coding and Conventional-V-BLAST (C-V-BLAST) techniques in Non-Orthogonal Multiple Access (NOMA) systems. We have devised a novel channel prediction function (CPF) that enhances the accuracy of channel estimation by using pilot signals, power allocation information, and partially decoded data symbols. Additionally, we provide a subcarrier selection approach that assigns priority to subcarriers depending on their impact on the channel estimation. This work further investigates the use of Gold sequences in NOMA systems. Gold sequences include distinctive correlation characteristics that facilitate the differentiation of users and the identification of data, especially in situations when subcarrier signals overlap. Our simulations demonstrate that our methods surpass others in terms of accuracy in channel estimation, separation of users, and overall system performance. Our findings indicate that the use of gold coding and channel prediction methodologies has the potential to enhance NOMA systems.

Table of Contents

	Page
List of Figures	iv
List of Tables	ix
List of Algorithms	xi
1 Introduction	1
1.1 Background	1
1.1.1 Towards 5G and Beyond	1
1.1.2 Multiple Access Techniques for 5G	1
1.1.3 Towards Non-orthogonal Multiple Access	2
1.1.4 5G Interference Management	3
1.2 Motivation and Contributions	4
1.3 Literature Review	6
1.3.1 Multi-Objective Optimization	7
1.3.2 NOMA with Multiple-Antenna Techniques	7
1.3.3 NOMA under Imperfect Channel Conditions	8
1.3.4 NOMA with Gold Sequence Spreading	9
2 Fundamentals Concepts	11
2.1 Basic principles of NOMA	11
2.1.1 Superposition Coding and Successive Interference Cancellation	11
2.1.2 Downlink NOMA	12
2.1.3 Uplink NOMA	13
2.1.4 Information-theoretic Views of NOMA	13
3 Multi-objective Optimization in NOMA Networks	15
3.1 Introduction	15
3.2 System Model	16

TABLE OF CONTENTS

3.2.1	Problem Statement	18
3.3	Multi-Objective Optimization	20
3.4	Proposed Architecture	21
3.4.1	MOGA	21
3.4.2	Proposed MOGA-RL Algorithm for Spectral Efficiency and Energy Efficiency	24
3.4.3	Reward Function	27
3.5	Comparative Analysis	29
3.6	Results and Discussion	31
3.7	Algorithm Analysis	35
3.7.1	Space Complexity	35
3.7.2	Time Complexity	36
3.8	Summary	36
4	Multiple Interference Cancellation in MIMO-NOMA Network	37
4.1	Introduction	37
4.2	System Model	38
4.3	PROBLEM FORMULATION	46
4.3.1	Sum Rate	46
4.3.2	Energy Efficiency	46
4.3.3	Multiple Interference Cancellation	47
4.3.4	Beamformer Design and Performance Analysis	49
4.4	Simulations Results and Discussion	50
4.5	Summary	60
5	Channel Estimation in NOMA Network	61
5.1	Introduction	61
5.2	System model	62
5.3	Proposed RNN-LSTM model	66
5.3.1	Data Preperation	66
5.3.2	Complexity Analysis	67
5.4	Results and Discussion	70
5.4.1	Simulation Setup and Results	70
5.4.2	Performance Metrics	71

5.4.3	Evaluation Of RNN-LSTM model	73
5.4.4	Comparative Analysis of RNN-LSTM	80
5.4.5	Application of the Proposed Technique to HLF/RLF	85
5.5	Summary	87
6	Improving Channel Estimation Through Gold Sequences	89
6.1	Introduction	89
6.2	System Model	90
6.3	Channel Estimation Problem in NOMA Network	92
6.4	Gold Sequences for NOMA Channel Estimation	95
6.5	Results and Discussion	96
6.5.1	Simulation Setup	96
6.5.2	Performance Comparison of NOMA with Gold Coding and C-V-BLAST	98
6.5.3	Performance Evaluation Via Deep Learning Model	99
6.5.4	Addressing Scalability Challenges for Larger Networks	101
6.6	Summary	104
7	Conclusions and Future Works	105
7.1	Conclusions	105
7.2	Future Works	107
	List of Publications	117

List of Figures

	Page
1.1 Key applications of 5G networks.	2
1.2 Cellular technology evolution, copied from [2].	3
1.3 Four-user 64×64 MIMO-NOMA system, copied from [22].	8
2.1 Two-user channel sharing strategies (a) NOMA (b) OMA, copied from [27].	12
3.1 Q-Learning.	26
3.2 Flow chart of MOGA-RL algorithm.	30
3.3 Pareto optimal solution at SINR = 4dB.	32
3.4 Pareto optimal solution at SINR = 8dB.	32
3.5 Pareto optimal solution at SINR = 12dB.	33
3.6 Convergence rate of the proposed scheme at different generations.	33
3.7 Trade-off between EE and SE: Comparison of MOGA and Weighted Sum Method for Different SNR Values.	34
3.8 Comparison of MOGA-RL, weighted Sum, constraint, sequential, and max- min method.	35
4.1 General MIMO-NOMA D2D network	39
4.2 Spectral efficiency comparison under transmit power Power 30 dBm	51
4.3 Spectral efficiency comparison under transmit power Power 40 dBm	52
4.4 Spectral efficiency comparison under transmit power Power 50 dBm	53
4.5 Energy efficiency comparison under different antenna setup, Antenna = 5	54
4.6 Energy efficiency comparison under different antenna setup, Antenna = 10	55
4.7 Energy efficiency comparison under different antenna setup, Antenna = 15	56
4.8 Spectral efficiency comparison	56
4.9 Energy efficiency comparison	57
4.10 Analysis of Spectral Efficiency vs. Cluster Count	58
4.11 Spectral Efficiency vs. Correlation Coefficient	59

4.12 Beamforming Scheme Performance Comparison	59
5.1 System model of NOMA-HO	64
5.2 System model of NOMA transceiver with RNN-LSTM model	65
5.3 Flowchart of algorithm 1	68
5.4 Distribution of original values	68
5.5 Distribution of augmented values	69
5.6 KDE plots	69
5.7 Training convergence of three architectures: CNN, RNN and RNN-LSTM .	73
5.8 NRMSE of near user and far user over epochs (UE2 and UE1)	74
5.9 Training MAE with PDD and without PDD	75
5.10 R-squared comparison with PDD and without PDD	76
5.11 R-squared score (without PDD): CNN, RNN, RNN-LSTM	77
5.12 Training SINR comparison over data frames	78
5.13 Testing SINR comparison over data frames	79
5.14 A Comparative Analysis of RNN-LSTM, SVM, and Random Forest Models Under Varying SNR Conditions.	81
5.15 A Comparative Study of LSTM, SVM, and Random Forest Models Using CSI and Partially Decoded Data.	82
5.16 Impact of Varying LSTM Units on Channel Estimation Performance with Fixed Dropout Rate (0.3) and Learning Rate (0.001).	83
5.17 Impact of Varying Learning Rate on Channel Estimation Performance with Fixed LSTM Units (256) and Dropout Rate (0.3)	84
5.18 Handover failure rates over UE speeds (km/hour)	85
5.19 Ping-pong rates over UE speeds (km/hour)	86
5.20 Number of false alarm vs. UE speeds (km/hour)	87
6.1 Transmission block structure at the BS in NOMA network.	91
6.2 SER performance comparison of a two-user NOMA system employing Gold sequence lengths 31, 63, and 127.	98
6.3 SER performance comparison of Gold coding and C-V BLAST for a two-user NOMA system.	99
6.4 A rolling window approach with a 2-minute window size was applied to the 10-minute dataset.	100
6.5 Loss function of training and validation dataset.	101

6.6	Enhanced channel estimation in NOMA via CPF with fractional power allocation.	102
6.7	Channel Estimation in NOMA Networks Using Gold Sequences: Evaluating Scalability, Interference, and MSE.	103

List of Tables

	Page
3.1 Table of parameters	17
4.1 Table of parameters	39
5.1 Parameters setup	71
5.2 Performance metrics of different ML models	79
6.1 Simulation Setup.	97
6.2 Model Parameters for LSTM-based Prediction Model	97

List of Algorithms

1	ε - Greedy Action Selection	26
2	Multi-Objective Genetic Algorithm with RL	29
3	D2D Communication in the Downlink MIMO-NOMA Network	43
4	D2D Pair formation	44
5	Computing performance indicator data	44
6	MIMO-NOMA-D2D with Multiple Interference Cancellation	45
7	Transfer Learning Algorithm to generate Regressor model	67
8	Channel Estimation using Weighted Power Allocation in NOMA	94
9	Channel Estimation using a two-step process in NOMA	94

Introduction

1.1 Background

1.1.1 Towards 5G and Beyond

The relentless pursuit of higher data rates, lower latency, and massive connectivity has driven the evolution of wireless communication systems. While 4G LTE networks have revolutionized mobile broadband, the burgeoning demands of emerging applications such as IoT, augmented reality, and autonomous vehicles necessitate a paradigm shift. 5G technology [1], with its promise of enhanced mobile broadband, ultra-reliable low-latency communications, and massive machine-type communications, is poised to address these challenges as shown in Fig 1.1. However, the rapid pace of technological advancement suggests that 5G may be just the first step in a continuous evolution towards even more sophisticated wireless networks, capable of supporting the ever-increasing complexity and diversity of future applications.

1.1.2 Multiple Access Techniques for 5G

Multiple access techniques have undergone significant evolution across generations of wireless networks. From the analog FDMA in 1G to the digital TDMA and CDMA in 2G and 3G, respectively, the industry has continuously sought to improve spectral efficiency and system capacity [2] as depicted in Fig 1.2. The introduction of OFDMA in 4G marked a significant step forward. However, the explosive growth of IoT devices and demanding applications



Figure 1.1: Key applications of 5G networks.

necessitate further advancements. Non-orthogonal multiple access (NOMA) has emerged as a promising candidate for 5G networks, offering the potential to substantially enhance spectral efficiency by allowing multiple users to share the same time and frequency resources. This is achieved through power domain multiplexing and successive interference cancellation, fundamentally differentiating NOMA from conventional orthogonal multiple access schemes like FDMA, TDMA, CDMA, and OFDMA, which assign orthogonal resources to different users.

1.1.3 Towards Non-orthogonal Multiple Access

Non-orthogonal Multiple Access (NOMA) [3] has emerged as a promising technology to address the increasing demand for higher spectral efficiency and massive connectivity in fifth-generation (5G) and beyond wireless networks. Unlike conventional orthogonal multiple access (OMA) schemes that assign orthogonal resources to different users, NOMA allows multiple users to share the same time, frequency, or code resources. This is achieved primarily through power-domain NOMA, where users are differentiated by power levels and successive interference cancellation (SIC) is employed at the receiver. NOMA's ability to







1G	2G	3G	4G	5G	6G
					
2.4 Kbps Voice call Analog signals	64 Kbps SMS Digital signals Larger service	2 Mbps Internet Web Applications Smartphones	100-1000 Mbps High Data Rate Mobile Applications Internet of Applications	1-10 Gbps Internet of Things Massive Broadband Smart City VR / AR	More than 10 Gbps New Spectrum Energy Efficiency Artificial Intelligence Blockchain
1980s	1990s	2000s	2010s	2020s	2030s

Figure 1.2: Cellular technology evolution, copied from [2].

serve multiple users within a single resource block offers significant advantages in terms of spectral efficiency and user fairness [4]. Furthermore, NOMA can be synergistically combined with other technologies, such as multiple-antenna [5] techniques and conventional OMA schemes [6], to create even more efficient and flexible wireless communication systems.

1.1.4 5G Interference Management

The advent of 5G technology has ushered in a new era of wireless communication, promising unprecedented data rates, low latency, and massive connectivity. However, interference [7] poses a critical challenge to achieving the promised benefits. The realization of these benefits is hindered by the ever-increasing interference challenges in network environments, necessitating advanced techniques to address this issue. Interference arises when signals from different sources overlap, leading to signal degradation and reduced performance. Effective interference management is crucial for realizing the full potential of 5G. To address these interference challenges, a combination of advanced techniques, including Multi-Objective Genetic Algorithms with Reinforcement Learning (MOGA-RL) [8], Recurrent Neural Networks with Long Short-Term Memory (RNN-LSTM) [9], Gold Coding [10], and Multiple Interference Cancellation (MIC) [11], has emerged as a promising solution.

Our work delves into the critical role of these techniques in mitigating interference in 5G networks. We will explore how the proposed techniques can effectively suppress interference. Gold codes are a family of binary sequences with good auto-correlation and cross-correlation

properties. They can be used in spread spectrum techniques to reduce interference between users. In NOMA, Gold codes can be used to spread the user signals over a wider bandwidth, reducing the impact of intra-cell interference. By carefully selecting and assigning Gold codes to different users, it is possible to minimize the interference between their signals. MOGA-RL and RNN-LSTM represent powerful AI-driven approaches to tackling the complex challenge of interference management in 5G networks. By exploring and refining these techniques, researchers aim to develop more intelligent and efficient solutions that enable higher data rates, lower latency, and improved user experience in future 5G and beyond networks. MOGA-RL combines evolutionary algorithms with reinforcement learning principles. It explores a diverse range of solutions by evolving a population of potential interference mitigation strategies. It leverages reinforcement learning to fine-tune these strategies based on real-time network feedback, optimizing performance metrics like throughput and fairness. This approach is particularly well-suited for complex scenarios with multiple objectives and dynamic environments, making it a promising solution for 5G interference management. On the other hand, RNN-LSTM employs deep learning to learn and predict interference patterns from historical data. LSTM's ability to capture long-term dependencies in time series data enables accurate predictions of future interference levels. RNN-LSTM can adapt to dynamic and time-varying interference conditions, making it suitable for rapidly changing network environments. This approach focuses on proactive interference mitigation by anticipating future interference and adjusting resource allocation accordingly.

1.2 Motivation and Contributions

The overarching motivation behind this research lies in the urgent need to overcome challenges associated with resource limitations, conflicting objectives, and the dynamic nature of wireless communication environments. Through innovative algorithms, cooperative communication strategies, and adaptive channel estimation methodologies, we aim to contribute to the advancement of wireless communication technology, ensuring its feasibility, versatility, and precision in meeting the demands of contemporary and future communication systems. In light of the above, we identify the following challenges:

Challenge #1: *Navigating Spectrum Scarcity: A Hybrid Algorithmic Solution for Dynamic NOMA Networks.*

The motivation for this research is deeply rooted in addressing critical challenges within the landscape of wireless communication networks, specifically in the context of NOMA 5G networks. One of the paramount issues revolves around the limited availability of radio spectrum resources, leading to intricate problems related to resource allocation and optimization, mainly when aiming to enhance the overall throughput of the network. When dealing with conflicting objectives, the complexity intensifies, where improving one aspect may compromise another. In response to these challenges, we propose a hybrid meta-heuristic algorithm, the Multi-Objective Optimization Genetic Algorithm based Reinforcement Learning Algorithm (MOGA-RL). By synergizing the simplicity of interaction with the environment offered by Reinforcement Learning (RL) with the optimization capabilities of Genetic Algorithms (GAs), our approach seeks to navigate the dynamic nature of networks, where rapid changes in user information demand simultaneous updates to both environmental information and optimization metrics.

Challenge #2: *Overcoming Interference Challenges with MIMO-NOMA-D2D Networks*

This research is motivated by the dual potential of Non-Orthogonal Multiple Access (NOMA) and Multiple Input Multiple Output (MIMO) techniques in wireless communication networks. NOMA's cost-effectiveness enhances spectrum efficiency, yet inter-user interference remains a challenge. Simultaneously, MIMO, with its multiple antennas, promises substantial spectral efficiency gains. Using Multiple Interference Cancellation (MIC) to increase system capacity and energy efficiency while minimizing total interference. Innovations like efficient resource allocation, ideal relay device selection, energy efficiency maximization, and power consumption reduction by doing away with decoders and regenerators make green communication essential. Thorough simulations conducted at various power and antenna levels confirm that the suggested system outperforms current MIMO-NOMA solutions in terms of interference mitigation and user clustering efficiency.

Challenge #3: *Leveraging Partially Decoded Data for CSI Prediction in NOMA-HO.*

This research is motivated by the critical role of accurate Channel State Information (CSI) in ensuring efficient and reliable NOMA communication. Existing CSI estimation methods face challenges due to dynamic channel conditions, imperfect models, and feedback

overhead. To address these limitations, we propose a novel CSI prediction technique that leverages partially decoded data (PDD) as a valuable source of information. By incorporating machine learning, our approach offers improved accuracy, reduced computational complexity, and enhanced adaptability compared to traditional methods. Our contributions include developing a CSI prediction model that effectively utilizes PDD, demonstrating its efficacy in handover failure prediction, and reducing the need for excessive pilot overhead, ultimately leading to improved NOMA system performance and user experience.

Challenge #4: Gold Coding and Fractional Power Allocation for NOMA Channel Estimation.

This research is motivated by the challenges associated with channel estimation in NOMA systems, where traditional pilot-based methods face limitations due to superimposed signals and reduced pilot power. To address these issues, we propose a novel channel estimation technique that combines the strengths of Gold coding, fractional power allocation, and partially decoded data. Our contributions include the development of a novel channel prediction function (CPF) that significantly outperforms existing methods. By leveraging a comprehensive dataset and comparing our approach to conventional techniques, we demonstrate the effectiveness of our proposed method in enhancing NOMA system performance.

1.3 Literature Review

Non-Orthogonal Multiple Access (NOMA) [3] is a promising technology for future wireless networks due to its potential to support diverse applications. Unlike traditional methods like TDMA and OFDMA, NOMA enables multiple users to share the same radio resources simultaneously. This technique is primarily categorized into power-domain NOMA and code-domain NOMA [12].

Power-domain NOMA assigns different power levels to users based on their channel conditions, the focus of this study. In contrast, code-domain NOMA uses unique code sequences for each user. This category includes variations like Low-Density Spreading CDMA (LDS-CDMA), LDS-OFDM, Sparse Code Multiple Access (SCMA), Pattern Division Multiple Access (PDMA), and Multi-User Shared Access (MUSA) [13].

1.3.1 Multi-Objective Optimization

Multi-objective optimization [14] is a critical aspect of NOMA system design due to the inherent trade-offs. NOMA systems typically aim to optimize multiple conflicting objectives simultaneously, such as Spectral efficiency (SE), Energy efficiency (EE), User fairness (UF) [15]. By employing multi-objective optimization techniques, NOMA system designers can explore the trade-off space between these objectives and identify optimal operating points that balance different performance metrics. This leads to more efficient and equitable resource allocation, ultimately enhancing overall system performance. The two types of algorithms used to tackle Multi-objective Optimization (MOO) issues are the classical method and the metaheuristic algorithm [16]. A few examples of metaheuristic algorithms that are used in evolutionary optimization include Multi-objective Genetic Algorithms (MOGA) [15], Vector Evaluated Genetic Algorithms (VEGA) [17], Non-dominated Sorting Genetic Algorithms (NSGA) [18], and Niched Pareto Genetic Algorithms (NPGA) [19]. Weighted sum method, ε -Constraint Method, the hierarchical optimization method, the goal programming method, and the optimization methods belong to the classical group for multi-objective optimization [20].

1.3.2 NOMA with Multiple-Antenna Techniques

Multiple-antenna techniques have emerged as a fundamental component of contemporary wireless communication systems, delivering substantial improvements in data transmission rates, error resilience, and interference suppression. By effectively harnessing the spatial dimension of the wireless channel, these systems can significantly enhance spectral efficiency and link robustness. Massive MIMO [21], a cutting-edge technology characterized by the deployment of a large number of antennas at the base station, takes these advantages to new heights. Through the creation of highly focused antenna beams, massive MIMO systems enable simultaneous communication with multiple users, thereby increasing system capacity and coverage. When integrated with NOMA [22], as illustrated in Fig 1.3, the resultant system can achieve remarkable gains in spectral efficiency, energy efficiency, and spatial diversity compared to traditional single-antenna systems. This synergistic combination unlocks the full potential of both technologies, paving the way for advanced wireless communication applications.

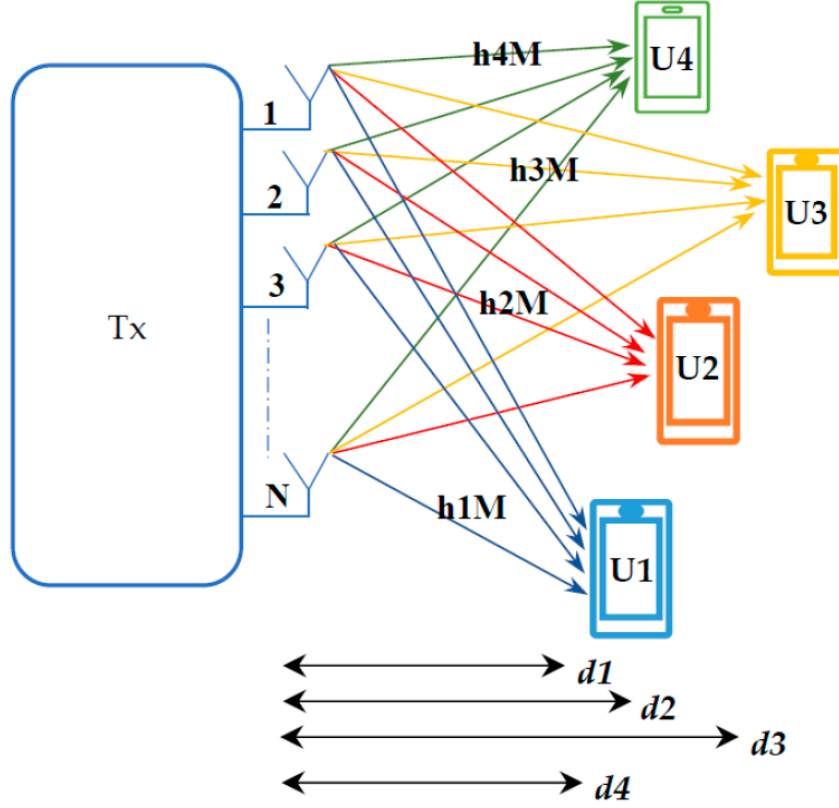


Figure 1.3: Four-user 64×64 MIMO-NOMA system, copied from [22].

1.3.3 NOMA under Imperfect Channel Conditions

The performance of NOMA systems is significantly impacted by the accuracy of channel state information (CSI). Imperfect CSI [23], arising from factors such as channel estimation errors, feedback delays, and dynamic channel variations, can degrade system performance. These imperfections lead to suboptimal power allocation, reduced user fairness, and increased interference among users. To mitigate the effects of imperfect CSI, robust power allocation algorithms [24] and advanced channel estimation techniques are crucial. Additionally, incorporating error correction coding and diversity schemes can enhance the system's resilience to channel uncertainties.

1.3.4 NOMA with Gold Sequence Spreading

To address the challenge of user separation in NOMA systems, where superimposed signals can cause interference, Gold sequences [25] can be employed as a spreading code. These sequences offer near-orthogonal properties, enabling better user differentiation compared to conventional power-domain NOMA. By spreading user signals across multiple subcarriers using Gold sequences, the system can achieve improved performance in terms of user fairness and system capacity. This approach can be considered as a hybrid of code-domain and power-domain NOMA [26], leveraging the benefits of both techniques.



Fundamentals Concepts

2.1 Basic principles of NOMA

NOMA operates on the principle of superposition coding and successive interference cancellation (SIC). Multiple users share the same time, frequency, and code resources, with different power levels assigned to each user. Users with better channel conditions are allocated lower power levels. At the receiver, users with higher channel gains decode their own signals first, treating signals from other users as interference. Subsequently, they decode signals for users with lower channel gains by subtracting their own signal from the received superposition. This process, known as SIC, enables the separation of users and improves spectral efficiency compared to conventional orthogonal multiple access schemes. A visual presentation of the NOMA and OMA systems is visually shown in Fig 2.1 from the reference [27].

2.1.1 Superposition Coding and Successive Interference Cancellation

Superposition coding (SC) is a signal-processing technique that enables the simultaneous transmission of information to multiple users from a single source. This contrasts traditional orthogonal multiple access (OMA) methods, which allocate orthogonal resources (time, frequency, or code) to different users. In SC, multiple users' signals are superimposed and transmitted together over the same resource block. To illustrate, users are ordered based on their channel conditions, such that user U_1 experiences the weakest channel, followed by U_2 , and so on, with U_N having the strongest channel. NOMA enables simultaneous

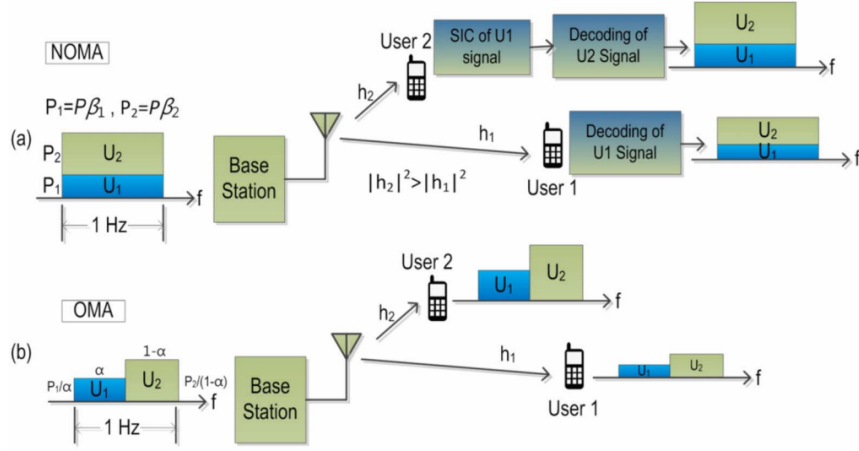


Figure 2.1: Two-user channel sharing strategies (a) NOMA (b) OMA, copied from [27].

transmission to all users within the same bandwidth by employing superposition coding at the base station and successive interference cancellation (SIC) at the user terminals. The BS superposes the modulated data of all N users into a single signal, allocating a power fraction β_i to user U_i . The received signal at user U_i can be expressed as:

$$y_i = h_i x + w_i \quad (2.1)$$

where h_i is the channel gain of user U_i , $x = \sum_{i=1}^N \sqrt{P\beta_i} S_i$ is the superimposed signal from the BS, and w_i is additive white Gaussian noise (AWGN). To decode its intended signal, user U_i first decodes the signals of users with weaker channels (i.e., users 1 to $i-1$) using SIC. Subsequently, it decodes its own signal, treating signals from stronger users (i.e., users $i+1$ to N) as interference. The achievable data rate for user U_i is given by:

$$R_i = \log_2 \left(1 + \frac{\beta_i P |h_i|^2}{P |h_i|^2 \sum_{k=i+1}^N \beta_k + \sigma_n^2} \right) \quad (2.2)$$

The user with the best channel U_N experiences no intra-cell interference and achieves the highest data rate.

2.1.2 Downlink NOMA

In the downlink, using the SC technique, the BS superimposes signal $x = \sum_{i=1}^N \sqrt{P\beta_i} S_i$ and transmits over the network. Here, the total number of users is N , S_i denotes the

message signal for user i . The received signal at user i is denoted by $y_i = h_i x + w_i$, where w_i is additive white Gaussian noise (AWGN) h_i is the channel gain. The process behind extracting the desired signal at user i , decoding signal one by one from user 1 to user $N - 1$, then re-modulating then subtracting them from the received signal x , represented pictorially in fig 1.2. Finally, user m decodes its signal.

2.1.3 Uplink NOMA

In the uplink, SIC is applied at the BS and the received signal at BS is defined by $x = \sum_{i=1}^N \sqrt{P\beta_i} h_i S_i + w_i$, where w_i indicates noise, the power for each user is different depending on the user's battery power. The BS sequentially decodes users, beginning with the user who has the maximum channel gain. Before decoding the next user, the received signal is subtracted from the decoded signal of each user. The channel model, denoted by β_i and h_i , encompasses signal propagation characteristics and fading occurrence. Precise channel assessment is crucial for the effective functioning of NOMA.

2.1.4 Information-theoretic Views of NOMA

Information-theoretic analysis has played a crucial role in comprehending NOMA's underlying boundaries and possibilities. Researchers have explored the capacity areas of NOMA systems by using ideas from information theory. Through this exploration, they have discovered the complex relationship between power allocation, user clustering, and SIC. The theoretical foundation has facilitated the creation of optimum power allocation techniques, which allow NOMA to achieve maximum spectrum efficiency and user fairness. [Moreover, Information theory, a cornerstone of communication systems, has provided critical insights into the error performance of NOMA systems \[28\] \[29\].](#) Researchers have been able to design robust error correction codes by quantifying the information capacity and error rates under various channel conditions. These codes are specifically tailored to the unique error patterns introduced by NOMA, such as those arising from interference and noise. Researchers can optimize the code rate and block length to achieve the best balance between error correction capability and spectral efficiency. By selecting modulation schemes that are robust to the non-orthogonal nature of NOMA and the associated interference and by adapting modulation parameters such as constellation size and coding rate to varying channel conditions and traffic

loads, researchers can significantly improve the performance of NOMA systems. Information theory provides a benchmark for practical system design by analyzing the theoretical limits of NOMA systems. This analysis allows for evaluating the impact of crucial factors such as power allocation strategies, user pairing decisions, and channel estimation accuracy on the overall system performance, enabling researchers to optimize these parameters for optimal system efficiency and reliability. By leveraging these information-theoretic insights, researchers and engineers can develop advanced NOMA techniques that can accommodate more users in a given bandwidth, leading to higher data rates and improved network capacity. Researchers can ensure reliable communication even in challenging environments by designing NOMA systems that are resilient to channel impairments like fading, interference, and noise. Information theory enables real-time applications such as video conferencing and autonomous vehicle communication by optimizing NOMA systems to minimize delay and jitter. By leveraging information-theoretic insights, NOMA can facilitate the exploration of new applications demanding high data rates, low latency, and reliable communication, such as the Internet of Things (IoT), virtual reality, and augmented reality. The future of wireless communication promises to be more efficient, reliable, and versatile by understanding the information-theoretic foundations of NOMA.



Multi-objective Optimization in NOMA Networks

3.1 Introduction

Considering the large scale of user equipment, multiple optimization problems exist, which we will discuss in this chapter. Here, we consider the tradeoff between spectral efficiency (SE) and energy efficiency (EE). Reinforcement learning algorithms were initially proposed for machine learning (ML) and decision-making applications. An RL agent takes information from the environment, and based on that information, it learns the optimal action policy via interaction over and over again. The agent decides which action is best for maximizing reward in each episode. RL algorithm is best suited for long-term decision-making purposes. A genetic algorithm is used for optimization purposes. After using this technique for single-objective optimization, the fitness function has been modified for multi-objective optimization purposes. The limited resource availability of the radio spectrum leads to a problem with resource allocation and optimization in a network when the primary goal is to improve the total throughput of the network. This must be an even worse situation when handling multiple objectives, especially those that are conflicting. Improvement of one objective deteriorates the performance of another objective [30] [31]. A simple solution for conflicting objectives can be to find a set of solutions satisfying each conflicting objective to a certain level, and those solutions are non-dominated solutions. Here, we propose a hybrid meta-heuristic algorithm, a multi-objective optimization genetic algorithm based on a reinforcement learning algorithm (MOGA-RL). The simple way of interacting with the environment makes the RL algorithm suitable for taking information from the environment,

whereas GA is used for optimization objectives. Most of the work for optimization using the RL algorithm uses backpropagation, weighted sum method [32], constraint method [33], sequential method [34] and max-min method [35]. This work has limitations of local minimization problems, which have been overcome in evolutionary optimization algorithms. GA can rival back propagation-based algorithms, and the joint work of GA and RL algorithms performs best in dynamic environments where user information changes rapidly and needs to update environment information as well as optimize metrics in the NOMA network. This work aims to determine the trade-off between the total power consumption of the network and spectral efficiency by formulating a MOO problem to maximize SE and minimize power consumption. Also, the work combines the benefits of both GA and RL algorithms with the Q-learning method to find an optimal action selection policy in a particular state.

3.2 System Model

The NOMA network is comprised of a base station (BS) and k number of users. The system's total bandwidth is denoted by B , which is divided into n number of sub-channels denoted by B_1, B_2, \dots, B_n such that $B_i = \frac{B}{n}; i = 1, 2, \dots, n$. The power allocation coefficients for n number of Resource Blocks (RB) are denoted as $\alpha_{1,n} \geq \alpha_{2,n} \geq \dots \geq \alpha_{k,n}$, subject to $\sum_{i=1}^k \alpha_i = 1$, where k is the number of users assigned to sub-channel n . Power allocation coefficients are the fractional power allocation to all the users for NOMA downlink transmission based on their distances from BS. The nearest user gets the lowest fractional power, and the farthest user gets the highest. The rest of the user's power allocation stays in between them. $h_{1,n}, h_{2,n}, \dots, h_{k,n}$ denotes the channel coefficients for all users allocated to n^{th} sub-channel. Without loss of generality, the channel gains are ordered as $|h_{1,n}|^2 \leq |h_{2,n}|^2 \leq \dots \leq |h_{k,n}|^2$. For simplicity, we assume BS holds perfect channel state information (CSI). The total power assigned to sub-channel n denoted as: $\sum_{i=1}^k \alpha_{i,n}$ and $\sum_{i=1}^n P_i = \alpha_{total}$ is the total power from BS. The total power is divided into n sub-channels, and hypothetically, each sub-channel gets equal power. The signal interference to noise ratio (SINR) for user k of subchannel n is denoted as :

$$SINR_{k,n} = \frac{\alpha_{k,n} |h_{k,n}|^2}{\sigma^2}. \quad (3.1)$$

Parameters	Names
k	Total number of number of users
B	Total bandwidth
n	Total number of sub-channels
α_i	Fractional power assigned to user i
α_{total}	Total power from BS
h_i	Channel coefficient for user i
R_{total}	Total sum rate
η_{SE}	Spectral Efficiency and
η_{EE}	Energy Efficiency
κ	Drain efficiency of the power amplifier at the BS
α_c	Total circuit power consumption
R_{min}	Minimum guaranteed data rate of each user
θ	The priority between power consumption and capacity

Table 3.1: Table of parameters

where k is the nearest user of BS. The SINR of j^{th} user of subchannel n denoted as:

$$SINR_{j,n} = \frac{\alpha_{j,n} |h_{j,n}|^2}{|h_{j,n}|^2 \sum_{i=j+1}^k \alpha_i + \sigma^2}. \quad (3.2)$$

R_{total} is the total sum rate for sub channel n indicating as:

$$R_{total}(n) = \log_2(1 + \frac{\alpha_{k,n} |h_{k,n}|^2}{\sigma^2}) + \sum_{j=1}^{k-1} \log_2(1 + \frac{\alpha_{j,n} |h_{j,n}|^2}{|h_{j,n}|^2 \sum_{i=j+1}^k \alpha_i + \sigma^2}). \quad (3.3)$$

The Spectral Efficiency and Energy Efficiency are indicated as follows:

$$\eta_{SE} = \frac{R_{total}}{B}. \quad (3.4)$$

$$\eta_{EE} = \frac{R_{total}}{B(\kappa \alpha_{total} + \alpha_c)}. \quad (3.5)$$

Where κ denotes the drain efficiency of the power amplifier at the BS. α_c is the total circuit power consumption. The abbreviation referenced in this chapter may be found in Table 3.1.

3.2.1 Problem Statement

Our goal is to maximize the total sum rate and minimize power consumption. The sum rate is denoted as R_{total} , which is the sum of all user's data rates. During sum rate maximization, each user should maintain user fairness, which is the minimum data rate requirement for each user, which must be greater than 0 if the user is active. Our goal is to maximize the total sum rate of each sub-channel so that the overall sum rate will be maximized. The problem statement can be formulated as:

$$R_{total} = \max \sum_{n=1}^N \sum_{k=1}^K R_{k,n} \quad (3.6)$$

subject to:

$$\sum_{n=1}^N R_{k,n} \geq R_{min} \quad \forall k \quad (3.7)$$

Constraints C1 indicates each user should maintain a minimum data rate greater or equal to R_{min} . R_{min} is the minimum guaranteed data rate of each user.

$$C2 : \alpha_K = \sum_{i=1}^k \alpha_{i,j}, \forall j \in \{1, 2, \dots, n\}. \quad (3.8)$$

Here n is the number of sub-channels, and k is the total number of users assigned to each sub-channel.

$$C3 : \alpha_{i,j} > 0. \quad (3.9)$$

$\alpha_{i,j}$ is the fractional power assigned to i^{th} user in j^{th} sub channel.

The formulation in Eqs. 3.10 and 3.14 adopts a weighted-sum approach to multi-objective optimization (MOO) rather than constraint-based prioritization for three key reasons: 1. Dynamic Trade-off Control: The priority index θ (or θ' in Eq. 3.13) allows adaptive balancing between SE and EE based on real-time network demands (e.g., peak vs. off-peak hours), whereas fixed constraints lack this flexibility. 2. Pareto Frontier Exploration: The weighted sum ($\lambda_{SE-EE} = \theta\eta_{SE} + (1 - \theta)\eta_{EE}$) explicitly generates Pareto-optimal solutions in a single run, revealing the full trade-off curve. Constraint-based methods require iterative tuning to approximate this frontier. 3. Algorithmic Compatibility: The MOGA-RL framework leverages Eq. 3.10's structure to efficiently explore the solution space

via genetic operations (crossover/mutation) and RL-guided weight adaptation (θ), avoiding the convergence issues of constrained methods in dynamic NOMA environments.

SE and EE both have contradictory objectives. Depending on different situational demands, the different objectives need to be taken care of. During peak hours, SE needs to improve, but during peak-off time, EE needs to improve. The MOO method uses priority index θ to find the optimal solution. So, the new objective can be defined as:

$$\lambda_{SE-EE} = \theta \times \eta_{SE} + (1 - \theta) \times \eta_{EE}. \quad (3.10)$$

Where θ defines the priority between power consumption and capacity. The problem statement can be defined as $\max \lambda_{EE-SE}$, where,

$$C2 : P_T = \sum_{i=1}^N P_i. \quad (3.11)$$

In Eq. 3.11, N represents the total number of sub-channels, P_i is the transmit power for the i -th element, and $P_T = \sum_{i=1}^N P_i$ is the aggregate transmit power. These directly affect the objective λ_{SE-EE} :

$$\lambda_{SE-EE} = \underbrace{\theta \left(\frac{R_{\text{total}}}{B} \right)}_{\eta_{SE}} + (1 - \theta) \underbrace{\left(\frac{R_{\text{total}}}{B(\kappa P_T + \alpha_c)} \right)}_{\eta_{EE}}$$

where:

- λ_{SE-EE} : Combined SE-EE objective function
- $\theta \in [0, 1]$: Priority weight between SE and EE
- $R_{\text{total}} = \sum_{k=1}^K \log_2(1 + \text{SINR}_k)$ (Sum rate)
- $P_T = \sum_{i=1}^N P_i$: Total transmit power
- κ : Power amplifier inefficiency factor
- α_c : Circuit power consumption
- B : System bandwidth

η_{SE} typically increases with higher P_i (more power \rightarrow better signal quality \rightarrow higher data rates). η_{EE} measures “bits transmitted per Joule” and decreases if P_T grows excessively. Higher P_T reduces EE because more energy is consumed for marginal gains in SE (η_{SE}). User Fairness should quantify minimum rate compliance as $\sum_{n=1}^N R_{k,n} \geq R_{\min} \forall k$ (refer equation. 3.7), ensuring no user falls below R_{\min} .

User fairness is a performance metric in the NOMA network, where each user needs to maintain a minimum data rate irrespective of its CSI value. Increasing the distance between BS and UE’s will require more power to maintain a fairness index, which in turn affects power requirements. The priority index θ' helps to find the optimal solution of the new objective:

$$\lambda_{EE-UF} = \theta' \times \eta_{EE} + (1 - \theta') \times UF. \quad (3.12)$$

3.3 Multi-Objective Optimization

To date, very little work has been done focusing on multi-objective optimization (MOO) in NOMA networks. Our work mainly focuses on multi-objective optimization using a Multi-Objective Genetic Algorithm (MOGA) that combines the features of Reinforcement learning (MOGA-RL). This framework helps to optimize multiple objectives while maintaining users’ quality of service (QoS). It removes the requirements of manual tuning to handle multiple objectives. Most of the MOO focuses on a random selection of objectives in different Episodes, which in this work has been eliminated using the Reinforcement Learning approach. Reference [36] presents a PD-NOMA and Deep Reinforcement Learning (DRL) framework for multi-objective optimization in satellite networks, balancing link utilization, latency, power efficiency, and throughput. The approach uses predictive network analysis, PD-NOMA for spectral efficiency, and DRL for dynamic resource allocation, enabling real-time adaptation. Reference [37] proposes an IRS-aided PD-NOMA system with multi-relay selection strategies to enhance physical-layer security against eavesdroppers. The study optimizes secrecy capacity and energy efficiency through: (1) Three relay selection methods (best-relay, max-min, harmonious); (2) Joint IRS phase-shift and NOMA power allocation control; (3) Artificial noise transmission to disrupt eavesdroppers. Reference [38] proposes a multi-vector optimization (MVO) framework for RIS-assisted NOMA in satellite-aerial-terrestrial networks (SATINs), addressing dynamic optimization challenges through a novel MV-DDPG

algorithm that jointly optimizes UAV energy efficiency, transmit beamforming, and RIS phase-shifts in real-time. The study demonstrates effective simultaneous optimization of three key objectives with adaptable weighting, showing significant improvements in spectral efficiency and network reconfigurability for next-generation communications. This work advances NOMA multi-objective optimization by integrating RIS with DRL for intelligent resource allocation in complex heterogeneous networks.

In this section, we present a detailed mathematical model for the multi-objective optimization method, which optimizes N number of objectives, and N must be greater than or equal to 2. The optimal solution for each objective must satisfy associated constraints. In MOO, a set of optimal solutions from different set of populations are obtained. [39], [40] ensure convergence guarantee of the MOO GA algorithm. The MOO problem can be defined as:

$$f(x) = \max(f_1(x), f_2(x)). \quad (3.13)$$

Since both of the functions, f_1 and f_2 , are maximization functions, equation 3.13 indicates maximizing both objectives. where $N = 2$. Here, we have taken spectral efficiency (SE) and energy efficiency (EE) as maximization functions.

Pareto Optimality In the MOO problem, it results in a set of non-dominated solution sets P' out of the total solution set P . P' is the solution set where any member of P' are not dominated by any member of P .

A point $x^* \in X$ is considered Pareto optimal if and only if there exists no point $x \in X$ such that $f_n(x^*) \geq f_n(x)$, for all $n = 1, 2, \dots, N$.

3.4 Proposed Architecture

3.4.1 MOGA

The concept of Genetic Algorithm (GA) came from evolutionary optimization algorithms. This is the most widely used and well-known optimization technique in the area of optimization. GA works on four basic principles: Initial random population, selection, crossover, and mutation. MOGA is a concept for optimizing multiple objectives when one objective may compromise another one. It is a simple approach and an extension of a single objective

3.4. PROPOSED ARCHITECTURE

genetic algorithm. The output of the algorithm is a set of Pareto optimal solutions. According to the preference of the decision maker, the best solution is then selected. Algorithm 1 shows step by step explanation of MOGA: Step 1: The algorithm starts with generating a random number of population P_0 at Episode $t = 0$;

Step 2: Evaluate the fitness function of each chromosome in the population. The evaluate function follows the steps below.

Step 2.1: Assigned rank $r(x, t)$ to each solution $x \in P$ in each generation t . The rank assignment follows the process below.

$$r(x, t) = 1 + nq(x, t) \quad (3.14)$$

$nq(x, t)$ represents the number of dominating solutions (chromosomes) x at generation t . Identify non-dominated solutions(P_1, P_2, \dots, P_n) in the population set P for each generation where $P_1 \cup P_2 \cup \dots \cup P_n = P$. Assign each non-dominated set to a non-dominated front F_i , where $i = 1, 2, \dots, n$.

Step 2.2: Assign fitness values to each chromosome based on the rank assigned in step 2.1.

$$f(x, t) = N - \sum_{k=1}^{r(x,t)-1} n_k - 0.5 * (n_{r(x,t)} - 1) \quad (3.15)$$

where n_k represents the number of solutions with rank k .

Step 2.3: GA tends to converge to a single solution as the diversity of the population diminishes. Calculate niche count $nc(x, t)$ of each solution in each generation to maintain diversity in the population based on the distance between the population members.

$$nc(x) = \sum_{y=1}^{\mu(r_i)} Sh(d_{x,y}) \quad (3.16)$$

$\mu(r_i)$ is the number of solutions with rank value equal to r_i . Sharing function value $Sh(d_{x,y})$ is a function of the distance between two solutions x and y and can be calculated as:

$$Sh(d_{x,y}) = \begin{cases} 1 - (\frac{d_{x,y}}{\sigma_{share}})^\alpha, & \text{if } d_{x,y} \leq \sigma_{share}, \\ 0, & \text{otherwise.} \end{cases} \quad (3.17)$$

α is a constant value used to regulate the shape of the sharing function, and it is usually set to 1.

$$d(x, y) = \sqrt{\sum_{k=1}^M \left(\frac{f_k(x) - f_k(y)}{f_k^{max} - f_k^{min}} \right)^2} \quad (3.18)$$

For the solution x , $d(x, y)$ represents the Euclidean distance for each solution y , which has the same rank. f_k^{max} and f_k^{min} indicates maximum and minimum k^{th} objective function values. M represents the number of objectives. The niching technique is used to maintain diversity and avoid genetic drift.

Step 2.4: Calculate the shared fitness value

$$f'(x, t) = \frac{f(x, t)}{nc(x, t)} \quad (3.19)$$

Step 3: Apply the selection method based on the fitness value f' , crossover, and mutation for generating the next generation of population.

Step 4: Check if t has not reached the maximum number of generations, set $t = t + 1$, and go to step 2.

f_k^{max} and f_k^{min} are the observed maximum and minimum values of the k -th objective function in the current population, calculated dynamically each generation as $f_k^{max} = \max_{x \in P} f_k(x)$ and $f_k^{min} = \min_{x \in P} f_k(x)$, where $f_k(x)$ is the k -th objective value for solution x . The calculation involves: (1) evaluating all objectives $f_1(x), \dots, f_M(x)$ for each $x \in P$, (2) extracting per-objective extremes across the population ($f_k^{max} = \max_{x \in P} f_k(x)$ and $f_k^{min} = \min_{x \in P} f_k(x)$), and (3) optionally normalizing values via $\frac{f_k(x) - f_k^{min}}{f_k^{max} - f_k^{min}}$ for distance metrics. Genetic drift [41] refers to the unintended loss of population diversity in evolutionary algorithms, where certain traits dominate by chance rather than fitness, leading to premature convergence. Our niching technique counters this through: (1) a sharing function (Eq. 3.18) that penalizes overcrowded solutions, (2) niche counts (Eq. 3.17) quantifying solution density via pairwise distances, and (3) shared fitness scaling (Eq. 3.20) that preserves diversity by adjusting raw fitness values. The selection method in Step 3 combines tournament selection (using shared fitness $f'(x, t)$) with elitism to prioritize high-quality, diverse solutions while retaining top non-dominated candidates between generations.

3.4.2 Proposed MOGA-RL Algorithm for Spectral Efficiency and Energy Efficiency

The MOGA-RL hybrid synergistically combines the population-based Pareto-front search of Multi-Objective Genetic Algorithms (MOGA) with Reinforcement Learning (RL) to overcome fundamental limitations of standalone MOGA in dynamic NOMA networks. While MOGA effectively solves static multi-objective problems, its fixed weight parameters (e.g., θ in Eq. 3.10) and predetermined genetic operators fail to adapt to real-time network dynamics like fluctuating user demands or channel conditions. The hybrid approach addresses this by: (1) dynamically adjusting SE/EE trade-off weights through Q-learning (Eq. 3.21), (2) intelligently selecting crossover/mutation operators (a_n/a_m) based on state-action rewards (Eq. 3.26), and (3) continuously refining solutions via environmental feedback. By preserving MOGA's optimization core while augmenting it with RL's decision-making adaptability, MOGA-RL maintains Pareto-optimality while gaining critical responsiveness to time-varying conditions

Reinforcement Learning

In recent years, the Reinforcement Learning (RL) [42] method has gained success in the area of decision-making approach and machine learning. The standard RL algorithm works with a learning agent and an environment. The agent receives state and reward information from the environment and gives an optimal result through trial and error interaction. In this chapter, we use a genetic algorithm for optimization purposes and a reinforcement learning approach for taking information from the environment. In each episode, the proposed MOGA-RL algorithm takes state information and generates a Pareto optimal solution using a multi-objective genetic algorithm. Markov decision process (MDP) is a mathematical model used to describe the RL algorithm. MDP can be formulated as a tuple (S, A, T, R, γ) , where S represents a set of states, A represents a set of actions, T is the transition probability from one state to another $p(s'|s, a)$, where $s', s \in S$ and $a \in A$, R is the reward function and $\gamma \in [0, 1]$ represents discount factor. MDP components are formally defined as: (1) State space \mathcal{S} comprising current spectral efficiency η_{SE} , energy efficiency η_{EE} , power allocations $\alpha_{i,n}$; (2) Action space $\mathcal{A} = a_c, a_m$ where a_c/a_m select genetic operators (Algorithm 2) and the continuous component adjusts priority weight θ (Eq. 3.10); (3) Reward function r_t

balancing SE/EE trade-offs; and (4) Transition probabilities $\mathcal{P}(s_{t+1}|s_t, a_t)$ modeled via Gaussian perturbations for $\alpha_{i,n}$ updates and deterministic efficiency recalculation.

Proposed MOGA-RL Algorithm

Evolutionary strategies are an alternative to gradient-based neural network training [43], which uses backpropagation. Most of the gradient-based algorithms for neural networks stagnate in local minima. The multi-objective genetic algorithm is a subclass of evolutionary algorithms. It avoids getting stuck in the local minima by using the niching technique, which maintains diversity based on the distance between the population members. Backpropagation usually takes too long to find an optimal solution so it is very difficult to get convergence in a short period of time. Our work is to replace backpropagation with GA to get better convergence in a short time duration.

Crossover and mutation are two different actions taken to generate Pareto optimal solutions and store them in the Q-Table. After completion of the predefined maximum number of generations, the scaled fitness values are the final set of Pareto solutions. Then, based on the decision maker's choice or the system's requirement, the solution is taken.

The first two parents are randomly selected from the population. Then, the crossover and mutation operations are applied as two different actions, and based on different actions in different states, the reward is generated. Q-Table holds all possible state-action values, which are initially set to 0. There is an iterative process that updates the Q-values over and over again. During the exploration of the environment, the Q-function gives better approximations by continuously updating the Q-values. The flow chart of the Q-learning algorithm is described in Fig 3.1. The reward function is calculated from $f'(x, t)$ of multi-objective genetic algorithm based on crossover or mutation process as an action taken. In Q-Table, columns represent actions, and rows represent states. The action set represented as: $a \in \{a_c, a_m\}$. The Q-table update rule [44], [45] can be calculated as:

$$Q(s_t, a_t)^{new} = Q(s_t, a_t) + \alpha'(r_t + \gamma \max_{a'} Q(s_{t+1}, a') - Q(s_t, a_t)) \quad (3.20)$$

where $a' \in a$,

$\gamma \in [0, 1]$: discount factor,

$Q(s_t, a_t)$: old value,

3.4. PROPOSED ARCHITECTURE

α' ($0 < \alpha' \leq 1$): learning rate,

$\alpha' r_t$: the calculated reward $r(s_t, a_t)$, if action a_t is taken in state s_t , weighted by learning rate

$\alpha' \gamma \max_{a'} Q(s_{t+1}, a')$: the maximum reward that can be obtained from state s_{t+1} , weighted by learning rate and discount factor.

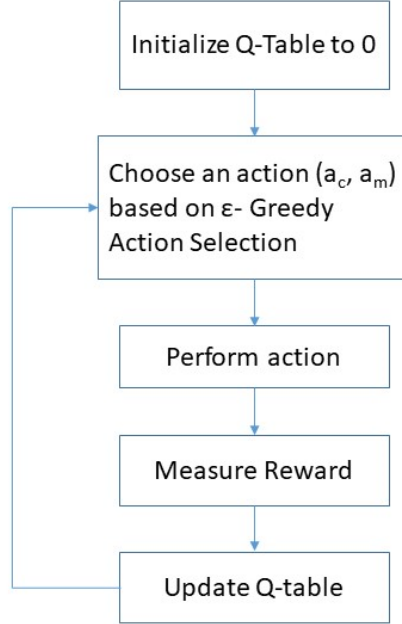


Figure 3.1: Q-Learning.

Q-learning is an iterative optimization method where state information in different episodes is fed into the agent. To avoid the exploration-exploitation problem in the RL algorithm, ϵ -greedy algorithm is used, which selects the action with the highest estimated reward, where $\epsilon \in [0, 1]$. The working principle of ϵ -Greedy Action Selection is described in Algorithm 1.

ALGORITHM 1: ϵ -Greedy Action Selection

- 1 Generate a random number R .
 - 2 **if** $R \leq \epsilon$ **then**
 - 3 Choose random action a_t
 - 4 **else**
 - 5 Choose the current best action $\underset{a}{\operatorname{argmax}} Q(a)$.
-

Where *argmax* specifies choosing the action a for which $Q_t(a)$ is maximized, the working principle of ε -Greedy Action Selection is based on a trial and error strategy. The ε -greedy approach is incorporated to avoid the exploration-exploitation problem. We set ε is set to 1 to explore the available actions with a probability of 1/2. This will obtain the best result for crossover and mutation. The flowchart of the proposed MOGA-RL algorithm (Algorithm 2) is represented in Fig 3.2.

3.4.3 Reward Function

The reward function r_t must incorporate both spectral efficiency (SE) and energy efficiency (EE). SE is calculated as:

$$SE = \sum_{i=1}^N B \cdot \log_2(1 + \text{SINR}_i) \quad (3.21)$$

where: B : Bandwidth, SINR_i : Signal-to-interference-plus-noise ratio for user i . EE is calculated as:

$$EE = \frac{P_{total}}{\sum_{i=1}^N R_i} \quad (3.22)$$

where: R_i : Data rate for user i , P_{total} : Total power consumption. Normalize SE and EE to ensure they are on the same scale and to facilitate a balanced comparison between the two objectives.

$$SE_{\text{norm}} = \frac{SE}{SE_{\text{max}}} \quad (3.23)$$

$$EE_{\text{norm}} = \frac{EE}{EE_{\text{max}}} \quad (3.24)$$

The reward r_t is a weighted sum of normalized SE and EE:

$$r_t = w_1 \cdot SE_{\text{norm}} + w_2 \cdot EE_{\text{norm}} \quad (3.25)$$

where: w_1 : weight for SE ($w_1 \in [0, 1]$), w_2 : weight for EE ($w_2 \in [0, 1]$) and $w_1 + w_2 = 1$. The weights w_1 and w_2 are selected using the ε -greedy strategy to balance exploration and exploitation:

Exploitation (with probability $1 - \epsilon$):

Select the weights w_1 and w_2 that maximize the reward based on the current knowledge (e.g., historical performance of SE and EE).

Exploration (with probability ϵ):

Randomly select w_1 and w_2 from the range $[0, 1]$ such that $w_1 + w_2 = 1$.

Integration with Q-Learning involves using the reward r_t in the Q-table update rule:

$$Q(s_t, a_t)_{\text{new}} = Q(s_t, a_t) + \alpha' \left(r_t + \gamma \max_{a'} Q(s_{t+1}, a') - Q(s_t, a_t) \right). \quad (3.26)$$

Each state s_t represents a configuration of the NOMA network, such as power allocation or user pairing, while actions a_t are either crossover (a_c) or mutation (a_m). For each action a_t , the resulting SE and EE are calculated, and the reward r_t is computed using the weighted sum of normalized SE and EE to guide the optimization process.

The implementation steps begin with initializing the Q-table, where states are represented as rows and actions (a_c , a_m) as columns. For each state s_t , the actions a_c and a_m are evaluated by performing crossover or mutation, calculating the resulting SE and EE, and computing the reward r_t . The Q-table is then updated using the Q-learning update rule based on the reward r_t . An exploration-exploitation strategy, such as ϵ -greedy, is employed to select the next action, and the process is repeated iteratively until convergence or a predefined stopping criterion is met.

ALGORITHM 2: Multi-Objective Genetic Algorithm with RL

Input: Population size P , max generations G , MOO problem

Output: Pareto optimal solution set \mathcal{P}^*

```

1  // Initialization
2  Initialize random population  $P_0$  of size  $P$ 
3  Initialize empty Pareto archive  $\mathcal{A}_0$ 
4  foreach state-action pair  $(s, a) \in Q$ -table do
5      | Initialize  $Q(s, a)$                                      //  $s = (\eta_{SE}, \eta_{EE}, UF)$ ,  $a \in \{a_c, a_m\}$ 
6  end
7  for  $t \leftarrow 1$  to  $G$  do
8      | // RL-Guided Evolution
9      | Evaluate fitness:  $\mathbf{f}(x) = [\eta_{SE}(x), \eta_{EE}(x)]$  for all  $x \in P_{t-1}$ 
10     | Observe current state  $s_t$  from population metrics
11     | Select action  $a_t \in \{a_c, a_m\}$  using  $\epsilon$ -greedy policy
12     | // Genetic Operations
13     | if  $a_t = a_c$  then
14         | Perform crossover to generate offspring
15     | else
16         | Perform mutation
17     | end
18     | // Multi-Objective Optimization
19     | Apply multi-objective genetic algorithm
20     | // RL Update
21     | Compute reward:  $r_t = w_1 \eta_{SE} + w_2 \eta_{EE} - \lambda \sum \max(0, R_{\min} - R_i)$ 
22     | Update  $Q(s_t, a_t) \leftarrow Q(s_t, a_t) + \alpha[r_t + \gamma \max_a Q(s_{t+1}, a) - Q(s_t, a_t)]$ 
23     | Update Pareto archive  $\mathcal{A}_t$  with current non-dominated solutions
24 end
25 return  $\mathcal{P}^* = \mathcal{A}_G$                                      // Final Pareto front

```

3.5 Comparative Analysis

In NOMA networks, optimizing for multiple objectives like sum rate and energy efficiency is crucial. While the weighted-sum method [46] is a common approach, MOGA demonstrates superior performance. The weighted-sum method relies heavily on predefined weights, which

3.5. COMPARATIVE ANALYSIS

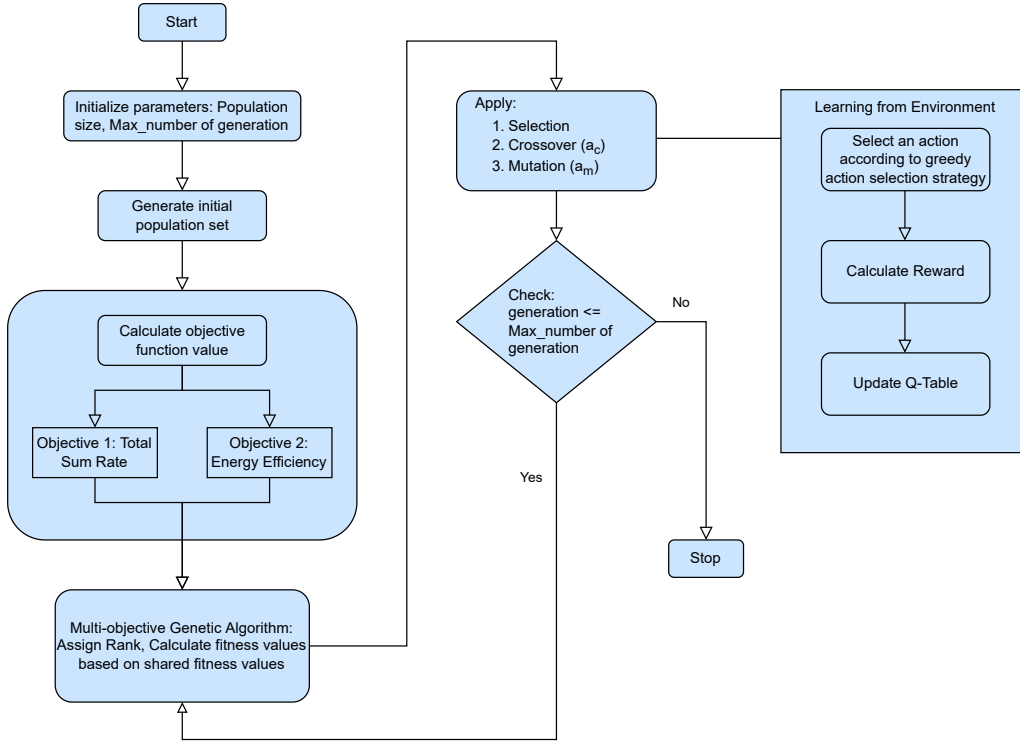


Figure 3.2: Flow chart of MOGA-RL algorithm.

can lead to skewed optimization and difficulty in capturing complex trade-offs between objectives. Moreover, it typically generates a single solution, limiting the exploration of the Pareto front. In contrast, MOGA directly addresses multiple objectives, avoiding arbitrary weight assignments and effectively exploring the solution space to discover a diverse set of Pareto-optimal solutions. Their flexibility and adaptability make them well-suited for complex optimization scenarios in NOMA networks. While the weighted-sum method provides a basic framework, MOGAs offer several advantages, particularly in achieving optimal trade-offs between sum rate and energy efficiency.

In a NOMA network, while the Weighted Sum Method offers a computationally efficient approach with a complexity of $O(T \cdot N)$, where N is the number of user equipment (UE) and T is the number of iterations, making it linearly scalable for smaller-scale problems, the Multi-Objective Genetic Algorithm (MOGA) is fundamentally superior for multi-objective optimization. Despite its higher computational cost, represented by $O(T \cdot (P \cdot N + P \cdot \log P))$, where P is the population size, MOGA's population-based approach and maintenance of Pareto-optimal solutions allow for a significantly more comprehensive exploration of the

objective space. This capability is crucial in complex, large-scale scenarios where balancing multiple, often conflicting, objectives is paramount. While the Weighted Sum Method's simplicity and lower cost are appealing, its inherent limitation in exploring the full Pareto front makes MOGA the preferred method for achieving truly optimal, multi-objective solutions, as evidenced by the substantial difference in computational overhead in the provided example, which underscores the trade-off for enhanced optimization quality.

3.6 Results and Discussion

In this section, we have evaluated the performance of the proposed system. The result shows the tradeoff between sum rate and energy efficiency. The Pareto optimal solutions are obtained at different SINR values depicted in Fig 3.3, Fig 3.4, and Fig 3.5. It is observed that improvement in energy efficiency is obtained at the cost of spectral efficiency. The Pareto optimal solution obtained by the proposed algorithm exhibits its performance in terms of search space and population diversity. Fig 3.6 tracks the evolution of the sum rate (measured in bps/Hz) over 140 generations for five different mutation rates: 0.01, 0.05, 0.1, 0.2, and 0.3. The graph shows how each mutation rate influences the convergence behavior, with lower rates (e.g., 0.01) potentially leading to slower but steadier improvements, while higher rates (e.g., 0.3) may result in faster initial gains but with possible instability or early plateaus. The comparison suggests an optimal mutation rate that balances speed and stability to maximize the sum rate, providing insights into the performance of evolutionary algorithms or optimization processes under varying genetic mutation intensities. The simulation employs the following parameters and models: The system configuration includes $K = 10$ users and $N = 5$ sub-channels with $B = 20$ MHz bandwidth, power constraints $P_{max} = 30$ dBm and $\alpha_c = 10$ dBm circuit power, and QoS requirements $R_{min} = 0.5$ Mbps/user, and RL parameters $\gamma = 0.9$, $\alpha' = 0.1$, $\epsilon = 0.2$. Channels follow Rayleigh fading ($h_{k,n} \sim \mathcal{CN}(0, 1)$) with 100ms coherence time and path loss $PL(d_k) = 128.1 + 37.6 \log_{10}(d_k)$ dB for uniformly distributed user distances $d_k \sim \mathcal{U}(50, 500)$ m. AWGN noise is modeled with $\sigma^2 = -174 + 10 \log_{10}(B/N) + 7$ dBm, where channels are fixed at each iteration (for simplicity).

Fig. 3.7 generates a graph illustrating the trade-off between EE and SE for two optimization methods: MOGA and the Weighted Sum Method [46] across varying signal-

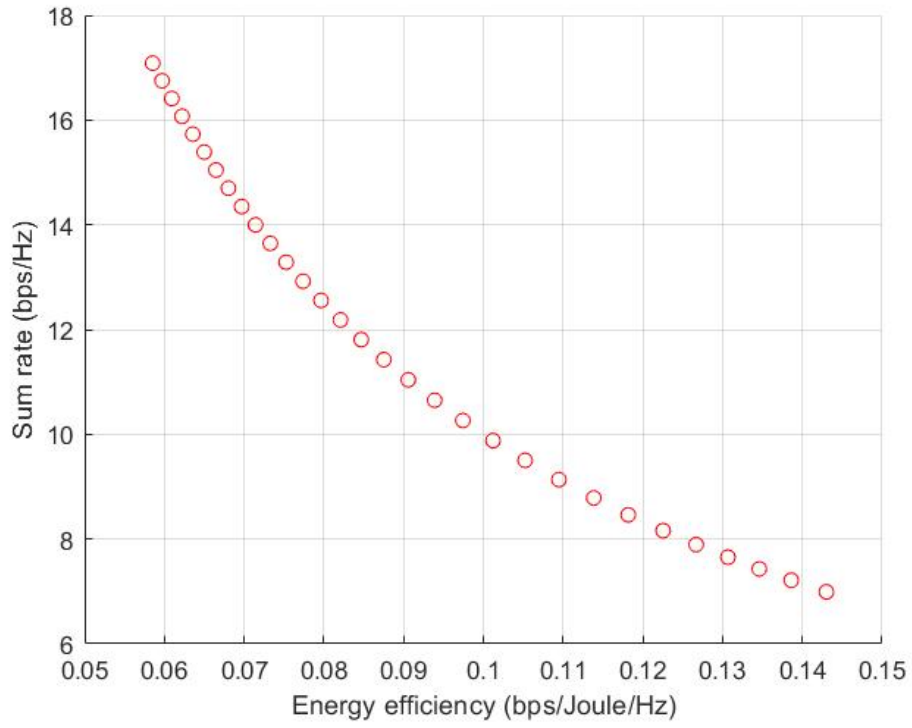


Figure 3.3: Pareto optimal solution at $\text{SINR} = 4\text{dB}$.

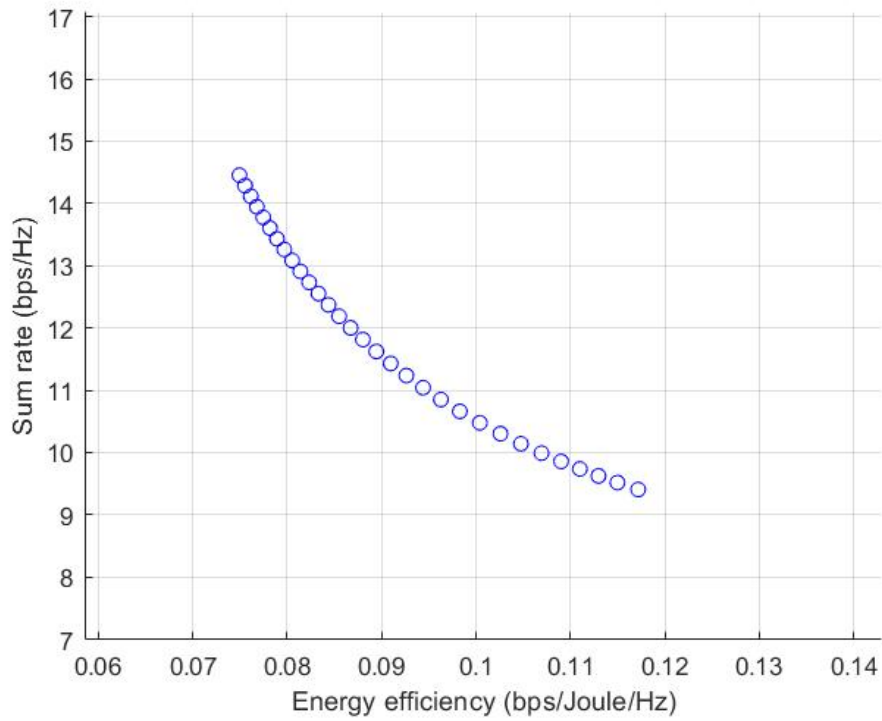


Figure 3.4: Pareto optimal solution at $\text{SINR} = 8\text{dB}$.

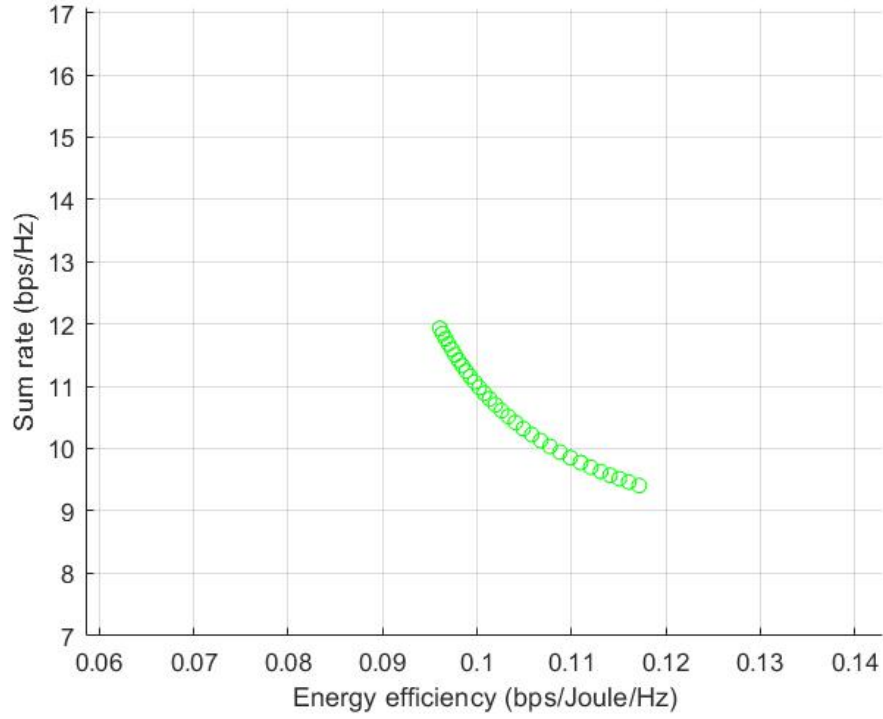


Figure 3.5: Pareto optimal solution at $\text{SINR} = 12\text{dB}$.

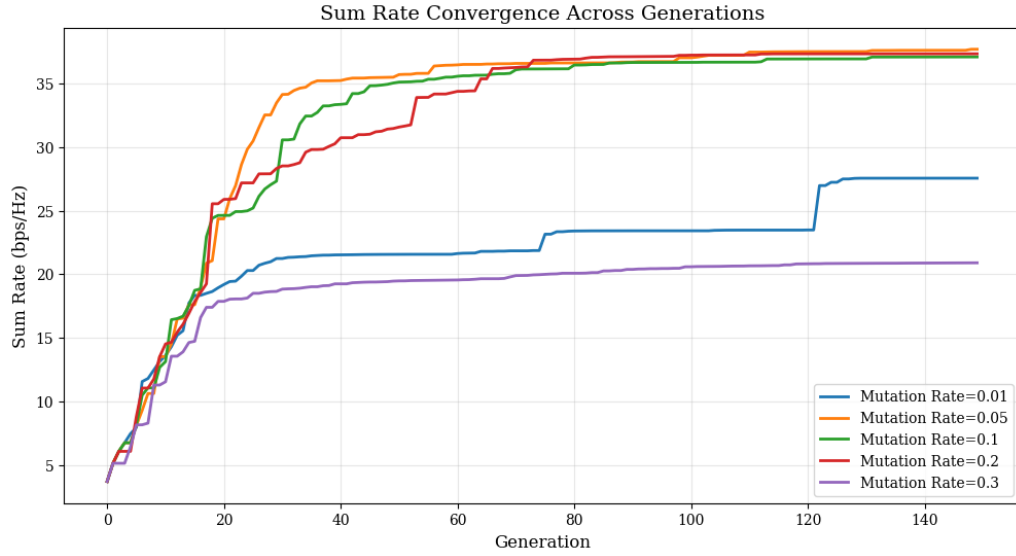


Figure 3.6: Convergence rate of the proposed scheme at different generations.

to-Noise Ratio (SNR) values. The graph reveals an inherent trade-off: increasing SE (e.g., via higher-order modulation) typically reduces EE due to higher energy demands while improving EE (e.g., by lowering transmission power) can decrease SE. Higher SNR improves EE for a given SE, as it reduces the energy needed for reliable communication. MOGA, a heuristic optimization technique, consistently outperforms the Weighted Sum Method, achieving higher EE values for the same SE and SNR, as the latter's performance is scaled down by 0.8 to reflect its suboptimal nature. The curves exhibit exponential decay in EE with increasing SE. These results highlight MOGA's effectiveness in balancing EE and SE, emphasizing the importance of energy-aware strategies in designing wireless systems, especially in varying SNR environments. Fig. 3.8 compares the performance of MOGA-RL

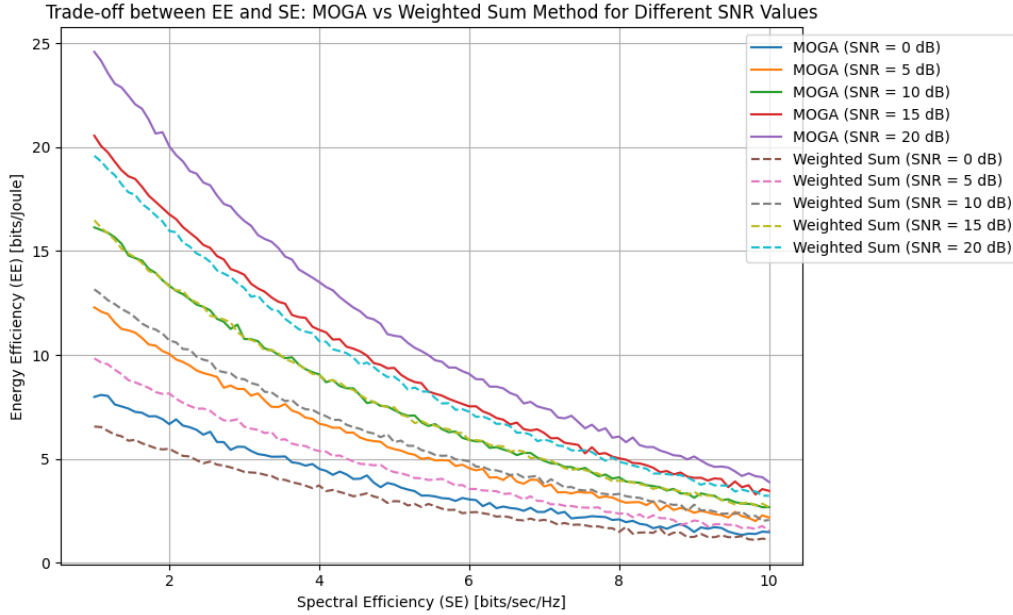


Figure 3.7: Trade-off between EE and SE: Comparison of MOGA and Weighted Sum Method for Different SNR Values.

with traditional optimization methods (Constraint, Weighted Sum, Sequential, and Max-Min). The x-axis represents SE (bps/Hz), while the y-axis shows EE (bits/Joule), where higher values on both axes indicate better performance. MOGA-RL's blue points form a Pareto front, demonstrating its ability to discover multiple optimal trade-offs between SE and EE, outperforming traditional methods that only produce single suboptimal solutions (marked by colored shapes). The graph clearly shows how MOGA-RL dominates by covering superior SE-EE combinations that other methods misses. This visualization highlights

MOGA-RL's advantage in exploring the full solution space and finding globally optimal trade-offs compared to traditional approaches that are limited to fixed constraints or weighted objectives.

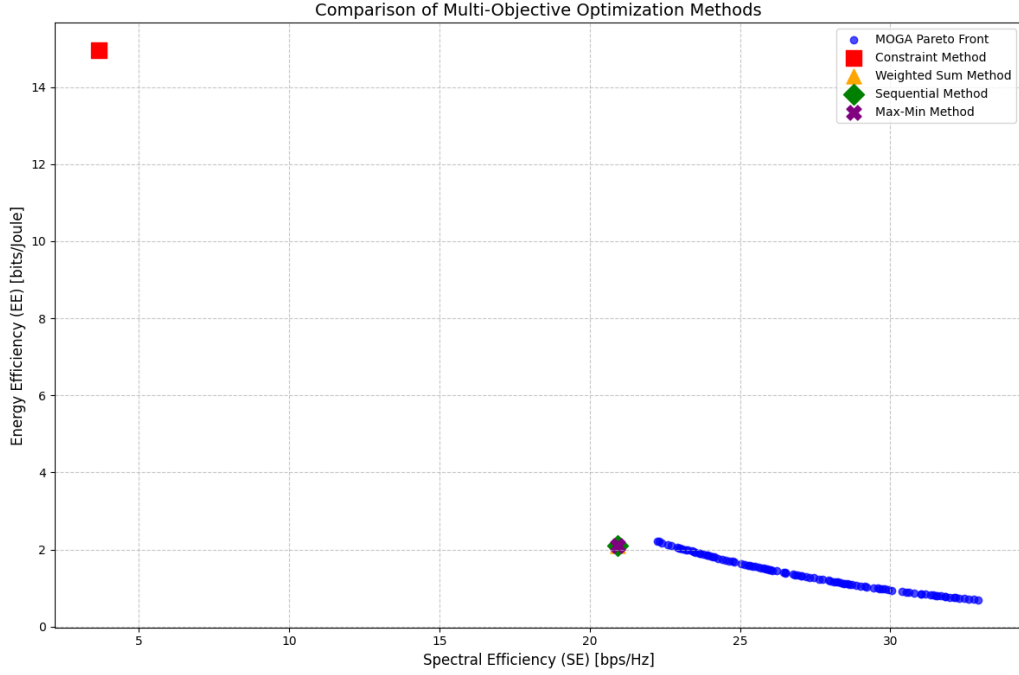


Figure 3.8: Comparison of MOGA-RL, weighted Sum, constraint, sequential, and max-min method.

The performance of the proposed multi-objective optimization algorithm works better than the conventional algorithms weighted sum method [32], constraint method [33], sequential method [34], and max-min method [35] in terms of the local minimization problem. Niching technique maintains diversity based on the distance between the population members to avoid genetic drift in a Multi-objective genetic algorithm. Also, the negative aspects of cognitive uncertainty are one of the major challenges in the MOO problem, which has been overcome in the proposed method.

3.7 Algorithm Analysis

3.7.1 Space Complexity

The space complexity to store Q-table is $O(|S| \times |A|)$, where $|A| = 2$. So the space complexity becomes $O(|S|)$. The space complexity of MOGA: $\Theta(max_pop)$, where max_pop : total

3.8. SUMMARY

number of population. The space complexity of the proposed algorithm: $O(max_pop \times |S|)$. The state space size is determined through discretization of key system parameters as $|S| = N_{\eta_{SE}} \times N_{\eta_{EE}} \times N_{\alpha}^{KN}$, where $N_{\eta_{SE}}$ = Number of bins for spectral efficiency (SE), $N_{\eta_{EE}}$ = Number of bins for energy efficiency (EE), N_{α} = Number of discrete levels for power allocation parameters, K = Number of users, and N = Number of resources (e.g., subcarriers, antennas)

3.7.2 Time Complexity

The time complexity of MOGA is $O(max_gen \times max_obj \times max_pop^2)$, where max_gen is the maximum number of generations and max_obj is the maximum number of objectives which here is 2. Therefore, the total time complexity of the proposed algorithm is $O(max_gen \times max_pop^2)$. We have used the worst-case $O(max_gen \times max_pop^2)$ analysis. We assume a maximum number of generations as a safeguard to ensure computational feasibility, preventing infinite runtime in cases of slow or non-convergence while balancing solution quality with resource constraints. This limit accounts for diminishing returns in later generations, where improvements become marginal, and guarantees termination with the best-available solution even if Pareto front convergence isn't achieved earlier.

3.8 Summary

In this chapter, maximizing the total sum rate of the network and minimizing power consumption can be formulated as a Multi-objective optimization (MOO) problem. The problem is solved by searching for the optimal set of solutions. The addition of reinforcement learning in multi-objective optimization helps to tune the parameter automatically to reduce manual interference. The proposed algorithm provides a Pareto optimal solution between conflicting objectives under a dynamic environment.



Multiple Interference Cancellation in MIMO-NOMA Network

4.1 Introduction

The increasing need for fast and dependable wireless access has driven the advancement of cellular networks to fifth-generation (5G) and beyond. NOMA is a fundamental aspect of 5G technology that improves spectrum efficiency by enabling multiple users to use the same time and frequency resources. In addition to NOMA, Multiple-Input Multiple-Output (MIMO) technology utilizes antenna arrays to enhance system capacity and coverage. Furthermore, Device-to-Device (D2D) communication has emerged as an auspicious approach to improve the efficiency of spectrum use and reduce the burden on the base station by transferring traffic. This study explores the incorporation of NOMA, MIMO, and D2D technologies to construct a resilient and effective wireless communication system. NOMA is a low-cost technology that boosts cell spectrum efficiency without needing additional resources or infrastructure. Inter-user interference is NOMA's main barrier. However, user clustering and power distribution may minimize it and boost spectral efficiency. In contrast, MIMO may triple spectral efficiency gain in proportion to spatial multiplexing order by using multiple antennas at the transmitter and receiving ends. Inter-cluster interference in MIMO may be eliminated when a cell has the same or fewer receive antennas than broadcast antennas. We want to build a groundbreaking multiuser MIMO-NOMA-D2D system employing Multiple Interference Cancellation (MIC) to maximize system capacity and energy efficiency while reducing net interference. Green communication will become necessary. We aim to improve system performance by using MIC approaches to reduce inter-

user and intra-user interferences. We prioritize optimizing resource allocation, enhancing spectral efficiency (SE), and improving energy efficiency (EE), considering the influence of D2D communication on the whole network. We conduct extensive simulations to compare our proposed MIMO-NOMA-D2D system with traditional MIMO-OMA and MIMO-NOMA schemes to emphasize the advantages of our method. This chapter discusses using correlated channel gains to allocate resources in the MIMO-NOMA-D2D network. MIMO-NOMA networks using MIC instead of SIC reduce intra-cluster interference to perfection. Instead of SIC, MIC is used at the receiving end to reduce interference. The final total sum rate is higher. The MIMO-NOMA network's huge antennas, decoders, detectors, and regenerator circuits need much power. Eliminating the receiver decoder and regenerator may promote green communication and a less power-hungry network. The system's hardware complexity is reduced.

4.2 System Model

Consider a single-cell downlink MIMO network where the base station (BS) has M broadcast antennas and k devices have N receive antennas on each of them (k ranges 1 to $K \approx 4M$ (2 pairs $\times M$ clusters)), whereas $M \geq 2N$, which are frequently seen in real-world settings involving IoT devices of low complexity and high-complexity BSs. All the devices can be equipped with one or more receiving antennas. The devices are grouped into M clusters. Wireless channels may be subject to any distribution, such as the Rayleigh distribution, assuming that fading is assumed to be quasi-static independent and identically distributed (i.i.d.). The network considers MIMO-NOMA transmission with D2D communication to serve multiple D2D pairs. For the l -th D2D pair in the m -th cluster denoted as $d_l \in \{d_1, d_2, \dots, d_l\}$ and $m \in \{1, 2, \dots, M\}$. In this chapter, we assume there are a maximum of up to two D2D pairs being assigned different power levels on the same cluster denoted as $\{d_1, d_2\}$ where d_1 denotes (w, x) pair and d_2 denotes (y, z) pair. The MIMO-NOMA network with D2D device communication is broadly described herein Figure 4.1. The abbreviation referenced in this chapter may be found in Table 4.1.

This chapter proposes a downlink MIMO-NOMA system with D2D integration to enhance spectral efficiency (SE) and energy efficiency (EE). The BS, equipped with M antennas, serves k devices grouped into M clusters, where each cluster contains a relay device

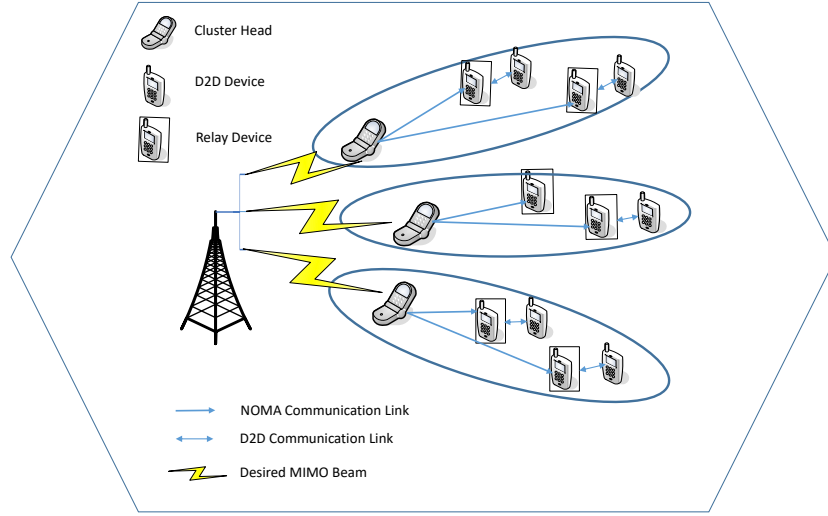


Figure 4.1: General MIMO-NOMA D2D network

Parameters	Names
M	Number of broadcast antennas
k	Number of devices
N	Number of receive antennas on each device
d_l	l -th D2D pair
$t_{m,i}$	modulated symbol for the i -th D2D pair in the m -th cluster
$\mathbf{t}_{m,i}$	modulated transmit symbol vector
\mathbf{X}	broadcast data vector
x_m	data stream for m -cluster
$p_{m,l}$	transmit power for the l -th D2D pair in the m -th cluster
\mathbf{B}	Beamforming precoding matrix
$\mathbf{H}_{m,k}$	Channel response matrix for device k in m -th cluster
\mathbf{G}_{wx}	Channel matrix between device w and device x
$ds_{m,l}$	decoding scaling weight factor
$y_{m,l}$	Received signal for the l th pair in the m th cluster
I_1	Intra-cluster interference
I_2	Inter-cluster interference
P_T	The total power from BS
p_m	The total power used by all pairings in a cluster
$h_{k,n}^*$	The channel between k -th device's send antenna and n -th receive antenna
y_k	The received signal at device k
d_1	The closest pair of BS
d_2	The farthest pair from BS
t_1	The signal detected at d_1
t_2	The signal detected at d_2

Table 4.1: Table of parameters

which is called cluster head (M relays) and two D2D pairs (e.g., (w, x) and (y, z)). The BS transmits superposed signals using a beamforming matrix B , with cluster heads receiving $y_{m,l} = ds_{m,l}[\tilde{h}_{m,l}BX + n_{m,l}]$. D2D pairs communicate locally ($\leq 20m$ apart) using NOMA principles: near users employ SIC to decode their signals first, while far users leverage MIC (Multiple Interference Cancellation) to bypass SIC complexity. Key innovations include (1) MIC for reduced far-user decoding power, (2) optimized power allocation (more power to weak channels), and (3) Algorithm-driven D2D pairing based on channel correlation ($R_{i,j} \geq 0.5$) and proximity. The model mitigates interference through orthogonal beams (inter-cluster) and MIC (intra-cluster), outperforming traditional MIMO-OMA in SE/EE by combining MIMO's spatial multiplexing, NOMA's spectral efficiency, and D2D's load reduction.

In this chapter, $t_{m,i}$ indicates i -th D2D pair of m -th cluster where $i \in \{w, x\}$ and $t_{m,j}$ indicates j -th D2D pair of m -th cluster where $j \in \{y, z\}$. The modulated transmit symbol vector $t_{m,i}$ for D2D cooperation may be utilized for symbol transmission for device w alone, device x only, or both, depending on the resource allocation. In this scenario, resource allocation implies a time-sharing method. The time slot can only be used for symbol transmission for device w if $t_{m,i}$ is dedicated to that device; otherwise, it can be used for device x or, in rare circumstances, for both devices in the m -th cluster. In this chapter, since NOMA is used, superposition coding (SC) is used at the transmitting end, and each D2D pair uses the SIC technique to decode its own messages at the receiver end.

In this work, we take into consideration that each cluster holds two D2D pairs which reduces the computational complexity. In the case of a downlink transmission from BS to users, licensed spectrums are being used, and for D2D transmission, all the devices use an unlicensed bandwidth spectrum. The D2D communication is for short-range communication relative to downlink communication from BS to users.

It is assumed that $X = [x_1, x_2, \dots, x_M]^T \in \mathbb{C}^{M \times M}$ is the broadcast data vector, where $x_m = \sum_{l=1}^{|d_l|} p_{m,l} t_{m,l}$ is the data stream for m -cluster in which $p_{m,l}$ and $t_{m,l}$ are the transmit power and modulated symbol, individually for the l -th D2D pair in the m -th cluster. where

$t_{m,l} \in \mathbb{C}^{M \times 1}$, $l \in \{\{i\}, \{j\}\}$ and $m \in \{1, 2, \dots, M\}$.

$$t_{m,l} = \begin{bmatrix} t_{1,i} + t_{1,j} \\ \vdots \\ t_{M,i} + t_{M,j} \end{bmatrix} \quad (4.1)$$

Let's further assume that a beamforming precoding matrix B modulates the data vector, and denotes the $M \times M$. The channel response matrix for device k in m -th cluster denoted as $H_{m,k} = [h_{mk,1}, h_{mk,2}, \dots, h_{mk,N}]^T$ (BS to 1st antenna of device k in the m th cluster). The dimension of $H_{m,k}$ is $N \times M$. Therefore, the transmitted superposed signal $\tilde{x} = BX$, where $\tilde{x} \in \mathbb{C}^{M \times 1}$.

The channel matrix provides information about the D2D link between device w and device x denoted as $G_{wx} = [g_{wx,1}, g_{wx,2}, \dots, g_{wx,N}]$. In D2D connections, the channel reciprocity is maintained as $G_{w,x} = G_{x,w}$. This essay makes the supposition that the BS has the ideal CSI on the channels. The channel matrix provides information about the D2D link between device w and device x denoted as

The decoding scaling weight factor, $ds_{m,l}$, is what multiplies the received signal before it is decoded at the l -th pair in the m -th cluster. Because of this, the signal that was received for the l th pair in the m th cluster is expressed as follows:

$$y_{m,l} = ds_{m,l} [\tilde{h}_{m,l} BX + n_{m,l}] \quad (4.2)$$

where, $l \in \{\{i\}, \{j\}\}$, $|\tilde{h}_{m,l}|^2$ = channel gain of l -th D2D pair and channel gains are expressed as $|\tilde{h}_{m,1}|^2 \geq |\tilde{h}_{m,2}|^2 \geq \dots \geq |\tilde{h}_{m,d_l}|^2$. The effective channel gain $\tilde{h}_{m,l}$ for the l -th D2D pair in the m -th cluster represents the composite downlink channel gain from the BS to the pair. While G models the D2D channel between paired devices (e.g., w and x) for local communication within a cluster (Algorithm 2). $\tilde{h}_{m,l}$ governs the BS-to-pair signal strength (impacting $SINR_{m,l}$ in Equation 4.4). $\tilde{h}_{m,l}$ is ordered by magnitude ($|\tilde{h}_{m,1}|^2 \geq |\tilde{h}_{m,2}|^2 \geq \dots$) to enforce NOMA power allocation, while G is used for D2D pair formation and local communication. $n_{m,l} \in \mathbb{C}$ represents circularly symmetric complex Gaussian noise with variance σ^2 . However, if b_m denotes the n -th column of the BF

precoding matrix B , then (2) can be expressed as follows:

$$y_{m,l} = ds_{m,l}\tilde{h}_{m,l}b_m p_{m,l}t_{m,l} + ds_{m,l}\tilde{h}_{m,l}b_m \sum_{j=1}^{|d_l|-1} p_{m,j}t_{m,j} + ds_{m,l}\tilde{h}_{m,l} \sum_{i=1, i \neq m}^M b_i x_i + ds_{m,l}n_{m,l} \quad (4.3)$$

The received signal-to-intra-cell interference-plus-noise ratio (SINR) for the l th pair of the m th cluster is as follows:

$$SINR_{m,l} = \frac{\left| \left(ds_{m,l}\tilde{h}_{m,l} \right) b_m \right|^2 p_{m,l}}{I_1 + I_2 + ds_{m,l}n_{m,l}} \quad (4.4)$$

where I_1 implies Intra-cluster interference, I_2 implies Inter-cluster interference and $ds_{m,l}n_{m,l}$ implies Noise. I_1 can be expressed as follows:

$$I_1 = \left| \left(ds_{m,l}\tilde{h}_{m,l} \right) b_m \right|^2 \sum_{j=1}^{|d_l|-1} p_{m,j} \quad (4.5)$$

I_2 can be expressed as follows:

$$I_2 = \sum_{i=1, i \neq m}^M \left| \left(ds_{m,l}\tilde{h}_{m,l} \right) b_i \right|^2 p_i \quad (4.6)$$

In the case of MIMO-NOMA-D2D communication, Intra-cluster interference can be expressed as $I_1 = I_{m,l}(1) + I_{m,l}(2)$ which is the n -th pair's interference with the l -th pair on the same subchannel at a distance of d_{max} , and because the pair has larger channel gains than the l -th pair, respectively. where

$$I_{m,l}(1) = \sum_{l' \in D, l' \neq l} p_{m,l'} |h_{m,l'}|^2 \quad (4.7)$$

and

$$I_{m,l}(2) = |h_{m,l}|^2 \sum_{j \in \{d_k | h_{m,k} > h_{m,l}\}} p_{m,k} \quad (4.8)$$

In this study, the number of D2D pairings in each cluster is fixed. Also, the distance between two different pairs also considered as the constraint during pair formation to minimize intra-cluster interference. Thus, we are able to eliminate $I_{m,l}(1)$ interference level which proves that our proposed scheme outperforms the conventional network. In Algorithm

1, we determine the D2D communication in the MIMO-NOMA network. The D2D pair formation technique using correlated channel gain is depicted in Algorithm 2.

ALGORITHM 3: D2D Communication in the Downlink MIMO-NOMA Network

Input: Number of D2D devices: k

Number of transmit antennas or clusters: M

Number of receive antennas of each device: N

Channel response matrix: H

Number of clusters and cluster-heads: M

- 1 **Initialization:** *All the higher channel gain devices are the cluster-head (within 150 metres of BS).*
 - 2 *Generate locations of each device randomly (minimum distance from BS = 200 metres).*
 - 3 *The total transmit power from BS is equally divided into all clusters.*
 - 4 *Taking an average of all channel gains of all antennas for each device in the network :*

$$h_{i,1}, h_{i,2}, \dots, h_{i,N}, h_i = \text{Average channel gain of } i\text{-th device, } i \in \{1, 2, \dots, k\},$$

$$n \in \{1, 2, \dots, N\}.$$
 - 5 *Device locations are sorted by channel gain in ascending order $h_1 \geq h_2 \geq \dots \geq h_k$, $h_i = i\text{-th}$ device's channel gain.*
 - 6 **Select set $A = \{1, 2, \dots, M\}$ of relay nodes for pair d_1 (closest to BS) depending on the channel gain, the higher channel gain devices are set as a relay device,**

$$h_1 \geq h_2 \geq \dots \geq h_M, h_i = i\text{-th device's channel gain}.$$
 - 7 **Include the second set of relay nodes for pair d_2 (far from BS),**

$$B = \{M + 1, M + 2, \dots, 2M\}. R_{i,j} = \text{correlation coefficient between } h_i \text{ and } h_j$$
 - 8 **for $t \leftarrow 1$ to M do**
 - 9 **for $s \leftarrow M + 1$ to $2M$ do**
 - 10 **if $R_{t,s} > R_{t,r} \geq 0.5, \forall r \neq s \in B$ then**
 - 11 add s -th device into t -th cluster
 - 12 update $A \leftarrow A - \{t\}, B \leftarrow B - \{s\}$
-

In Algorithm 3, complex channel coefficients h_i (with magnitude and phase) are re-ordered for clustering using a three-step magnitude-based approach: First, the average magnitude per device $|h_i| = \frac{1}{N} \sum_{n=1}^N |h_{i,n}|$ is computed across all N receive antennas. Second, devices are sorted in descending order of these magnitudes ($|h_1| \geq |h_2| \geq \dots \geq |h_k|$). Finally, cluster heads are selected from the top- M devices with strongest channels. This magnitude-focused method is justified because (1) phase information is irrelevant for NOMA power allocation, (2) it prioritizes devices with the strongest channels as relays, and (3) aligns with prac-

4.2. SYSTEM MODEL

tical implementations where Channel Quality Indicator (CQI) feedback typically uses magnitude measurements. Notably, while the sorting uses magnitudes, the channel correlation calculation $R_{i,j} = \frac{|\mathbf{h}_i^H \mathbf{h}_j|}{\|\mathbf{h}_i\| \|\mathbf{h}_j\|}$ retains the complex inner product to properly assess spatial relationships between devices, ensuring optimal cluster formation despite the scalar-based sorting.

ALGORITHM 4: D2D Pair formation

Input: Number of devices: k

Number of transmit antennas or clusters: M

Number of receive antennas of each device: N

Channel response matrix: H

Number of relay devices: L

Relay set: $C = A + B$, $A = \{1, 2, \dots, M\}$ and $B = \{M + 1, M + 2, \dots, 2M\}$

Non-relay set: $D = \{L + 1, L + 2, \dots, k\}$

Number of D2D pairs in each cluster: 2

Maximum distance between two D2D pairs = 20 metre.

- 1 **Initialization:** *Generate locations of each D2D device randomly.*
- 2 *Set D2D pair count d to zero.*
- 3 **for** $p \leftarrow 1$ **to** number of relay devices: L **do**
- 4 **for** $q \leftarrow L + 1$ **to** k **do**
- 5 Measure the distance between devices: $\sqrt{dist} = (x_p - x_q)^2 + (y_p - y_q)^2$
- 6 **if** $dist \leq 20$ **AND** $d \leq 2$ **then**
- 7 Device p and device q will form pair.
- 8 Set D2D count $\leftarrow d + 1$

ALGORITHM 5: Computing performance indicator data

Input: Number of clusters: M

- 1 **for** $i \leftarrow 1$ **to** M **do**
 - 2 **for** $j \leftarrow 1$ **to** d_i
 - 3 Compute t_1 and t_2 from Equation (4.22) and (4.24)
 - 4 Compute R
 - 5 Compute SE
 - 6 Compute EE
-

ALGORITHM 6: MIMO-NOMA-D2D with Multiple Interference Cancellation

Input: Number of BS antennas M , devices k , receive antennas N , channel matrix H , total

power P_T

Output: solution set \mathcal{P} with optimized SE and EE

```

1 // Network Initialization
2 Randomly deploy devices with minimum 200m from BS, cluster heads within 150m
3 Divide  $P_T$  equally among  $M$  clusters
4 Compute average channel gains  $h_i = \frac{1}{N} \sum_{n=1}^N h_{i,n}$  for all devices
5 // D2D Pair Formation
6 for each relay device  $p \in \{1, \dots, M\}$  do
7     if  $\text{dist}(p, q) \leq 20m$  AND pair count  $\leq 2$  then
8         Form D2D pair  $(p, q)$  with correlation  $R_{p,q} \geq 0.2$  AND  $R_{p,q} \leq 0.8$ 
9     end
10 end
11 Transmission Phase
12 Construct broadcast vector  $X = [x_1, \dots, x_M]^T$  where  $x_m = \sum_{l=1}^{|d_l|} p_{m,l} t_{m,l}$ 
13 Apply beamforming precoding:  $\tilde{x} = BX$ 
14 Transmit superposed signal to each cluster
15 Receiver Processing with MIC
16 for each cluster  $m \in \{1, \dots, M\}$  do
17     Compute SINR:  $\text{SINR}_{m,l} = \frac{|ds_{m,l} \tilde{h}_{m,l} b_m|^2 p_{m,l}}{I_1 + I_2 + \sigma^2}$ 
18     Multiple Interference Cancellation
19     For user  $d_1$  (stronger channel):
20         Detect  $t_1 = \langle \frac{y_k - \sum_{l=1}^{|d_l|-1} \sqrt{p_l} t_l}{\sqrt{p_1}} \rangle$ 
21     For user  $d_2$  (weaker channel):
22         Cancel  $d_1$ 's signal:  $y_2 = y_k - \sqrt{p_1} t_1$ 
23         Detect  $t_2 = \lfloor y_2 / \sqrt{p_2} \rfloor$  (no decoder needed)
24     Eliminate  $I_{m,l}(2)$  interference through MIC
25 end
26 // Performance Metrics Calculation
27 Compute sum rate:  $R_T = \sum_{m=1}^M \sum_{l=1}^{|d_l|} \log_2(1 + \text{SINR}_{m,l})$ 
28 Compute energy efficiency:  $EE_T = \max \sum_{m=1}^M \frac{R_m}{\zeta \sum p_{m,l} + p_{ckt}}$ 
29 Update solution set  $\mathcal{P}$  with optimized SE and EE
30 return  $\mathcal{P}$ 

```

4.3 PROBLEM FORMULATION

This section initially introduces the computation of the MIMO-NOMA-D2D network's spectral efficiency (SE) and energy efficiency (EE).

4.3.1 Sum Rate

The data rate of the l -th D2D pair may be given as follows using the formulas derived for SINR at the receiver of the l -th D2D pair, as in (4) of the m -th cluster:

$$R_{m,l} = \log_2(1 + \text{SINR}_{m,l}) \quad (4.9)$$

Therefore, the total sum rate achievable for all M clusters in the system can be expressed as:

$$R_T = \sum_{m=1}^M \sum_{l=1}^{|d_l|} R_{m,l} \quad (4.10)$$

4.3.2 Energy Efficiency

Through efficient resource management and improved EE, the goal of an energy-efficient network is accomplished. As a result, a MIMO-NOMA-D2D network performs EE calculations as the sum of the proportion of the total sum rate achieved from a cluster to the total power assigned to the cluster. In this chapter, we assign an equal power allocation to all clusters. Inside each cluster, the power allocation assignments are different, depending on the channel gain for each device. The sum of the l -th pair's transmission power and circuit power consumption is used to determine how much power it uses overall. The formula for the overall amount of power used by all pairings in a cluster is:

$$p_m = \zeta \sum_{l=1}^{|d_l|} p_{m,l} + p_{ckt,l} \quad (4.11)$$

where ζ denotes the drain efficiency of the amplifier, $p_{ckt,l}$ implies the total amount of power used by the regenerator, decoder, and detector, and the total power from BS is denoted as P_T :

$$P_T = \sum_{m=1}^M p_m \quad (4.12)$$

The EE maximization problem of the network can be formulated as:

$$EE_T = \max \left(\sum_{m=1}^M \frac{\sum_{l=1}^{|d_l|} R_{m,l}}{p_m} \right) \quad (4.13)$$

$$C1 : p_m \leq P_T \quad (4.14)$$

$$C2 : \sum_{l=1}^{|d_l|} p_{m,l} \leq p_m \quad (4.15)$$

4.3.3 Multiple Interference Cancellation

The pairs in each cluster get the super-positioned signal from the cellular user. The signal that the m -th cluster receives at each of the D2D pairings is as stated in (2). The suggested approach focuses on extracting the information of pairs with the maximum channel gain from the received signal because the n -th pair experiences interference from other pairs for $|h_{1,m}|^2 \geq |h_{2,m}|^2 \geq \dots \geq |h_{n,m}|^2$. As a result, the interference is removed.

The matrix form of the signal received at the receiving end is thus represented as:

$$y_{m,l} = ds_{m,l} \left[\tilde{H}_{m,l} B X' + n_{m,l} \right] \quad (4.16)$$

where

$$X' = \begin{bmatrix} x_1 & x_1 - p_{1,1}t_{1,1} & \dots & \sum_{l=1}^{|d_l|-1} p_{1,l}t_{1,l} \\ x_2 & x_2 - p_{2,1}t_{2,1} & \dots & \sum_{l=1}^{|d_l|-1} p_{2,l}t_{2,l} \\ \vdots & \vdots & \vdots & \vdots \\ x_M & x_M - p_{M,1}t_{M,1} & \dots & \sum_{l=1}^{|d_l|-1} p_{M,l}t_{M,l} \end{bmatrix} \quad (4.17)$$

$$y_{m,l} = \begin{bmatrix} y_{1,1} & y_{1,2} & \dots & y_{1,|d_l|} \\ y_{2,1} & y_{2,2} & \dots & y_{2,|d_l|} \\ \vdots & \vdots & \vdots & \vdots \\ y_{M,1} & y_{M,2} & \dots & y_{M,|d_l|} \end{bmatrix} \quad (4.18)$$

$$\tilde{H}_{m,l} = \begin{bmatrix} h_{1,1} & h_{1,2} & \dots & h_{1,|d_l|} \\ h_{2,1} & h_{2,2} & \dots & h_{2,|d_l|} \\ \vdots & \vdots & \vdots & \vdots \\ h_{M,1} & h_{M,2} & \dots & h_{M,|d_l|} \end{bmatrix} \quad (4.19)$$

4.3. PROBLEM FORMULATION

$$n_{m,l} = \begin{bmatrix} n_{1,1} & n_{1,2} & \dots & n_{1,|d_l|} \\ n_{2,1} & n_{2,2} & \dots & n_{2,|d_l|} \\ \vdots & \vdots & \vdots & \vdots \\ n_{M,1} & n_{M,2} & \dots & n_{M,|d_l|} \end{bmatrix} \quad (4.20)$$

Equation (4.16) represents the received signal after Multiple Interference Cancellation (MIC), derived by modifying the original signal from Eq. (4.2) through three key steps: First, the interference-cancelled signal matrix X' is constructed by subtracting intra-cluster interference components from the original signal X , where each column of X' progressively removes more interference terms (Column 1: original signal; Column 2: minus the first pair's component; etc.). Second, the scalar effective channel gain $\tilde{h}_{m,l}$ is expanded to a matrix $\tilde{H}_{m,l}$ to handle multiple signal components, with dimensions matching the number of antennas (M) and pairs ($|d_l|$). Finally, these components are combined with noise to yield the MIC-processed signal $y_{m,l} = ds_{m,l}\tilde{H}_{m,l}BX' + ds_{m,l}n_{m,l}$. Crucially, this approach proactively removes intra-cluster interference in the signal domain (via X') rather than relying on successive cancellation at the receiver, enabling far users (d_2) to decode directly without SIC as shown by $t_2 = \lfloor y_2/\sqrt{p_2} \rfloor$, while maintaining the beamforming gain through B and the channel adaptation through $\tilde{H}_{m,l}$.

Since each device has N antennas at the receiving end, at device $k \in \{w, x, y, z\}$, the corresponding received signal vector is represented as $y_k = [y_{k,1}, y_{k,2}, \dots, y_{k,N}]^T$, where $y_{k,n}$ represents the signal received at k -th device's n -th ($n = 1, 2, \dots, N$) receive antenna and $h_{k,n}^*$ represents the channel between k -th device's send antenna and n -th receive antenna. The received signal at device k is denoted as:

$$y_k = \frac{\sum_{n=1}^N h_{k,n}^* y_{k,n}}{\sum_{n=1}^N |h_{k,n}^*|^2} \quad (4.21)$$

where $k \in \{1, 2\}$ are the relay devices. The signal detected at the closest pair of BS which is here d_1 can present as:

$$t_1 = \left\langle \frac{y_k - \sum_{l=1}^{|d_l|-1} \sqrt{p_l} t_l}{\sqrt{p_1}} \right\rangle \quad (4.22)$$

Here, $\langle \cdot \rangle$ denotes the detection of the symbol as well as its demodulation and decoding. The $\langle \cdot \rangle$ operator in Equation (4.22) represents a joint demodulation-decoding process for

the near user (d_1) in NOMA systems, defined as $\langle x \rangle \triangleq \text{Decode}(\text{Demodulate}(x))$. It first normalizes the interference-cancelled signal $x = (y_k - \sum_{l=1}^{|d_l|-1} \sqrt{p_l} t_l) / \sqrt{p_1}$, then performs QAM demapping to convert the analog signal to digital symbols, followed by error-correction decoding (e.g., LDPC/Polar codes) to recover the transmitted bits \hat{t}_1 . Unlike the far user's $\lfloor \cdot \rfloor$ operator (Eq. 4.24) that only demodulates, $\langle \cdot \rangle$ is nonlinear (combining thresholding and algebraic operations) and operates across domains (complex baseband \rightarrow bitstream). This two-stage process is implemented physically as: demodulation (e.g., 16-QAM constellation mapping) \rightarrow decoding (e.g., LDPC syndrome checking), is critical for SIC at near users where full decoding precedes interference cancellation.

The signal received at d_2 is given by the first pair's signal, which is canceled after reception.

$$y_2 = y_k - \sqrt{p_1} t_1 \quad (4.23)$$

The signal at d_2 (farthest pair from BS) is the demodulated signal because SIC receivers do not decode the signal at the second pair. Thus d_2 is represented as:

$$t_2 = \left\lfloor \frac{y_2}{\sqrt{p_2}} \right\rfloor \quad (4.24)$$

The last pair only receives its own signal with MIC; therefore, in this case, $\lfloor \cdot \rfloor$ stands for symbol demodulation. Decoders and regenerators are no longer necessary because of this. This also signifies $I_{m,l}(2)$ has been eliminated from the received signal because the decoding mechanism eliminates higher gain pairs to interfere with the lower gain pairs [47]. Elimination of $I_{m,l}(2)$ significantly improves the SINR performance. It also reduces the power consumption of the decoder and regenerator circuits.

4.3.4 Beamformer Design and Performance Analysis

In MIMO-NOMA-D2D systems, beamformers are designed by optimizing antenna weights to jointly maximize spectral efficiency (SE), energy efficiency (EE), and interference management through various approaches. Heuristic methods include MRT (maximizing signal power but ignoring interference), ZF (suppressing interference while amplifying noise at low SNR), and RZF which balances these trade-offs via regularization. Optimality is verified by benchmarking against theoretical bounds like DPC or weighted MMSE to quantify

performance gaps, while respecting system constraints such as power budgets ($\|\mathbf{W}\|_F^2 \leq P_{\max}$) and D2D interference thresholds ($\|\mathbf{w}_k^H \mathbf{g}_j\|^2 \leq \epsilon$). For dynamic environments, adaptive optimization techniques like reinforcement learning further refine beamformer selection in real-time to minimize optimality gaps and maintain robust performance across varying channel conditions.

4.4 Simulations Results and Discussion

In this section, we show simulation results that show how the proposed MIMO-NOMA-D2D system improves spectrum and energy efficiency. We also compare these results to those of other MIMO-OMA and MIMO-NOMA networks. The relay and non-relay devices are dispersed at random throughout the cellular network. All cluster heads are believed to be within 150 metres of the BS. The 400-meter cell radius is commonly accepted, and it is presumed that the perfect CSI is available. Also, all the devices have been scattered a minimum of 200 metres from BS and formed NOMA networks with a parameter restriction of $R_{i,j} \geq 0.5$ mentioned in Algorithm 1, i.e., device i , and device j , the correlation coefficient should be greater or equal to 0.5. All the transmissions transpire in two phases. Data is sent from BS to the relay device during the first phase. In a specific cluster, the relay device transmits data to the non-relay devices in the network during the second phase of transmission. In order for all of the clusters to utilise full spectrum resources, it is also anticipated that the number of BS transmit antennas will be equal to the number of MIMO-NOMA-D2D clusters. We consider all MIMO-NOMA-D2D cluster sizes to be the same for a given simulation. In this work, MATLAB simulations are used to look into the effectiveness of the suggested MIMO-NOMA-D2D strategy. Comparisons are made between the performance of the proposed system and that of conventional MIMO-NOMA and MIMO-OMA. The spectral efficiency of the MIMO-NOMA system greatly increases with increasing transmit power and when strongly correlated users are grouped, as shown in Figure 4.2, Figure 4.3, and Figure 4.4. Based on Equation (4.10), Figure 4.2, Figure 4.3, and Figure 4.4 analyze the overall sum rate performance for various numbers of clusters. The image makes it obvious that the MIMO-OMA network will have the lowest attainable sum rate. The experiment takes place in three different transmit power scenarios from the BS. It is clear that increasing the transmit power also improves the overall spectral efficiency

of the whole network.

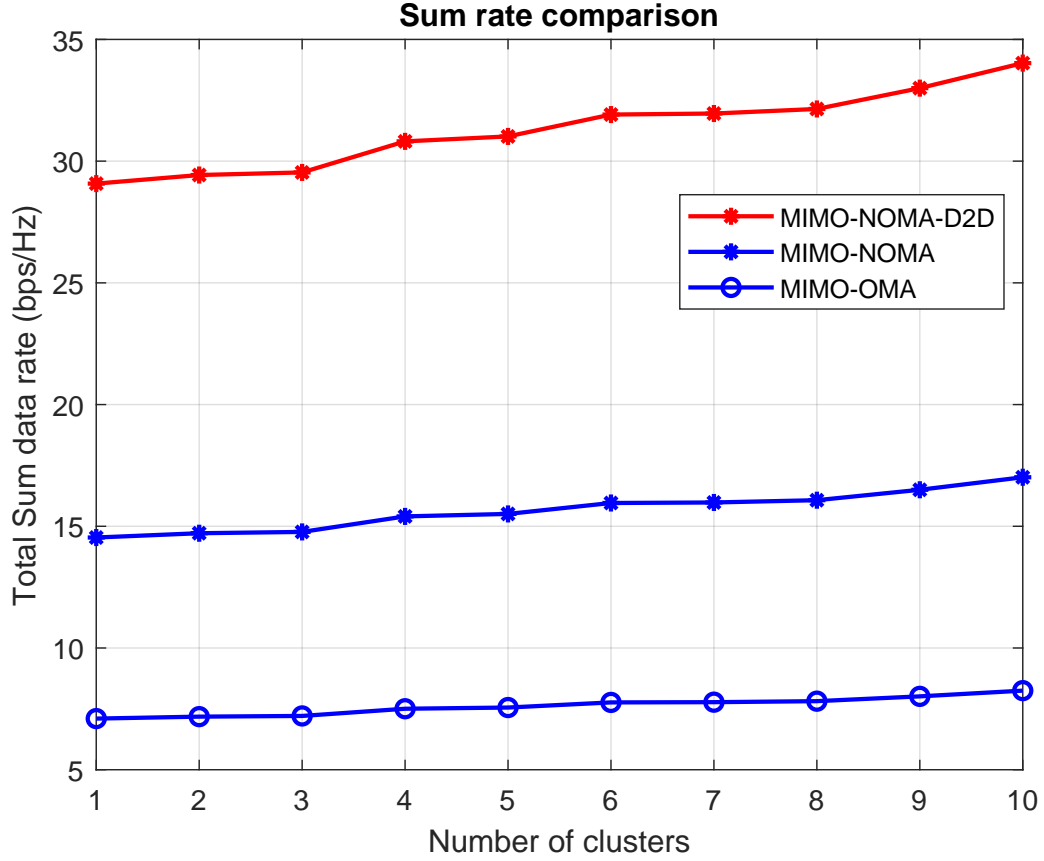


Figure 4.2: Spectral efficiency comparison under transmit power Power 30 dBm

Fig 4.5, Fig 4.6, and Fig 4.7 shows the improvement of EE as the number of clusters, which is equivalent to the number of transmit antennas, grows. The graph shows that compared to MIMO-NOMA and MIMO-OMA networks, MIMO-NOMA-D2D networks are much more energy-efficient. The experimental setup for calculating energy efficiency takes a transmit power = 30 dBm for different antenna configurations. Also, our pivotal attention is on cell-centered devices since all the devices are located at a significant distance from BS. The value of circuit power decreases due to the power savings realized with the suggested approach's regenerator circuit, as mentioned in Equations (4.22) and (4.24). The EE benefits from this in a favorable way. Figure 4.8 illustrates the spectral efficiency of MIMO-OMA, MIMO-NOMA, and MIMO-NOMA-D2D networks at various transmit powers. Energy efficiency comparison in different antenna setups is shown in Figure 4.9.

In Figure 4.10, the SE for all curves is very close for the first few clusters but diverges

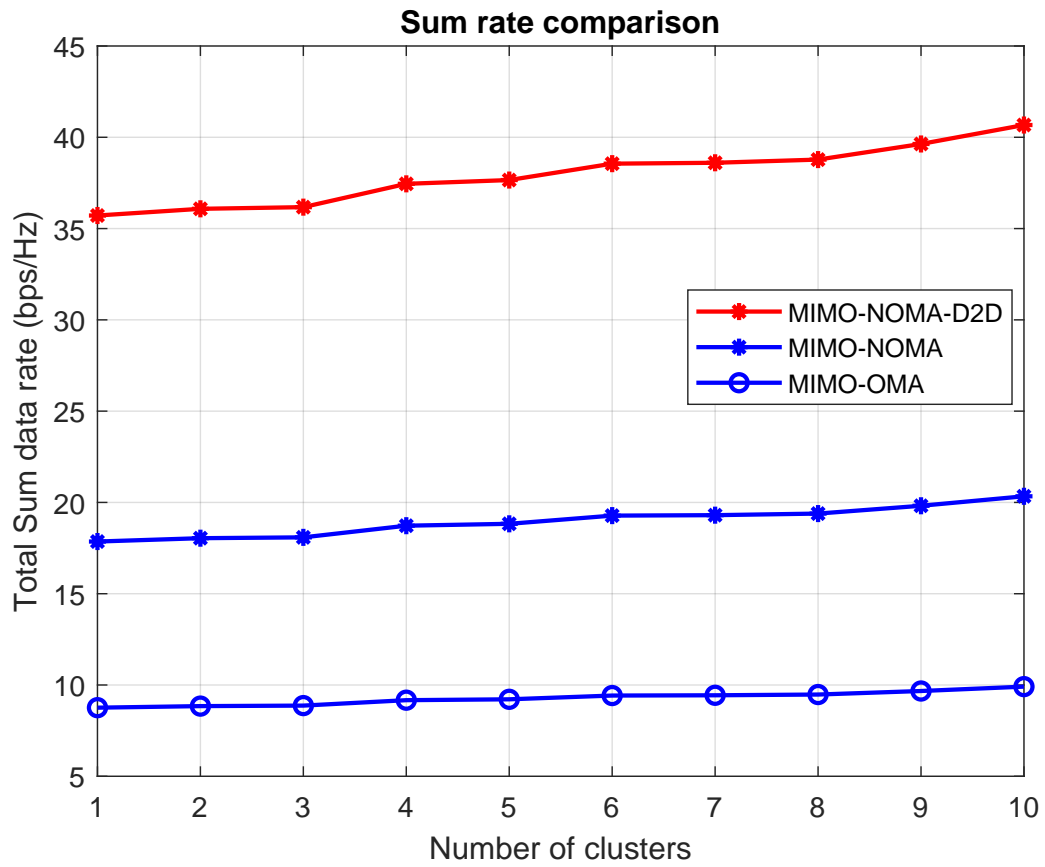


Figure 4.3: Spectral efficiency comparison under transmit power Power 40 dBm

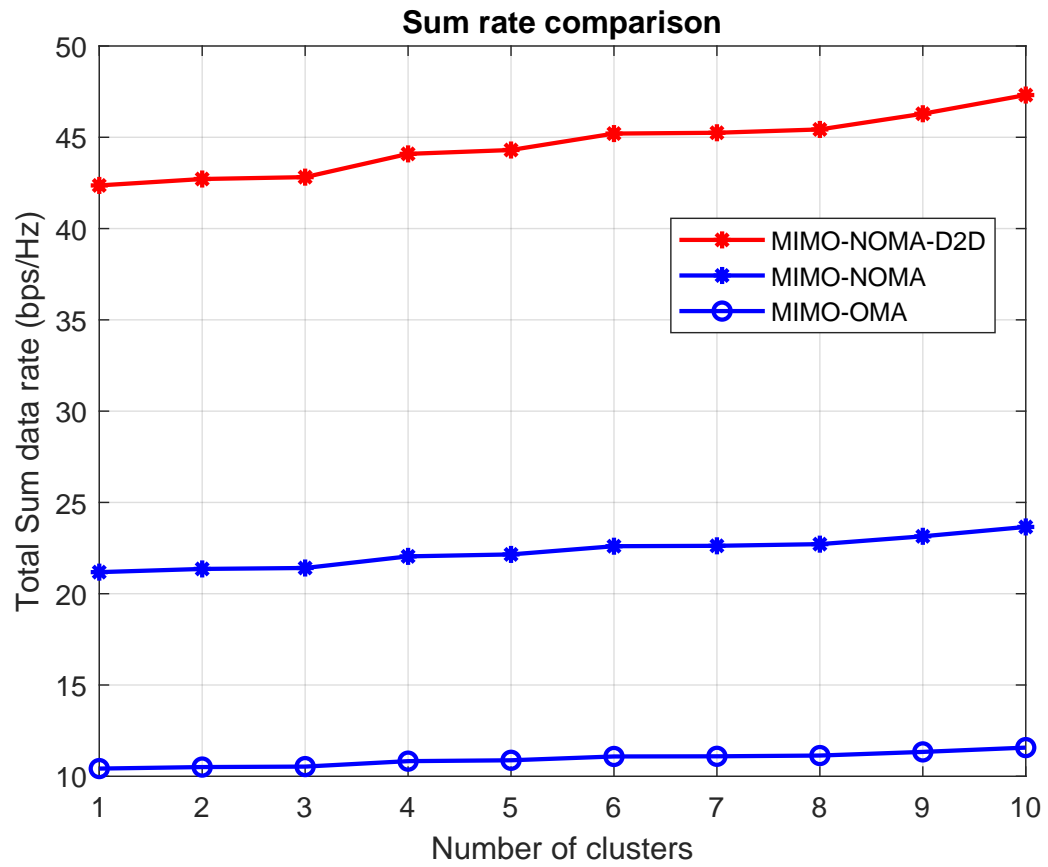


Figure 4.4: Spectral efficiency comparison under transmit power Power 50 dBm

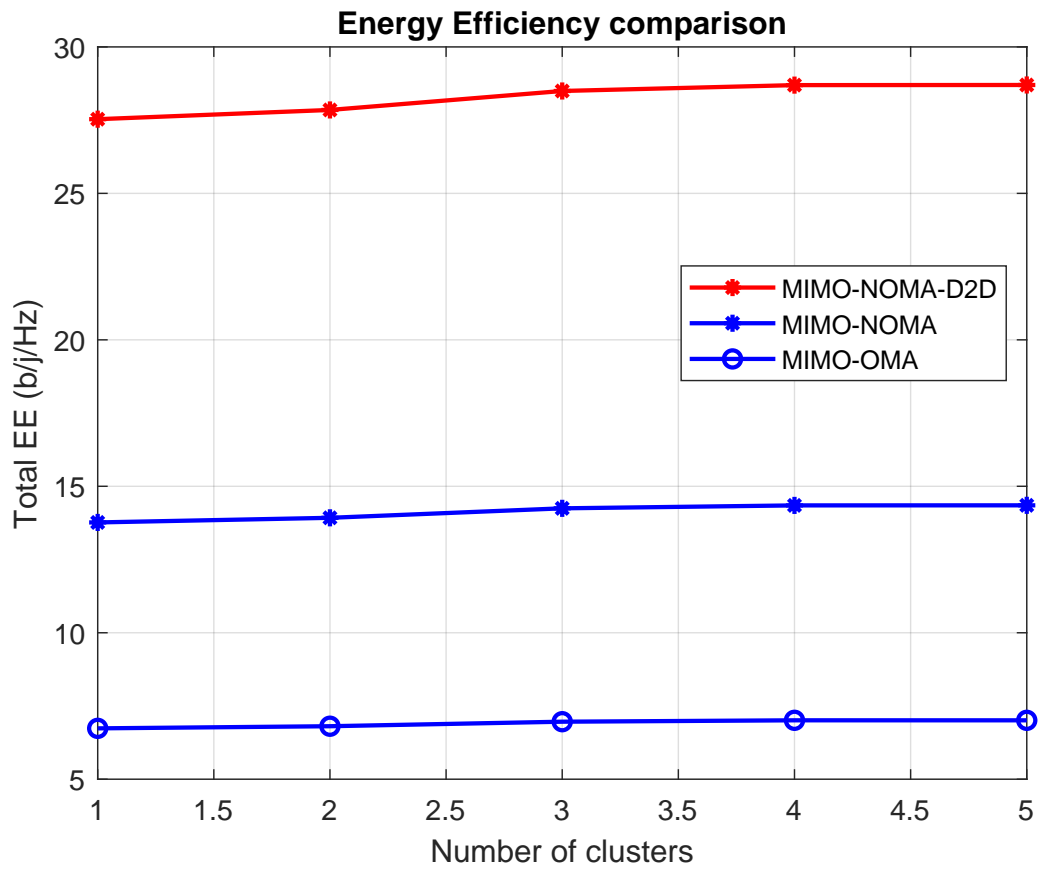


Figure 4.5: Energy efficiency comparison under different antenna setup, Antenna = 5

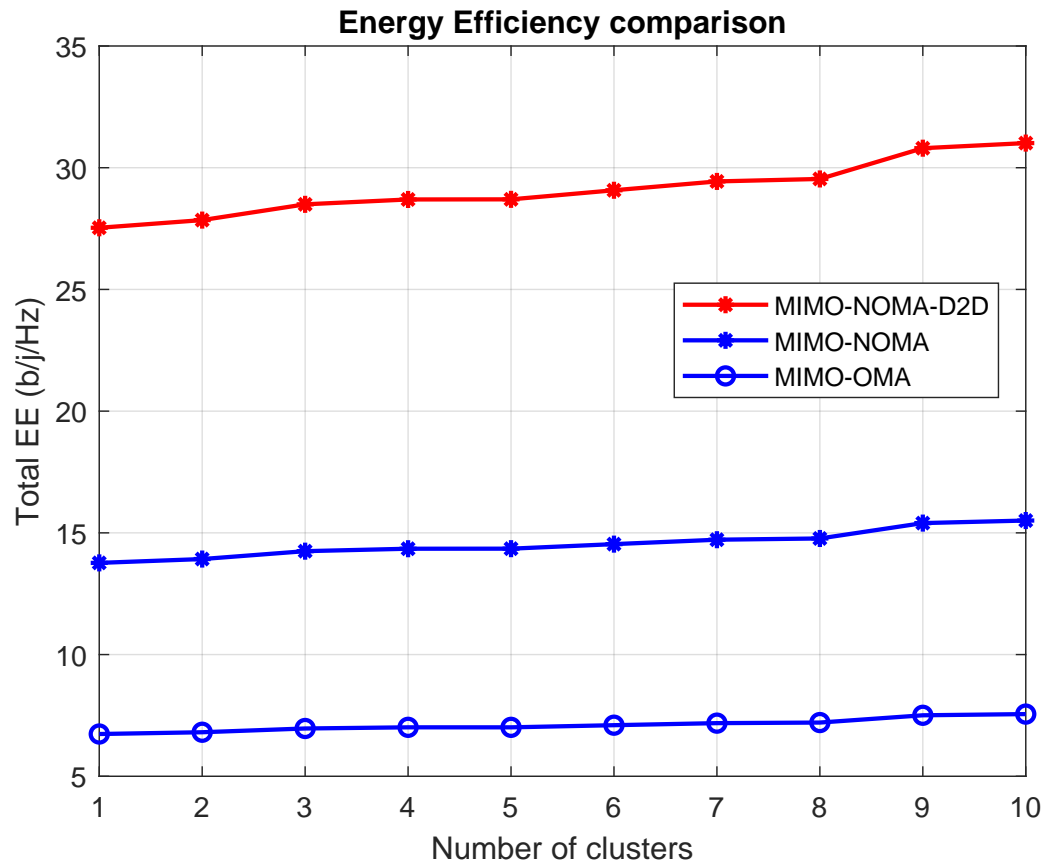


Figure 4.6: Energy efficiency comparison under different antenna setup, Antenna = 10

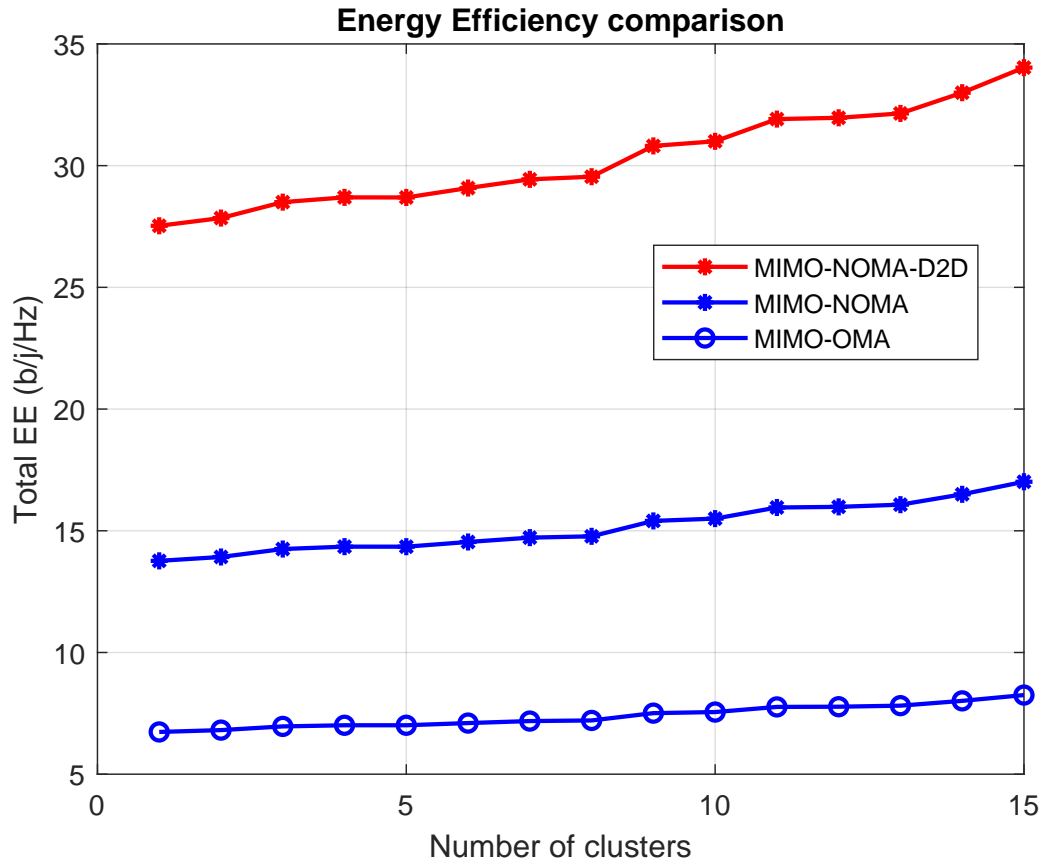


Figure 4.7: Energy efficiency comparison under different antenna setup, Antenna = 15

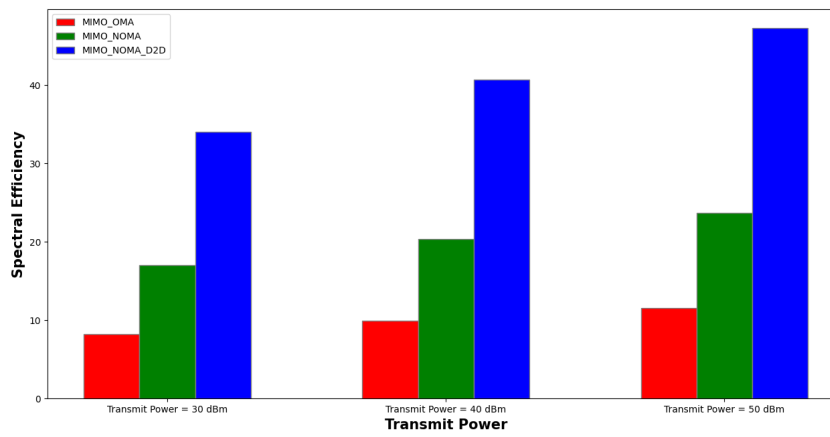


Figure 4.8: Spectral efficiency comparison

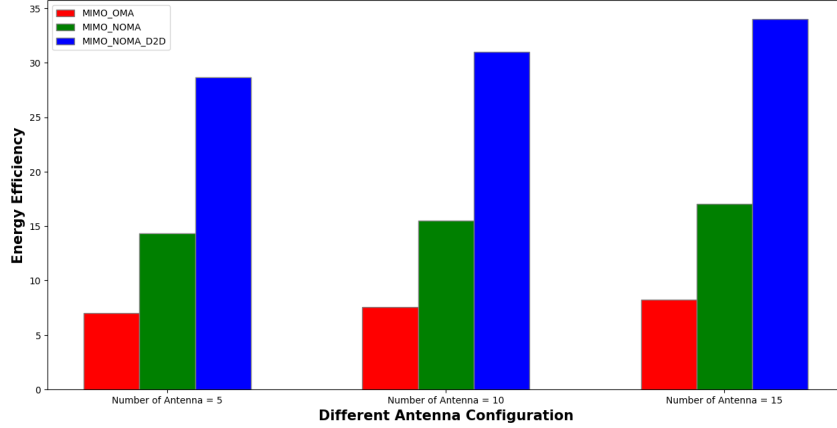


Figure 4.9: Energy efficiency comparison

significantly afterward due to the interplay between signal power, interference, and correlation. For $M \leq 3$, the power per cluster is high, leading to strong signal power that dominates interference, making SE less sensitive to correlation. Additionally, with fewer clusters, interference is low, and the limited number of D2D pairs means the benefits of D2D communication (e.g., interference reduction and signal power enhancement) are not fully utilized, resulting in high and similar SE for all correlation coefficients. However, for $M \geq 4$, the power per cluster decreases, reducing signal power and making the system more sensitive to interference. With more clusters, interference increases, and the impact of correlation becomes significant: a higher correlation ('corr = 1.0') increases interference by making channels more similar, while a lower correlation ('corr = 0.2') reduces interference by making channels less similar. Although more D2D pairs can be formed for larger M , enhancing signal power and reducing interference, the benefits are more pronounced for lower correlation coefficients, as higher correlation counteracts these benefits by increasing interference. This explains that SE diverges from $M = 4$ onward, with lower correlation coefficients showing better SE due to reduced interference and higher correlation coefficients showing worse SE due to increased interference.

Figure 4.11 compares the SE of MIMO-NOMA and MIMO-NOMA-D2D systems across increasing channel correlation ($\rho = 0$ to 0.9), where MIMO-NOMA (blue curve) shows consistent degradation from ~ 7 to ~ 3.5 bps/Hz due to reduced spatial diversity, while MIMO-NOMA-D2D (red dashed curve) demonstrates significant improvement from ~ 4.5 to

4.4. SIMULATIONS RESULTS AND DISCUSSION

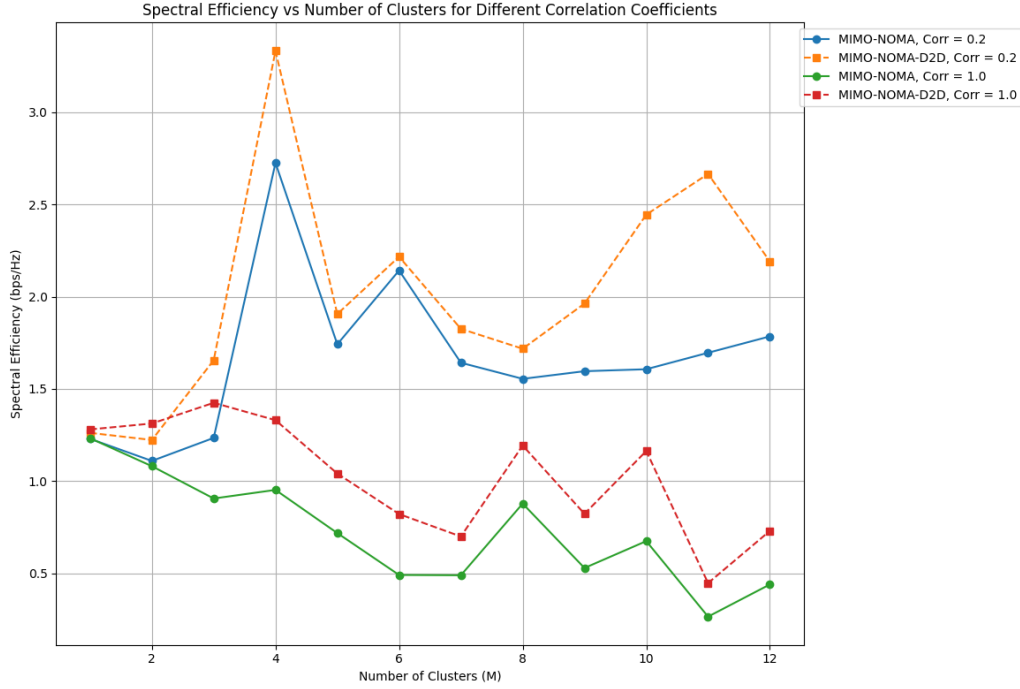


Figure 4.10: Analysis of Spectral Efficiency vs. Cluster Count

~ 9.5 bps/Hz by leveraging D2D links to mitigate correlation effects, eventually saturating beyond $\rho \approx 0.70$ – 0.80 as channel similarity limits further gains. The performance gap widens progressively from -2.5 to $+6$ bps/Hz, highlighting D2D's advantage in correlated environments, with a $\sim 2.7\times$ higher SE than NOMA at $\rho = 0.9$, though the saturation indicates diminishing returns at extreme correlation levels.

Figure 4.12 presents a performance comparison of beamforming schemes in a MIMO-NOMA-D2D system, analyzing three key metrics: Spectral Efficiency (Sum Rate in bps/Hz), which compares MRT, ZF, and the proposed RZF-MRT schemes to show variations in achievable rates; Energy Efficiency (EE in bps/Hz/W), highlighting power-efficiency trade-offs among the methods; and User SINR Distribution, displaying cumulative probability curves for SINR (dB) to demonstrate signal quality across users. The graph labels suggest the proposed RZF-MRT method may outperform conventional MRT and ZF by balancing spectral and energy efficiency while maintaining robust SINR performance.

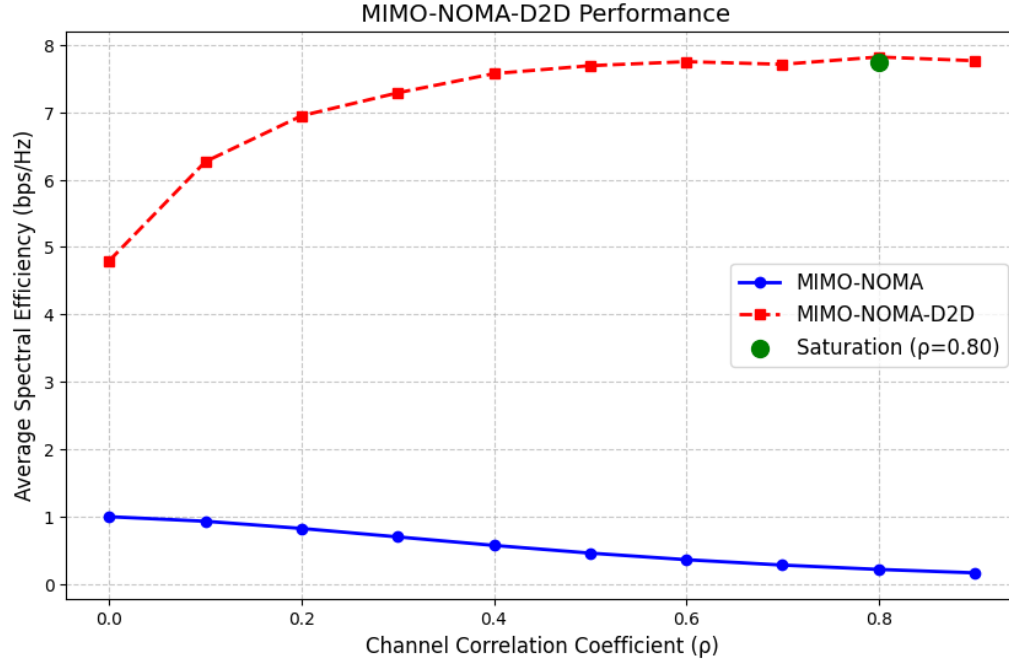


Figure 4.11: Spectral Efficiency vs. Correlation Coefficient

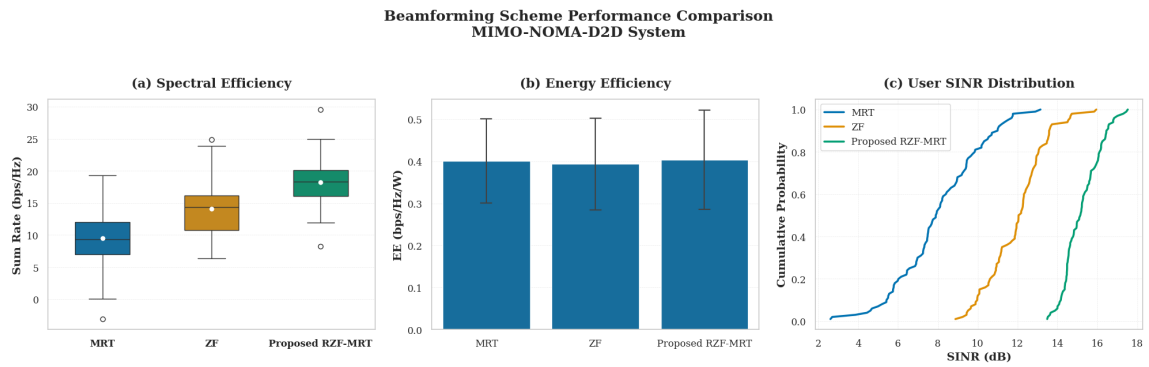


Figure 4.12: Beamforming Scheme Performance Comparison

4.5 Summary

A viable strategy for improving spectral and energy efficiency is using the MIC technique in MIMO-NOMA wireless cellular systems. This work focused on the downlink multiuser MIMO-NOMA, in which there are many more devices with receiving antennas than BS broadcast antennas in a cell. Each MIMO-NOMA cluster is supplied by a single MIMO beam that is orthogonal to the beams of the other clusters, and all users in a cluster are scheduled in accordance with NOMA. Most of the MIMO-NOMA solutions in the literature address inter-cluster interference; very little work has been done to address intra-cluster interference. Our work using the MIC technique and applying it to the MIMO-NOMA network significantly improves spectral and energy efficiency. Also, we have used the correlation coefficient to form the NOMA network inside each cluster, which significantly enhances the system's SE and EE performance. In Algorithm 1, we determine the relay nodes based on the channel state information of the device and work on two time stamps. The future direction of this study could be taken from the imperfect channel state information for further improvement.



Channel Estimation in NOMA Network

5.1 Introduction

The relentless pursuit of enhanced wireless communication capabilities has led to the development of advanced technologies such as NOMA. While NOMA offers significant advantages regarding spectral efficiency and user capacity, it relies heavily on accurate channel state information (CSI) for optimal performance. Conventional channel models might not fully capture the intricacies of real-world situations [48], leading to suboptimal system performance and potential service disruptions. This chapter addresses the critical challenge of accurate CSI estimation in NOMA networks by exploring the potential of utilizing a rich set of channel metrics, including reference signal received quality (RSRQ), signal-to-interference-plus-noise ratio (SINR), channel quality indicator (CQI), and partially decoded data (PDD). We aim to develop a robust and adaptive channel prediction model by incorporating these metrics and leveraging machine learning techniques. Our contributions focus on demonstrating the effectiveness of PDD as a valuable source of information for CSI estimation and investigating the impact of accurate channel prediction on NOMA system performance, particularly regarding handover management and resource allocation. By addressing the limitations of existing approaches, this research seeks to advance the state-of-the-art in NOMA channel estimation and contribute to developing more reliable and efficient wireless communication systems. Handover failures [49], [50] in NOMA networks happen when a user switches between cell towers and needs to pair with a new device in the next cell base station, as shown in Fig 5.1, but the handoff doesn't go through. These can result in dropped calls, slow data connections, and an unpleasant user experience. Predicting

CSI is essential to ensuring seamless handovers. The network is able to make educated judgments about when and to which cell tower to hand off a user by precisely forecasting future channel conditions. By doing this, the likelihood of a faulty handover and the feared "ping-pong" effect in which a user switches between two towers as a result of poor handover decisions is decreased. Essentially, smooth handovers and enhanced network performance are dependent on accurate CSI prediction.

5.2 System model

Within the scope of a downlink NOMA system, the analytical model consists of a base station of M antennas and N user equipment (UEs), each equipped with a single antenna. The Rayleigh fading channel model is used to describe the probabilistic behavior of wireless channels. The formulation of the received signal y is achieved by taking into account parameters such as channel matrices $h_i = \{h_1, h_2, \dots, h_N\}$, transmitted signals $x_i = \{x_1, x_2, \dots, x_N\}$, $\forall i \in \{1, 2, \dots, N\}$, and the additive white Gaussian noise n . The equation is denoted as:

$$y = \sum_{i=1}^N h_i x_i + n \quad (5.1)$$

We can rewrite Equation 5.1:

$$y_1 = \underbrace{h_1 x_1(j)}_{User1} + \sum_{i \neq 1}^N h_i x_i(j) + n_1(j) \quad (5.2)$$

where j indicates the time index and $j \in \{1, 2, \dots, J\}$. Equation (5.1) does not explicitly include beamforming. The equation represents the received signal as a sum of products of channel matrices (h_i) and transmitted signals (x_i), plus noise.

In this article, we have taken a new parameter, PDD, as a supplementary CSI metric. The analytical equation is expressed below. To understand this, we have taken two user scenarios in a NOMA network for easy understanding; user 1 indicated near user, and user 2 indicated far user from BS. Equation (5.3) is the received signal at User 1 after SIC, then the interference term reflect residual errors from imperfect SIC

$$y_{1,SIC} = h_1 \widetilde{x_1} + h_1 x_2 + n_1 \quad (5.3)$$

where $\widetilde{x}_1 = x_1 - \widehat{x}_1$ is the residual interference (PDD). PDD (\widetilde{x}_1) Represents undecoded residual interference. In the pre-SIC scenario, User 2 receives the original signal $y_2 = h_2x_1 + h_2x_2 + n_2$ where both x_1 and x_2 experience the same channel fading. During post-SIC processing, after imperfect decoding, the received signal at User 2 becomes:

$$y_{2,SIC} = h_2x_1 + h_2\widetilde{x}_2 + n_2 \quad (5.4)$$

where the partially decoded data (PDD) term $\widetilde{x}_2 = x_2 - \widehat{x}_2$ represents only the undecoded portion of x_2 and is generated locally during SIC. Crucially, all terms (including the residual interference) are properly scaled by h_2 , addressing the concern about fading consistency. Within the context of NOMA networks operating in the Rayleigh fading channel model, the need for efficient channel estimation to make the handover choice becomes apparent. As the number of UEs increases, the likelihood of user pairing based on handover decisions to improve the total sum rate also becomes difficult. In order to guarantee the resilience and effectiveness of these networks, it is important to cultivate channel status and different CSI parameters in the NOMA network. Fig 5.1 illustrates the concept of the NOMA handover. We have considered a two-cell scenario for ease of understanding. We have checked the condition for making a handover decision, $CSI_0 + PDD_0 < CSI_1 + PDD_1$, then the handover has been made, and user U_0^F will connect to the base station BS_1 .

Fig 5.2 illustrates the architecture of the NOMA transceiver using the RNN-LSTM model. The exclusive error information for channel status will be given after the demodulation state to the SIC/PIC module through the RNN-LSTM model to predict channel status. Channel prediction relies on exploiting information extracted after demodulation but before final data decoding. Following CP removal and FFT, demodulation recovers the symbols, potentially containing channel errors. These errors themselves become valuable clues. By analyzing these post-demodulation symbols with error patterns, techniques can estimate the channel's characteristics (fading, noise) and create CSI to predict future channel behavior and improve transmission reliability.

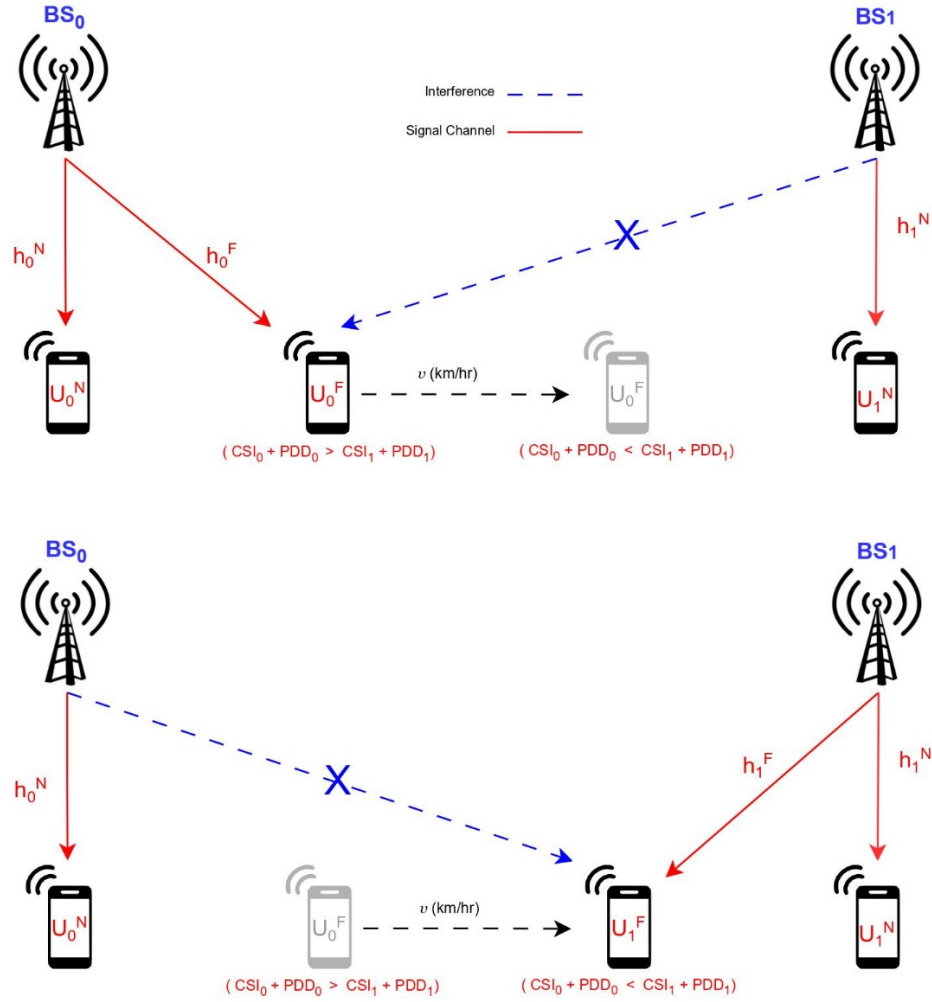


Figure 5.1: System model of NOMA-HO

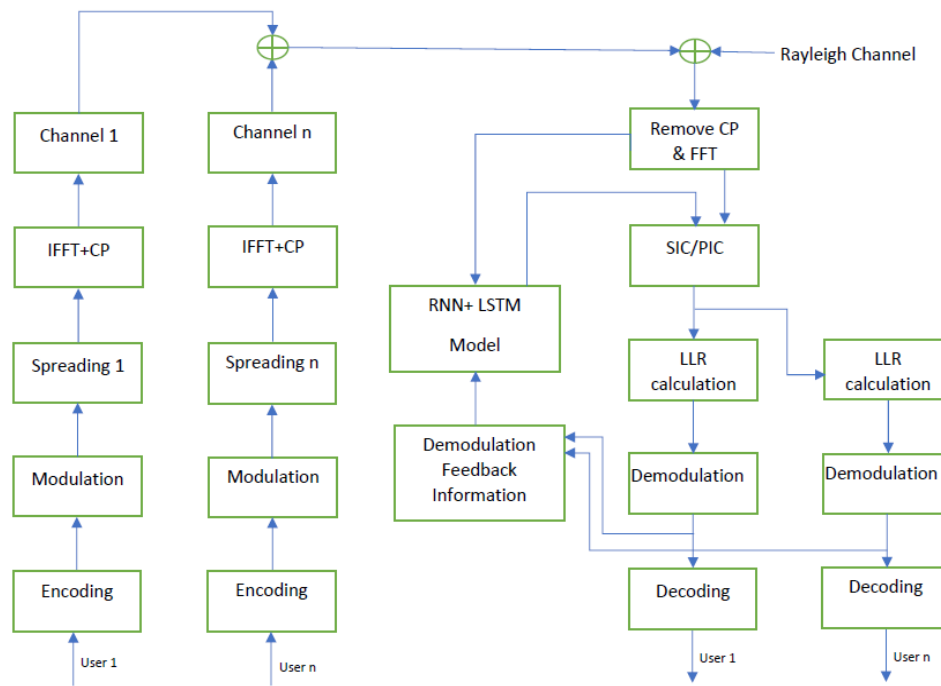


Figure 5.2: System model of NOMA transceiver with RNN-LSTM model

5.3 Proposed RNN-LSTM model

5.3.1 Data Preperation

Algorithm 1 outlines a transfer learning approach for predicting future channel state information in a wireless communication system using RNNs. It leverages a pre-trained RNN model, originally trained on a different but relevant task, to extract informative features from current and historical channel measurements CSI data like RSRQ, CQI, SNR, and PDD). These features are then fed into a newly trained regressor model to predict future values. This approach aims to improve channel prediction accuracy by utilizing the knowledge learned by the pre-trained RNN model and fine-tuning it for the specific task of channel state prediction. Fig 5.3 provides a pictorial representation of the workflow outlined in Algorithm 1. As evidenced in Fig 5.4, Fig 5.5, and Fig 5.6 (data source: [51]), we can visualize the impact of data augmentation. Fig 5.4 presents the initial distribution of the data, while Fig 5.5 showcases the transformed distribution after augmentation. To enhance our understanding of these changes, Fig 5.6 utilizes kernel density estimation (KDE) plots, providing a smoother representation of the data distributions in both figures. This comparative analysis allows for a clear assessment of how augmentation has modified the data. The new data set will be available in [52]. The number of epochs E and batch size B determine the number of times the regressor model processes the features extracted from the pre-trained model h . The total complexity depends on the product of these factors multiplied by the complexity per batch $T_{new}(h)$. The total time complexity of the algorithm becomes $O(E * B * T_{new}(h))$.

ALGORITHM 7: Transfer Learning Algorithm to generate Regressor model

- 1 **Input:** Pre-trained RNN model $M_{pre}(x; \theta_{pre})$, Training data set $\{x_i\}$,
 $i \in \{RSRQ, CQI, PDD, SNR\}$
- 2 **Output:** Regressor model $M_{new}(h; \theta_{new})$ **Feature Extraction:** $M_{pre}(x; \theta_{pre})$ takes an input vector x containing current and historical CSI measurements and outputs h .

$$h = M_{pre}(x; \theta_{pre}) \quad (5.5)$$

Regressor Model $M_{new}(h; \theta_{new})$ takes the extracted hidden state sequence h as input and predicts \hat{y} , where $y_i \in \{RSRQ, SNR\}$.

$$\hat{y} = M_{new}(h; \theta_{new}) \quad (5.6)$$

Training the Regressor model $M_{new}(h; \theta_{new})$ by minimizing the MSE loss function L .

$$L(\hat{y}, y) = (y - \hat{y})^2 \quad (5.7)$$

where y represents the actual RSRQ and SNR values.

5.3.2 Complexity Analysis

The complexity of a simple RNN-LSTM model is determined by examining the comparable operations that are involved. The fundamental operations of RNN-LSTMs depend on performing matrix multiplications and activation functions inside a backpropagation algorithm during the training process. An RNN-LSTM architecture comprises an RNN layer, often including LSTMs, followed by a final dense layer to provide the output. The internal gate actions (input, forget, output) and cell state update inside each LSTM unit contribute to the complexity every time step. The commonly used notation for this complexity is $O(D_i * D_o + D_o^2)$, where D_i represents the input dimension (the number of features in the input vector) and D_o represents the output dimension (the number of hidden units in the LSTM). The complexity of the final dense layer stays constant at $O(D_o * D_{out})$, where D_o represents the output dimension from the RNN layer (number of hidden units) and D_{out} represents the number of neurons in the output layer (typically 1 for RSRQ/SNR prediction). RNN-LSTMs sequentially process data. Hence, the intricacy increases with each successive time step T , whereas S is the number of training samples (iterations). The RNN-LSTM

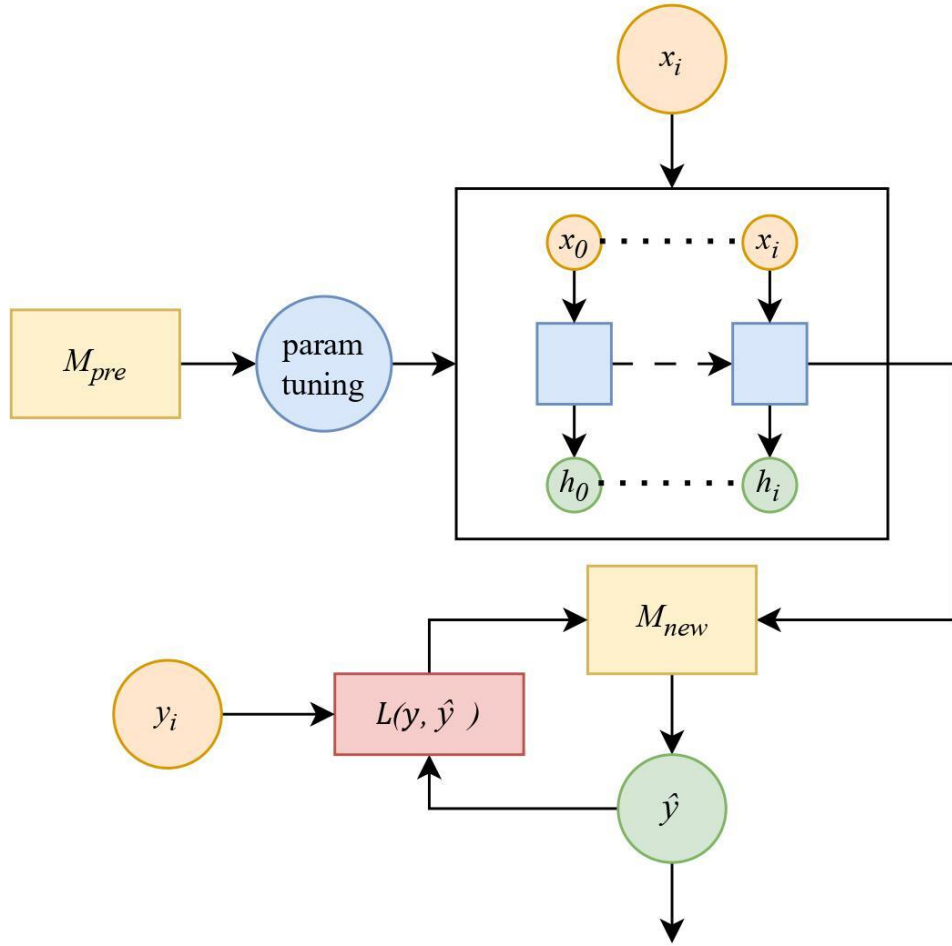


Figure 5.3: Flowchart of algorithm 1

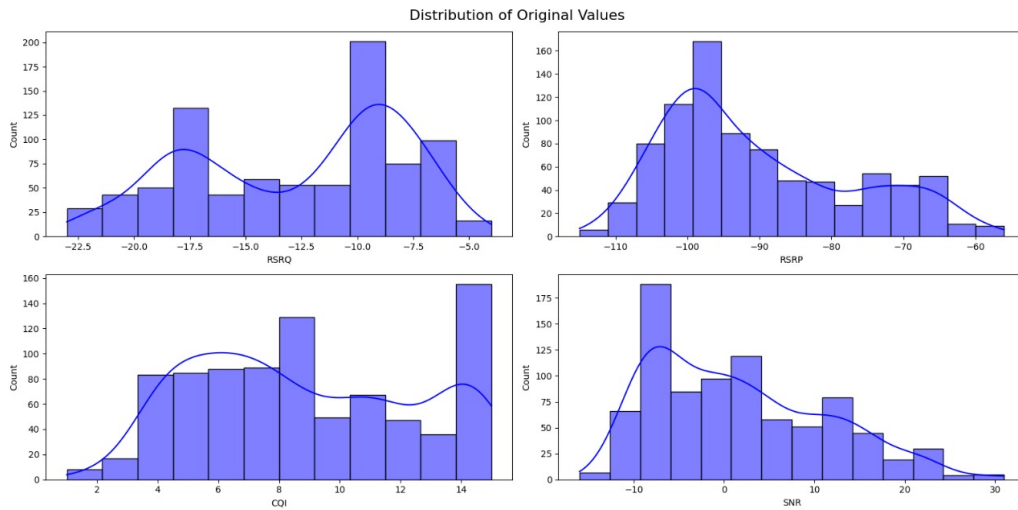


Figure 5.4: Distribution of original values

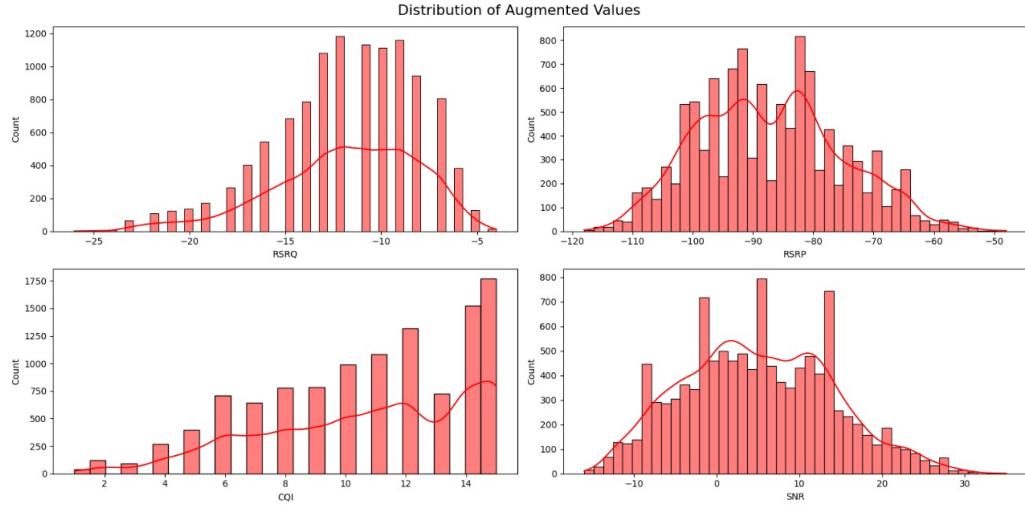


Figure 5.5: Distribution of augmented values

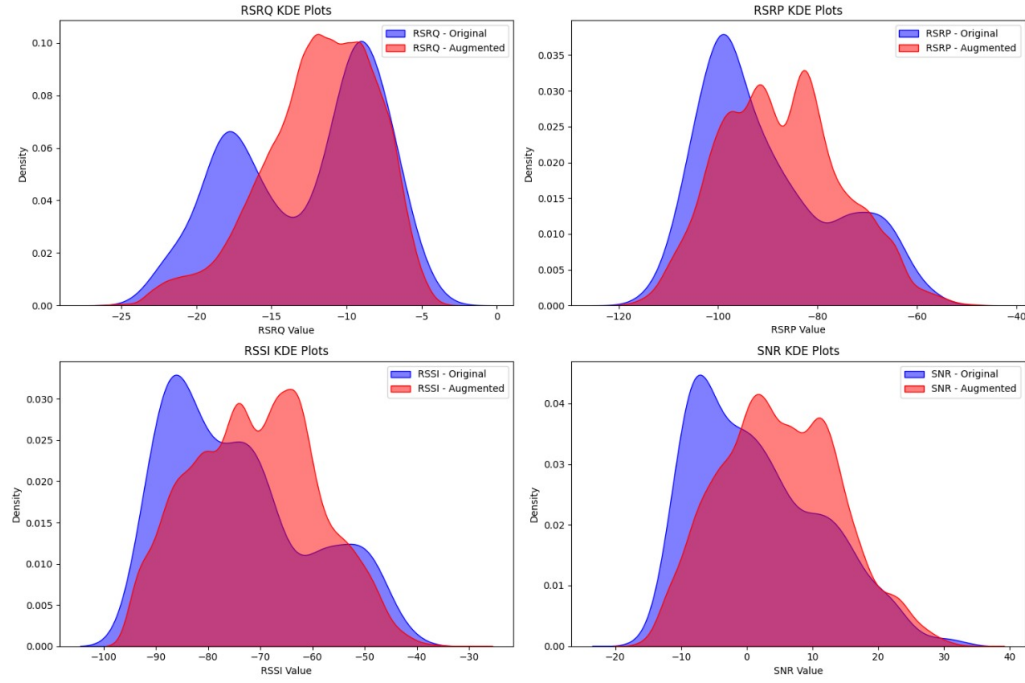


Figure 5.6: KDE plots

model's overall computational complexity is estimated as follows:

$$O(T * S * (D_i * D_o + D_o^2 + D_o * D_{out}))$$

The primary factors contributing to its complexity are the quantity of time steps (T) and the calculations performed inside the LSTM unit (D_i, D_o). The level of complexity may exhibit variability based on the number of hidden units (D_o) and the input sequence length (T).

5.4 Results and Discussion

This research investigates three key aspects of NOMA networks. The first part explores the application of an RNN-LSTM model for improving CSI prediction. The second part analyzes the relationship between handover frequency (switching between cell towers) and UE speeds within the network. The third part compares BER performance with existing pilot-based channel estimation techniques. All of the given pronged approaches aim to optimize network performance in NOMA systems by understanding handover behavior at different UE speeds and leveraging machine learning for more accurate CSI prediction.

5.4.1 Simulation Setup and Results

This study presents a feasible parameter configuration for the NOMA system model in the context of 5G. In this case, we have two BSs that are responsible for servicing two different cells. The number of Users per Cell is 2. Each Base Station has 4x4 antenna configurations. Each UE is equipped with a single antenna. In Table III, we have mentioned a precise description of network parameter configuration. We will establish precise channel models for the base station-to-user equipment connections, taking into account issues like route loss and fading. Regarding the fading feature, we will make the assumption that the distribution of $x(t)$ conforms to a Rayleigh distribution, which is often used to model real-world fading situations. The simulation will assess the NOMA system's performance under several scenarios, such as altering the Transmit SNR at the BSs and the power allocation factor of different UEs within each cell. The precise values for these parameters will be specified in Table III.

The number of hidden units (Ncell) in the LSTMs is set at 16. In addition, configure distinct activation functions such as Rectified Linear Unit (ReLU) for the Long Short-Term

Parameters	Names	Values
K	Number of time steps	1000
t_i	Number of input time steps	10
t_o	Number of future time steps	1
N	Number of users	4
B	Number of BS	2
C	Number of cells	2
v	Uniform speed per one time step	0.1m
γ	Transmit SNR	-9dB to 14dB
ρ	Transmit RSRQ	-8dB to -20dB
d_{bn}	Distance from BS to near user	20
d_{bf}	Distance from BS to far user	50
M	Number of antennas at BS	4
a	Number of antennas at UE	1

Table 5.1: Parameters setup

Memory (LSTM) units. Using three LSTM layers might be advantageous for capturing intricate temporal connections. The duration of the input sequence, referred to as the look-back window, also has a significant impact. Usually, the window size is set at $L = 10$ in order to provide context. Ultimately, using methods such as dropout regularization with a dropout rate of around 0.2 may effectively mitigate overfitting by randomly eliminating neurons throughout the training process.

5.4.2 Performance Metrics

A mix of scale-free and scale-dependent measurements will be the most appropriate performance metrics. Normalized Root Mean Square Error (NRMSE) is a kind of scale-free metric. The Root Mean Square Error (RMSE) is normalized by partitioning it by the standard deviation of the actual target values ($RSRQ/SNR$). This facilitates the comparison of performance by using datasets that include varying scales. Standardized RMSE and Mean

Absolute Scaled Error (MASE) are examples of scale-free metrics. The NRMSE is calculated by:

$$NRMSE = \frac{1}{\sigma_{actual}} \left(\sqrt{\frac{\sum (predicted_i - actual_i)^2}{N}} \right) \quad (5.8)$$

In this context, N represents the total number of samples, σ_{actual} denotes the standard deviation of the actual $RSRQ/SNR$ values, and $predicted_i$ and $actual_i$ represent the predicted and actual values for sample i .

MASE is a statistical technique that involves comparing the average absolute errors of a model with the average absolute difference of a naïve prediction that replicates the prior value. This measure serves as a valuable tool for evaluating and comparing performance across datasets that include varying sizes. MASE is calculated as:

$$MASE = N * \frac{\sum |predicted_i - actual_i|}{\sum |actual_i - actual_{i-1}|} \quad (5.9)$$

One example of a scale-dependent metric is the Mean Squared Error (MSE). Although not optimal for cross-dataset comparisons, the MSE may nonetheless provide valuable insights into assessing the overall accuracy of predictions within a particular dataset. It is calculated by:

$$MSE = \frac{\sum (predicted_i - actual_i)^2}{N} \quad (5.10)$$

In this context, N represents the total number of samples, whereas $predicted_i$ and $actual_i$ denote the predetermined and observed values for sample i , respectively.

The R-squared (R^2) score quantifies the extent to which the model's predictions account for the variability seen in the actual $RSRQ/SNR$ values. Although not devoid of scale, it offers insight into the degree to which the model aligns with the observed data. The use of NRMSE and MASE enables the evaluation of the model's efficacy across diverse datasets characterized by varied magnitudes of RSRQ and SNR values. MSE may provide valuable insights into the overall accuracy of predictions within our particular dataset. The R^2 score is a measure of how well the model captures the fundamental patterns in the data. Evaluating performance across different datasets is essential, and NRMSE and MASE play a vital role in this aspect. While the main emphasis is on comprehending the overall accuracy of predictions within the dataset, the MSE may also be a beneficial tool in conjunction with R^2 .

5.4.3 Evaluation Of RNN-LSTM model

The graph in Fig 5.7 illustrates the convergence of three architectures, namely Convolutional Neural Network (CNN), Recurrent Neural Network (RNN), and RNN-LSTM, in forecasting RSRQ values for a given User located distant from the BS (far user). The models are trained using normalized RSRQ data with a sequence length of 10. Their performance is then compared using RMSE metrics. The objective is to choose the model that produces the most optimal convergence by evaluating their RMSE on a time series dataset for a specified UE. Based on the training RMSE plots, it can be seen that RNN-LSTM has the ability to achieve superior convergence compared to CNN and RNN models. A lower RMSE implies superior model performance since it suggests that the model's predictions are, on average, more accurate and closer to the actual values. This indicates that the RNN-LSTM architecture is more appropriate for capturing the sequential characteristics of RSRQ data and acquiring knowledge of temporal relationships in order to make precise predictions.

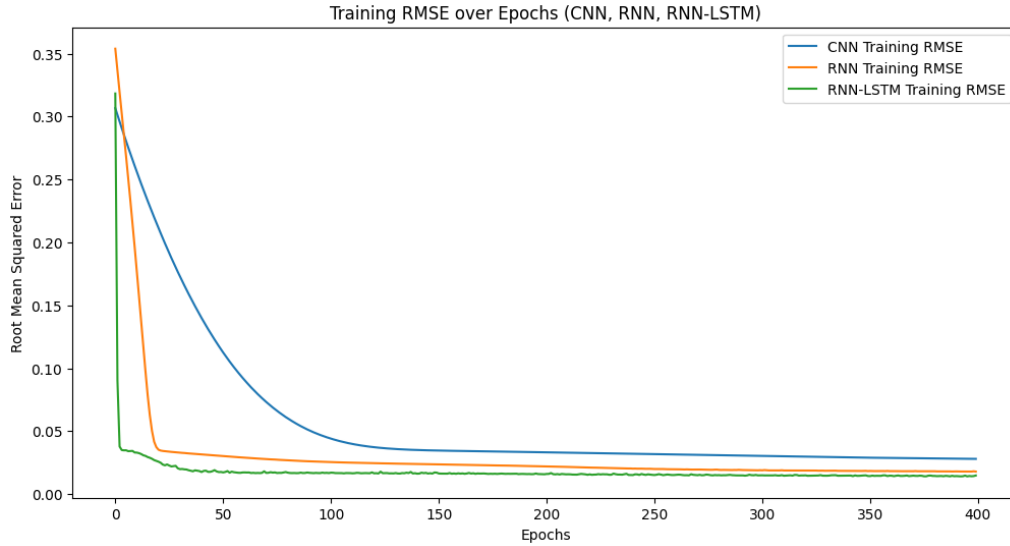


Figure 5.7: Training convergence of three architectures: CNN, RNN and RNN-LSTM

This graph in Fig 5.8 displays the Normalized Root Mean Squared Error (NRMSE) for predicting RSRQ on two User equipment (UE2 and UE1) located at different distances from the Base Station (BS). The RNN-LSTM model yielded projected RSRQ values that were more closely aligned with the actual values for nearby users. This would result in a decreased NRMSE for the nearby user and an increased NRMSE for the distant user in comparison to the nearby user. UE that is in close proximity to the providing cell tower

usually has a greater RSRQ, indicated by a higher number. UE that is situated at a greater distance from the providing cell tower often encounters a weaker RSRQ, which is indicated by a lower value and eventually more fluctuating NRMSE graph.

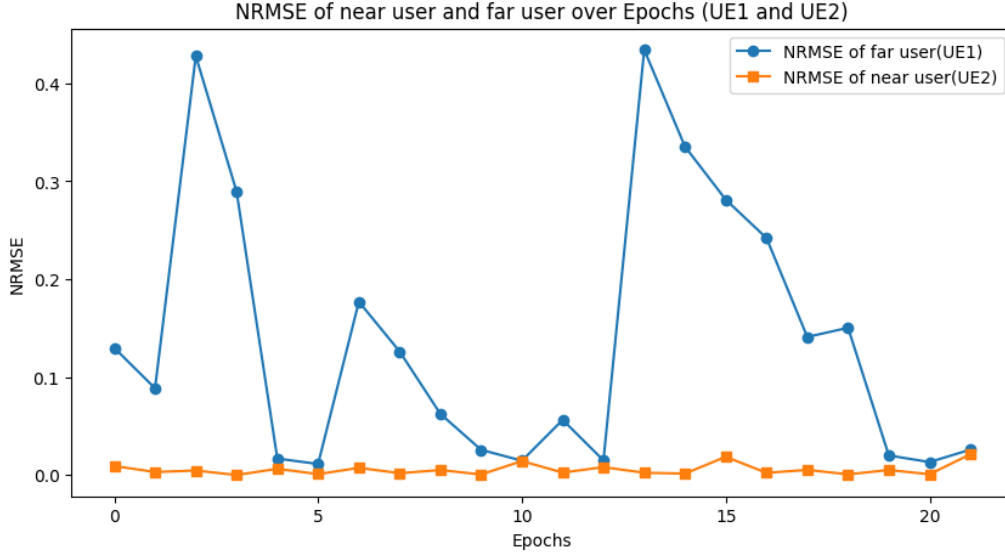


Figure 5.8: NRMSE of near user and far user over epochs (UE2 and UE1)

The graph in Fig 5.9 illustrates the MAE performance of two situations in forecasting channel information using an RNN-LSTM model. The blue curve indicates the MAE measure when the model is trained on channel data that does not contain partially decoded information, whereas the orange curve reflects the MAE when the model is trained using partially decoded data. It is noteworthy that both curves have variations instead of a completely smooth drop, which is a typical occurrence during the training of LSTM models. The variations occur due to the random characteristics of gradient descent, the optimization process used to train the model. Although there may be some variations, it is preferable to have a continuous decreasing trend in the MAE curve across epochs. Through a comparison of the curves, we can assess the influence of including partly decoded data on the model's convergence and prediction accuracy. If the orange curve (representing partly decoded data) exhibits a more pronounced and persistent reduction in MAE in comparison to the blue curve, it indicates that integrating additional information aids in the model's more efficient learning. In contrast, if the orange curve exhibits comparable or more pronounced variations, it suggests that partly decoded data has little impact on the model's convergence or may potentially contribute unwanted random signals.

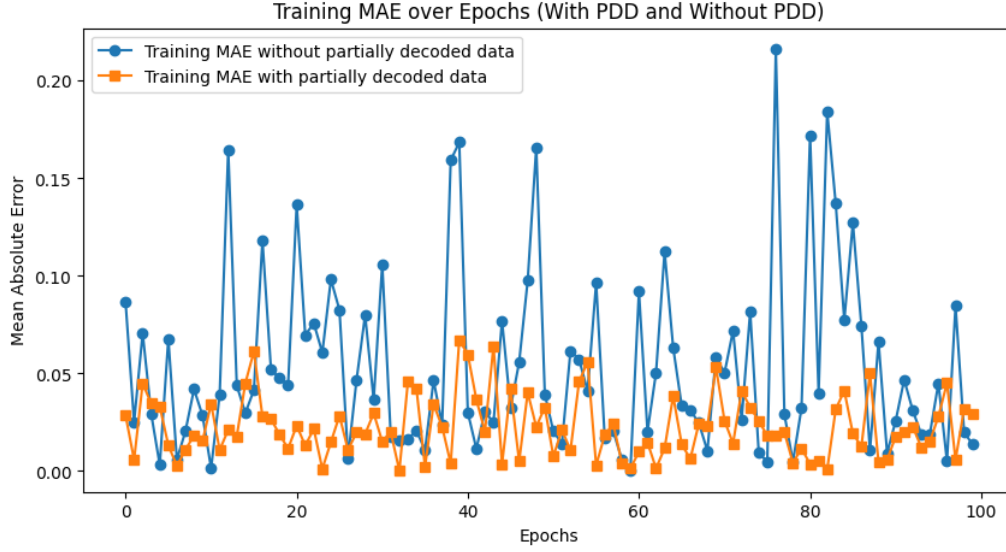


Figure 5.9: Training MAE with PDD and without PDD

R-squared (R^2) is a statistical measure used to assess the degree to which a regression model accurately represents a dataset. The coefficient of determination quantifies the amount of variability in the predicted values of the dependent variable that can be attributed to the independent variable(s) included in the model. The R^2 values vary between 0 and 1. A value of 0 shows no connection between the predicted and actual values, while a value of 1 indicates a perfect fit, where the model accurately predicts the dependent variable. By including PDD information, the model achieves a more accurate alignment between the predicted and actual channel information, demonstrating its enhanced effectiveness. The inclusion of PDD in the model is anticipated to enhance its ability to account for the effects of signal delays on CSI, hence resulting in more precise predictions. By processing the raw signal to extract PDD characteristics, the model gains more comprehensive knowledge about the behavior of the signal. This eventually leads to a deeper understanding of the link between the features and the target state of CSI. By visually comparing the graphs in Fig 5.10, we can verify if the model trained with PDD regularly achieves a better R^2 compared to the model without PDD. If the errors in partially decoded data are excessive or incomprehensible, they may introduce noise rather than useful information, resulting in a paradoxical scenario. This might result in a decreased R^2 in comparison to only using CSI. In the NOMA network we are studying, a user located far away may experience an abrupt change in the R-squared value during training. This might be due to difficulties

in accurately recording the signal behavior for remote users. If the learning algorithm of the model can detect patterns that are unique to distant user signals, it may encounter a dramatic increase in R-squared. This indicates the enhanced capability of the model to address the difficulties related to predicting signals from distant users.

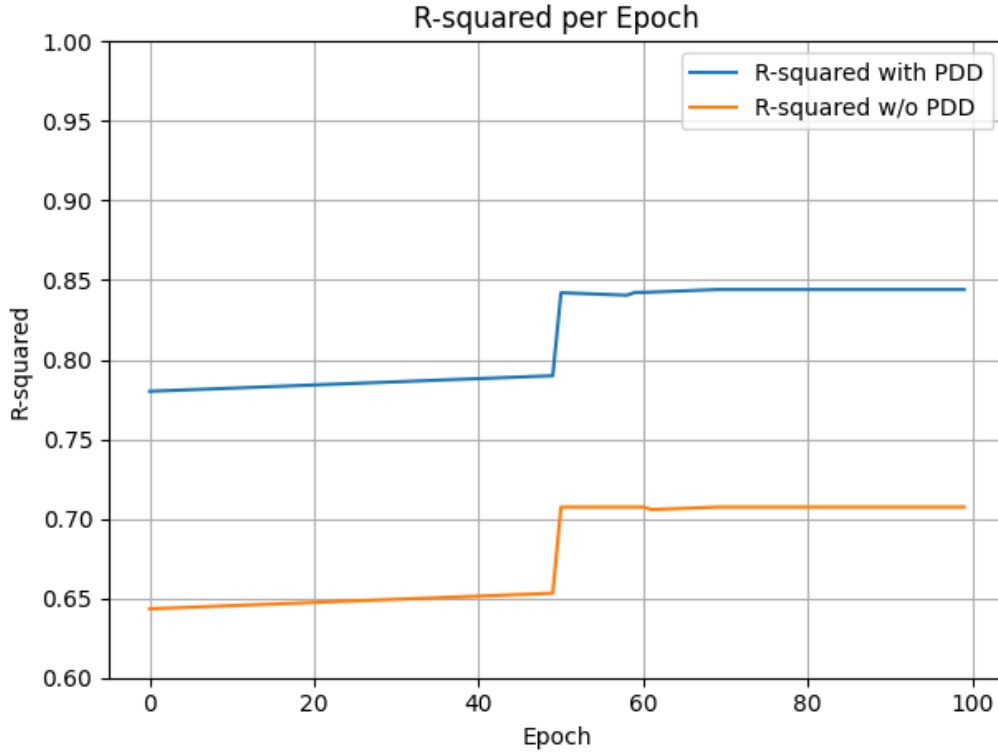


Figure 5.10: R-squared comparison with PDD and without PDD

The R-squared score curve in Fig 5.11 demonstrates a distinct ranking in the effectiveness of different models in predicting RSRQ results. The RNN-LSTM model regularly attains the greatest R-squared scores throughout the training phase, showing its better capacity to capture the underlying connections between the input data and the target variable. The training data may include a fresh data point or a group of points that have a noticeable and well-defined connection to RSRQ at that particular time period. The CNN uses 1D convolution with 32 filters and utilizes the Rectified Linear Unit (ReLU) activation function to extract features. The RNN model uses a single LSTM layer with 20 units and a ReLU activation function to capture the temporal dependencies present in the data effectively. The RNN-LSTM model consists of two LSTM layers, with the first layer having 50 units and the second layer having 20 units. The ReLU activation function is used to facilitate the learning

of intricate associations. Nevertheless, the constraints of the CNN design result in negative R-squared values. This suggests a worse match compared to the reference point. The

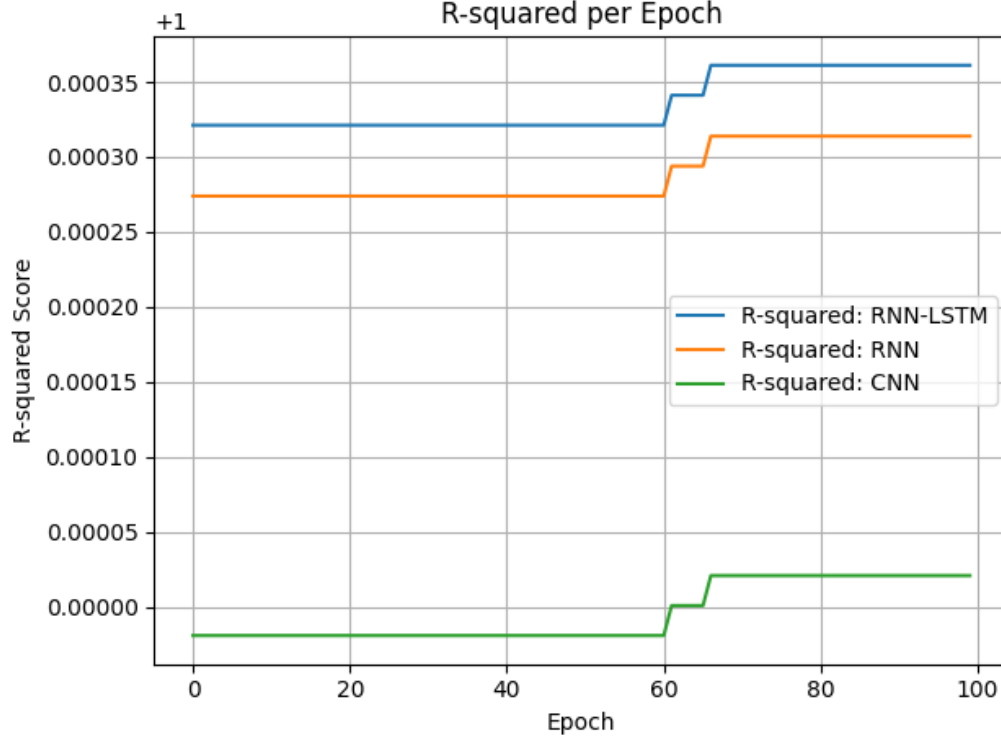


Figure 5.11: R-squared score (without PDD): CNN, RNN, RNN-LSTM

findings and discussion center on the influence of using PDD to evaluate the status of the channel. The RNN-LSTM model makes predictions on the Signal-to-interference-plus-Noise Ratio (SINR), which is an important measure of channel quality. The quantity of data frames defines the quantity of training data used for prediction. Fig 5.12 depicts the training patterns of models that use CSI exclusively and those that include PDD as input. The CSI-exclusive model shows a curve that falls below 0 in some epochs. This suggests that the model may not be well-suited for some data points, indicating that it has difficulty capturing the intricacies of the channel without more information. On the other hand, the model that includes partially decoded data regularly produces a curve that is higher than 1, indicating a more pronounced positive relationship with the goal values. Fig 5.13 of the testing comparison between SINR values illustrates the superiority of taking PDD as CSI, which results in a better SINR output. This emphasizes the advantage of PDD in improving the model's comprehension of channel fluctuations. Comparable trends are noted while

comparing testing data sets.

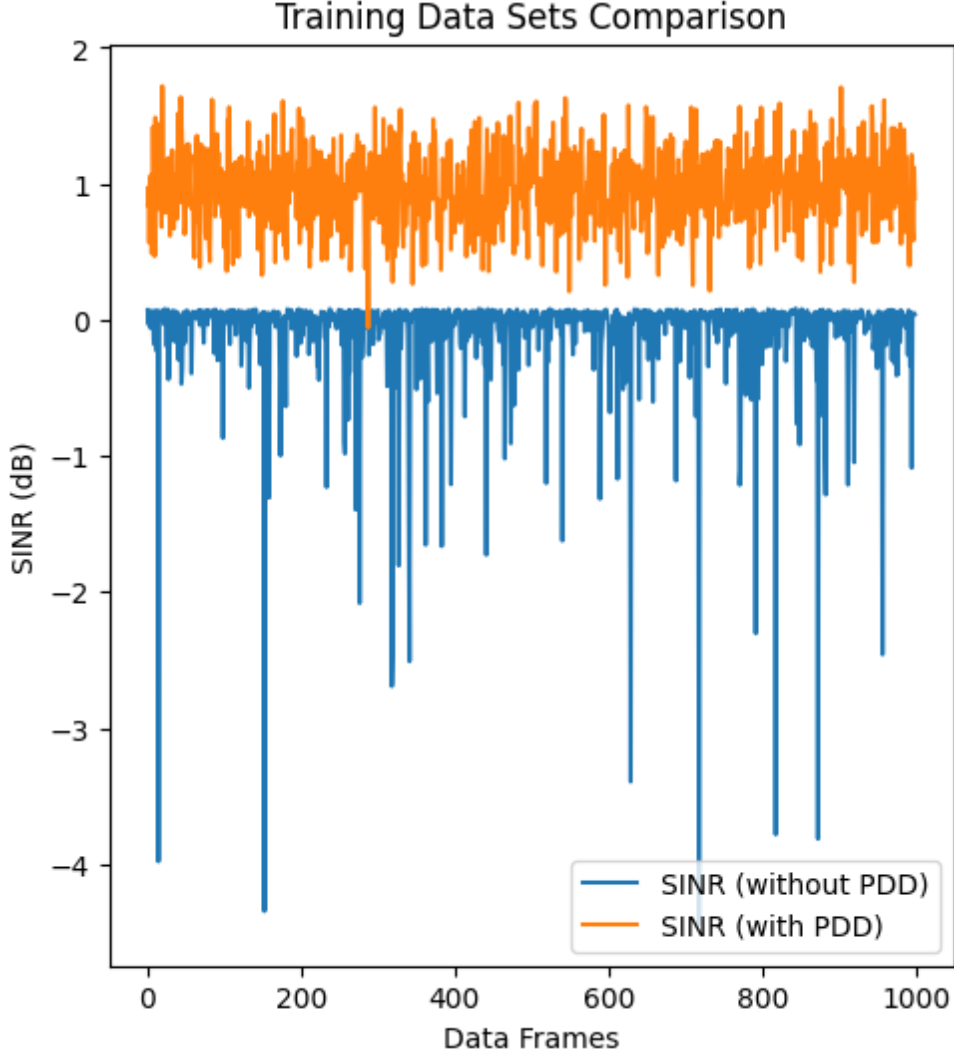


Figure 5.12: Training SINR comparison over data frames

We employ scale-free and scale-dependent measures, such as RMSE, MAE, and MSE scores in TABLE IV, to assess the behavior of various models on a dataset. Table IV lists the performance metrics for several ML models, such as CNN, RNN, and RNN-LSTM. Table IV presents the accuracy superiority of the proposed RNN-LSTM model over the two remaining models, namely CNN and RNN, based on different datasets from [51]. The complete code related to simulation can be found in [52].

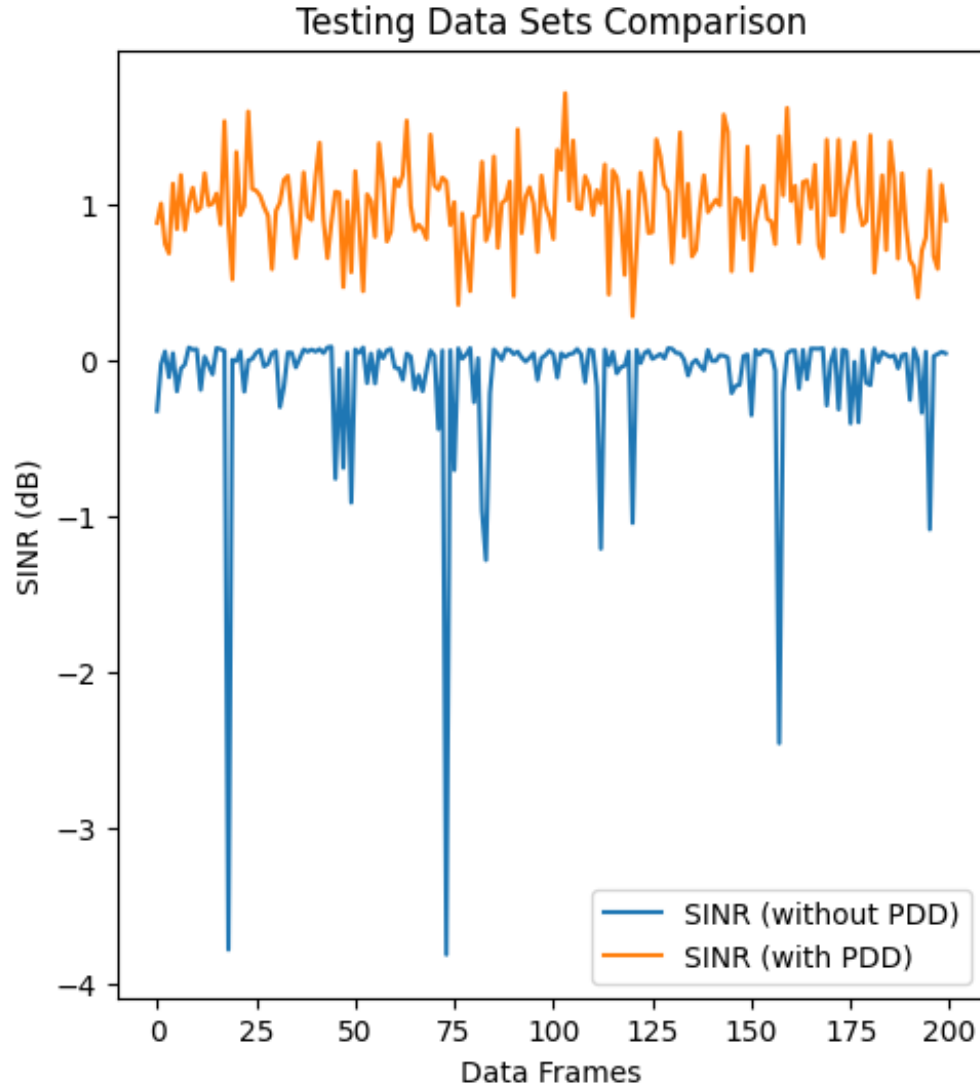


Figure 5.13: Testing SINR comparison over data frames

Metrics	Models	Amazon Prime		Download		Netflix	
		Driving	Static	Driving	Static	Driving	Static
RMSE	CNN	0.0798	0.0364	0.1092	0.1889	0.1116	0.1056
	RNN	0.0722	0.0323	0.0845	0.1478	0.0764	0.0837
	RNN-LSTM	0.0608	0.0119	0.0737	0.1322	0.0685	0.0712
MAE	CNN	0.0695	0.0069	0.0949	0.1543	0.0816	0.0853
	RNN	0.0585	0.0065	0.0543	0.1014	0.0489	0.0541
	RNN-LSTM	0.0386	0.0021	0.0502	0.0922	0.0343	0.0429
MSE	CNN	0.0075	0.0013	0.0136	0.0346	0.0117	0.0095
	RNN	0.0054	0.0009	0.0075	0.0218	0.0068	0.0062
	RNN-LSTM	0.0034	8.3417e-01	0.0063	0.0173	0.0046	0.0047

Table 5.2: Performance metrics of different ML models

5.4.4 Comparative Analysis of RNN-LSTM

In NOMA networks, accurate channel estimation is crucial for efficient resource allocation and reliable communication. Three baseline machine learning methods, RNN-LSTM, SVM, and Random Forest have been applied for channel estimation using two approaches: (1) using only CSI and (2) using CSI combined with PDD. RNN-LSTM excels in handling temporal dependencies and non-linear relationships, making it highly suitable for time-varying channel conditions and achieving superior accuracy, especially when PDD is included. However, it comes with high computational complexity due to its sequential processing and large parameter space. SVM performs well in high-dimensional spaces and generalizes effectively with CSI alone but struggles with scalability and temporal data handling, leading to lower accuracy. Random Forest, an ensemble method, reduces overfitting and provides feature importance insights, performing well with CSI alone but lacking in temporal dependency handling and scalability for high-dimensional data. In terms of computational complexity, RNN-LSTM is the most demanding, followed by SVM (moderate to high, depending on the kernel) and Random Forest (moderate, scaling with the number of trees). While all three methods have merits, RNN-LSTM stands out as the best in terms of accuracy and adaptability, making it the preferred choice for channel estimation in NOMA networks. Fig 5.14 predicts and analyzes the spectral efficiency of a NOMA network under varying SNR conditions. It begins by simulating NOMA network parameters, including channel gains and spectral efficiency, using synthetic data. Three models are trained: an RNN-LSTM with Bidirectional LSTM layers and dropout regularization for handling complex patterns, an SVM with an RBF kernel for capturing non-linear relationships, and a Random Forest regressor for robust generalization. The models predict spectral efficiency across SNR values ranging from 0 dB to 20 dB, with results visualized using ‘matplotlib’ to compare the performance of RNN-LSTM (solid blue line), SVM (dashed orange line), and Random Forest (dash-dotted green line). The RNN-LSTM model is expected to outperform the others, as indicated by its higher R^2 score, due to its ability to model complex dependencies and prevent overfitting. The SVM and Random Forest models, while effective, may struggle with high-dimensional data or fail to capture intricate patterns as effectively as the RNN-LSTM. The plot of spectral efficiency vs. SNR should show an increasing trend, with the RNN-LSTM closely following the theoretical curve, while the other models may deviate slightly

at higher SNR values. Limitations include the use of synthetic data, which may not fully reflect real-world NOMA network dynamics, and fixed power allocation coefficients, which simplify the problem. Future work could involve experimenting with advanced architectures like Transformers, incorporating real-world data, and exploring adaptive power allocation strategies. Overall, the code highlights the potential of deep learning models, particularly RNN-LSTM, in optimizing spectral efficiency for wireless communication systems, though further validation and optimization are needed for practical applications.

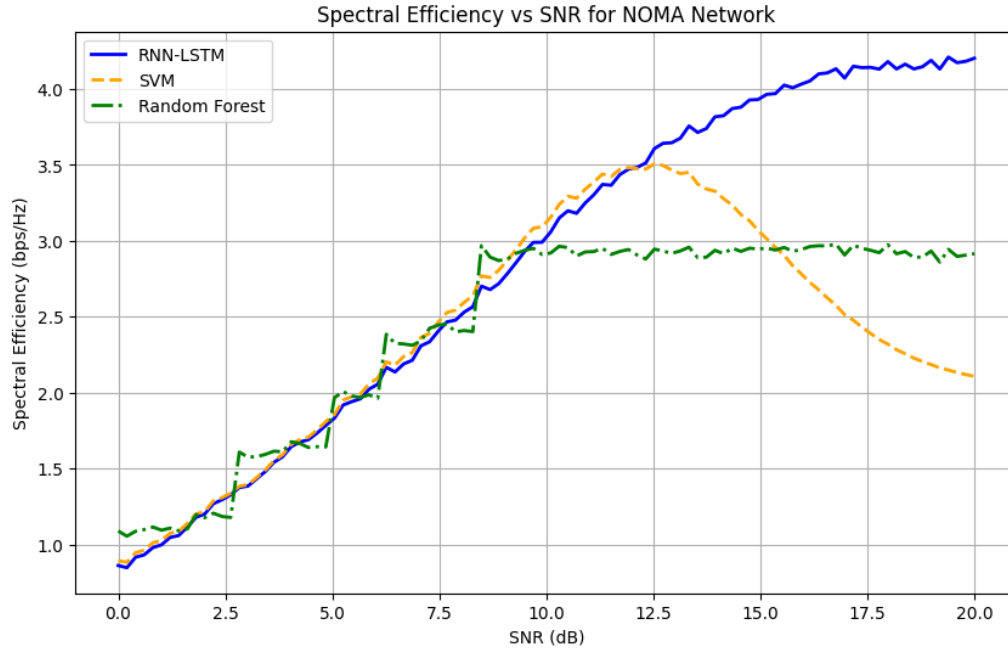


Figure 5.14: A Comparative Analysis of RNN-LSTM, SVM, and Random Forest Models Under Varying SNR Conditions.

Fig 5.15, evaluates the performance of three models RNN-LSTM, SVM, and Random Forest in predicting the symbol error rate for two scenarios in a wireless communication system, Scenario 1: using only CSI, and Scenario 2: using both CSI and PDD. The data [51] is split into training and testing sets. An RNN-LSTM model with dropout and batch normalization is trained for both scenarios, with early stopping to prevent overfitting, while SVM and Random Forest models are trained with varying hyperparameters. The models predict the channel state, and the symbol error rate is calculated using 'mean squared error'. Results show that RNN-LSTM outperforms SVM and Random Forest in both scenarios due to its ability to capture temporal dependencies, with the performance gap potentially

widening in Scenario 2 as RNN-LSTM leverages the additional data. A plot compares the symbol error rate of the models across scenarios, highlighting RNN-LSTM's superior performance. Limitations include the use of fixed hyperparameters, while future work could explore advanced architectures like Transformers, and optimize feature selection.

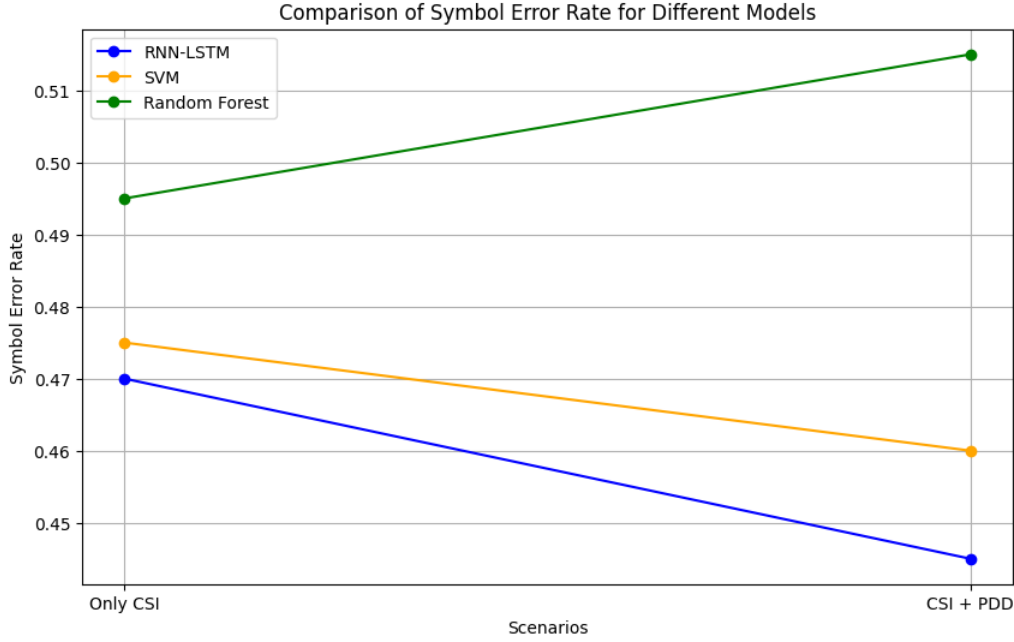


Figure 5.15: A Comparative Study of LSTM, SVM, and Random Forest Models Using CSI and Partially Decoded Data.

In Fig 5.16, the LSTM model architecture includes two LSTM layers to capture temporal dependencies, with dropout (fixed at 0.3) and batch normalization for regularization, and a dense output layer to predict channel gains for all users. The Adam optimizer, with a fixed learning rate of 0.001, minimizes the Mean Squared Error (MSE) loss function. Hyperparameter tuning evaluates the model's performance across different LSTM unit configurations (64, 128, 256, 512, 1024), using parallel training and early stopping to optimize computational efficiency and prevent overfitting. Performance is assessed using MSE, with results visualized to analyze the impact of model complexity on accuracy. Key findings reveal that increasing LSTM units improves performance up to a point beyond which overfitting occurs, while dropout and batch normalization enhance generalization. The study highlights the trade-offs between model complexity, computational cost, and performance, providing insights for designing deep learning models in NOMA systems. However, limitations include

a restricted hyperparameter search suggesting future work should explore comprehensive hyperparameter tuning. In Fig 5.17, the LSTM model architecture includes two LSTM

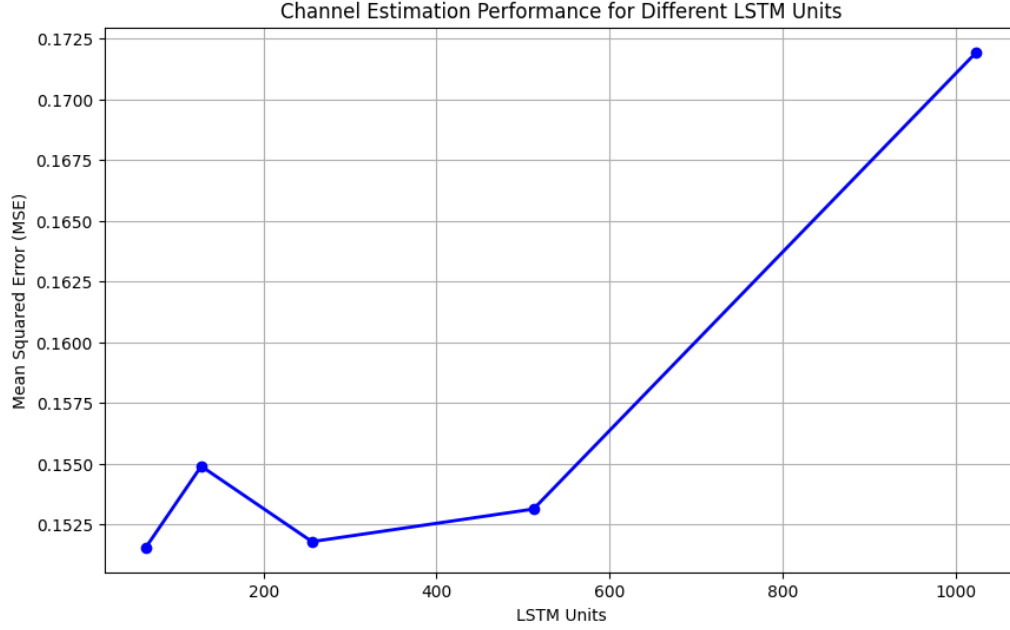


Figure 5.16: Impact of Varying LSTM Units on Channel Estimation Performance with Fixed Dropout Rate (0.3) and Learning Rate (0.001).

layers with a fixed number of units (256) to capture temporal dependencies, with dropout (fixed at 0.3) and batch normalization for regularization, and a dense output layer to predict channel gains for all users. The Adam optimizer, with varying learning rates (0.0001, 0.0005, 0.001, 0.005, 0.01), minimizes the MSE loss function. Hyperparameter tuning evaluates the model's performance across different learning rates using parallel training and early stopping to optimize computational efficiency and prevent overfitting. Performance is assessed using MSE, with results visualized to analyze the relationship between learning rate and accuracy. Key findings reveal that the learning rate significantly impacts model performance, with very low rates leading to slow convergence and very high rates causing instability, while dropout and batch normalization enhance generalization. The study highlights the trade-offs between learning rate, convergence speed, and performance, providing insights for designing deep learning models in NOMA systems.

The computational complexity of RNN-LSTM, SVM, and Random Forest, applied in NOMA networks for channel estimation using only CSI and CSI+PDD, varies significantly based on implementation details, dataset size, and hyperparameters. For RNN-LSTM, the



Figure 5.17: Impact of Varying Learning Rate on Channel Estimation Performance with Fixed LSTM Units (256) and Dropout Rate (0.3)

complexity is dominated by sequential processing and parameter size, with a single time step complexity of $O(T \cdot (n_h \cdot n_x + n_h^2))$, where T is the number of time steps, n_h is the number of hidden units, and n_x is the input dimension. For training over N samples and E epochs, the total complexity becomes $O(E \cdot N \cdot T \cdot (n_h \cdot n_x + n_h^2))$. SVM's complexity depends on the kernel choice, with a nonlinear kernel (e.g., Radial Basis Function) having a complexity of $O(N^2 \cdot d)$, where N is the number of training samples and d is the input dimensionality, while a linear kernel reduces this to $O(N \cdot d)$. Random Forest's complexity is determined by the number of trees T , features M , and dataset size, with a single tree's complexity being $O(M \cdot d \cdot N \log N)$ and the total complexity for the forest being $O(T \cdot M \cdot d \cdot N \log N)$. When applied in NOMA networks, using only CSI keeps the input dimension d limited to CSI features, but incorporating PDD increases d , raising complexity for all methods. RNN-LSTM, despite its higher computational cost, handles this increased dimensionality and temporal dependencies effectively, making it the most suitable choice. In contrast, SVM and Random Forest struggle with scalability and temporal data handling, making them less effective for scenarios involving CSI+PDD. Thus, while RNN-LSTM is computationally demanding, its superior adaptability and accuracy make it the preferred method for channel estimation in NOMA networks.

5.4.5 Application of the Proposed Technique to HLF/RLF

This research aims to examine the influence of handover decision-making, which is based on changing CSI, on the frequencies of handover failures. We use five handover profiles obtained from [53], each of which may reflect different network setups defined by specific values for Time to Trigger (TTT), $A3$ Offset, and $L3$ Filter K . Next, we model handover situations for UE moving at different velocities. Each profile is evaluated using two CSI configurations: 1) using only RSRQ and 2) employing both RSRQ and PDD. The generated graph effectively illustrates how the selection of CSI affects handover performance. This is done in Fig 5.18 by comparing the handover failure rates for these two CSI setups at various UE speeds and handover profiles. This analysis will provide valuable insights into optimizing handover strategies based on the available CSI and network conditions. We

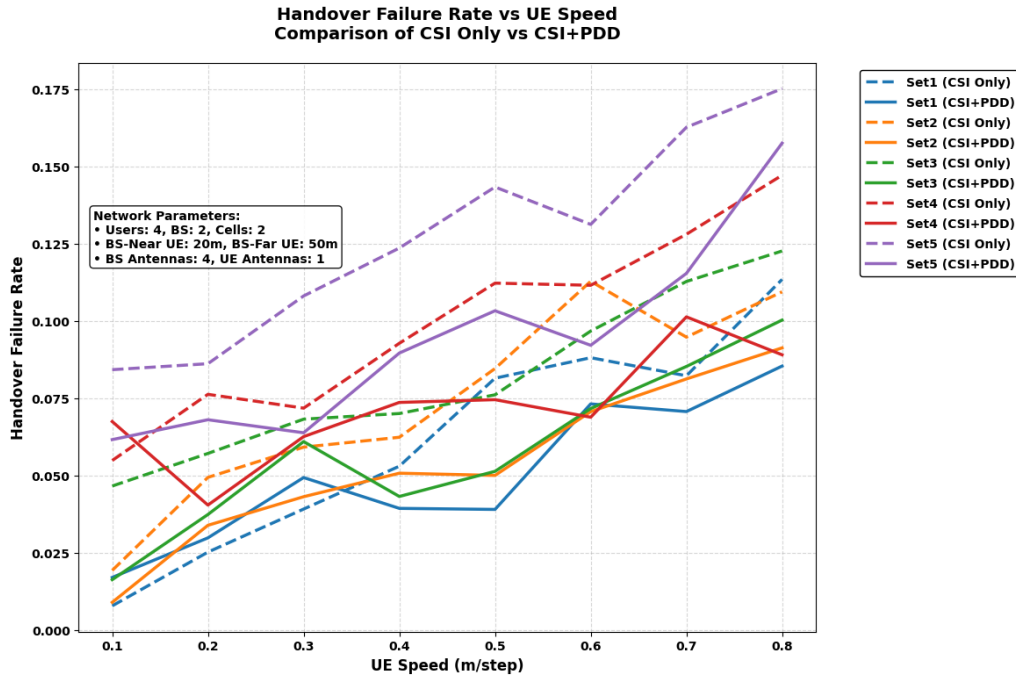


Figure 5.18: Handover failure rates over UE speeds (km/hour)

examine how handover decision-making affects ping pong rates (handover frequency) for UEs moving at different speeds. Five handover profiles from [53] reflect various network settings. We evaluate two CSI setups for each profile. We have given a complete graph in Fig 5.19 that shows how CSI and network design (as specified by handover profiles) affect handover frequency by comparing ping-pong rates across various UE speeds, handover profiles, and

CSI configurations. PDD provides more real-time channel quality information than signal strength (RSRQ), which improves handover choices and reduces ping pong. Handover failures arise from inaccurate forecasts of forthcoming channel conditions. Unsuccessful transfers might result in a consistent pattern in the curves that represent the rate of failure in transferring responsibilities. The ping pong rate takes into account both successful and unsuccessful handovers, which might result in less predictable patterns. The setup of the network and the information about the PDD may have a significant influence on both the success and failure rates, therefore affecting the distribution of ping-pong rates. The analysis

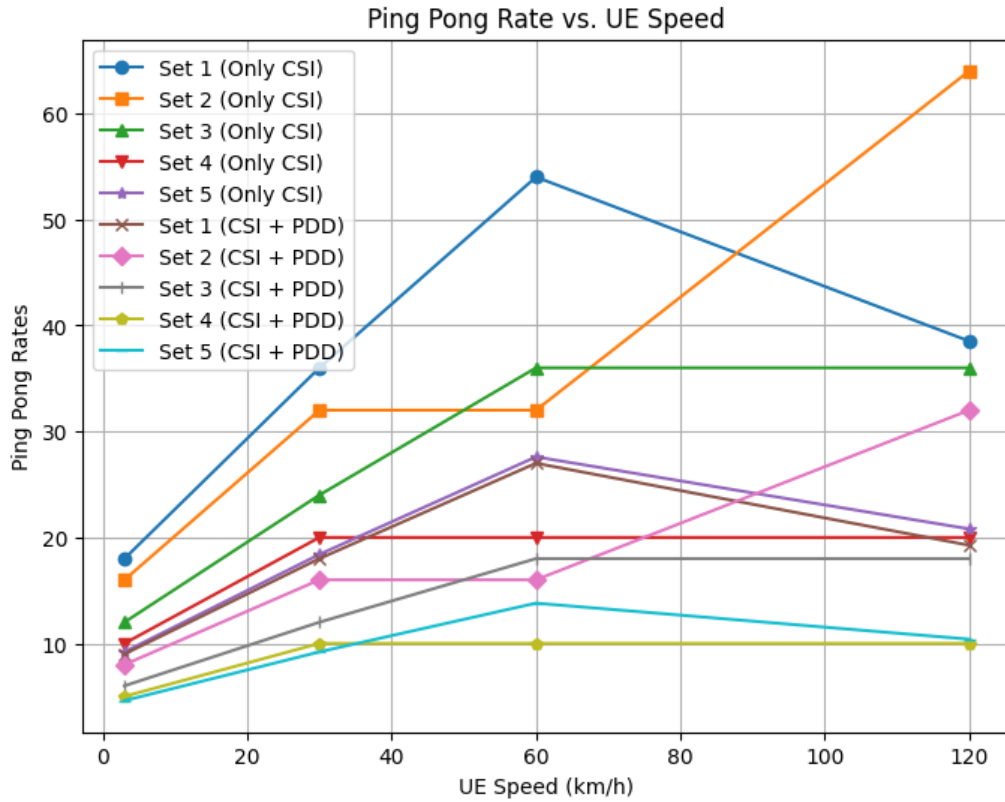


Figure 5.19: Ping-pong rates over UE speeds (km/hour)

of false alarm rates reveals a U-shaped curve when plotted against UE speeds. At very low speeds, even minor fluctuations in the channel, which might appear significant, can trigger unnecessary handover attempts (false alarms) due to limitations in predicting future channel conditions based solely on Received Signal Strength Received Quality (RSRQ). However, as UE speeds increase dramatically, the channel environment changes rapidly, making frequent handovers inevitable to maintain a good connection. This contrasting behavior at both ends

of the speed spectrum leads to a peak in the number of false alarms at moderate speeds. Here, the challenge lies in accurately distinguishing between temporary fluctuations and actual signal degradations, making handover decisions more critical. The graph in Fig 5.20 incorporates two curves representing the impact of CSI used for handover decisions, one only relying on RSRQ and another one considering both RSRQ and PDD. The data suggests that utilizing both CSI and PDD leads to generally lower false alarm rates compared to relying solely on RSRQ across most UE speeds.

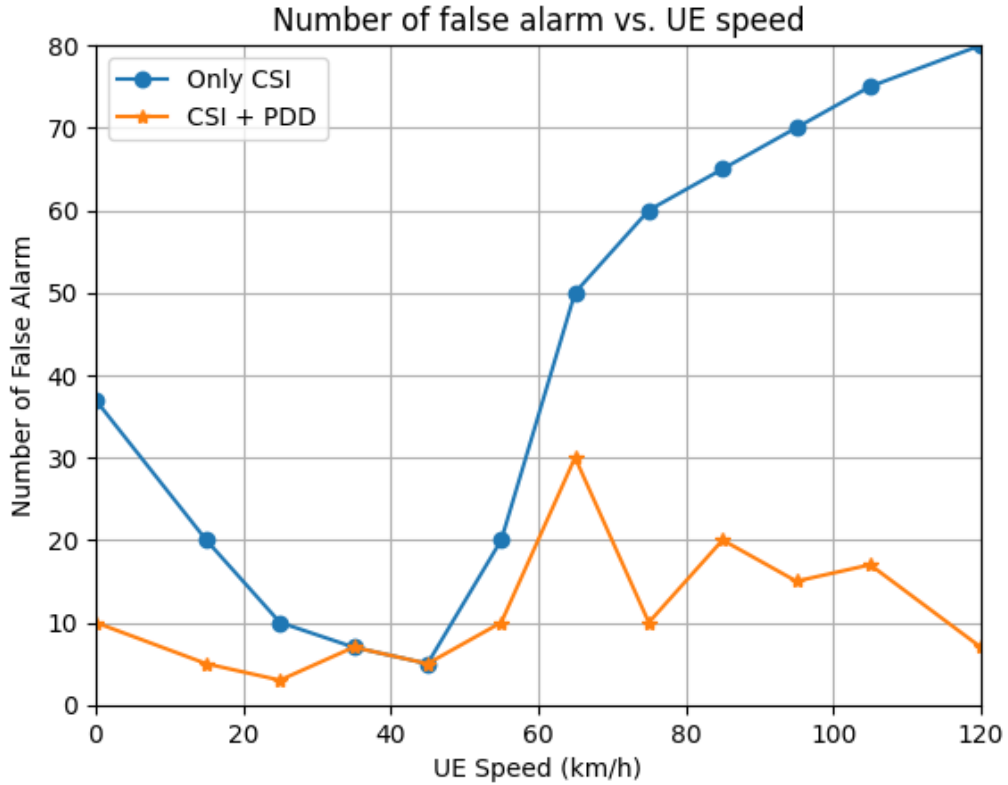


Figure 5.20: Number of false alarm vs. UE speeds (km/hour)

5.5 Summary

A novel method for NOMA channel prediction was introduced in this study, which makes use of a larger variety of CSI parameters, such as RSRP, RSRQ, CQI, SNR, and, most importantly, PDD. System-level simulations showed that low CSI has a major effect on radio link and handover failures. Our results demonstrate the benefits of PDD as a supplementary CSI metric. By doing away with the requirement for specialized pilot signals, PDD lowers

signaling overhead while providing a more realistic depiction of channel dynamics than conventional techniques. Additionally, this method is adaptable to shifting user traffic patterns. In comparison to a deterministic model, our suggested approach performed better in terms of MSE and BER. This is the first study to investigate the application of PDD in NOMA networks to forecast handover and radio link failures. Realizing that ML can be used for channel estimation because it doesn't require as many strict assumptions. In addition, we used a transfer learning strategy to get around dataset size constraints. Furthermore, we exhibited the competitive performance of our model in comparison to earlier research and investigated the use of scale-free and scale-dependent metrics. By using PDD as a useful source of channel information for forecasting channel behavior in NOMA networks, this study sets itself apart. In subsequent deployments, this strategy could enhance network performance and handover decision-making. Future objectives for the study include examining the effects of PDD on network performance under different traffic scenarios and delving deeper into the incorporation of ML algorithms for channel estimation.



Improving Channel Estimation Through Gold Sequences

6.1 Introduction

NOMA has emerged as a viable solution for improving spectral efficiency and ensuring fairness among users in wireless communication networks. Although NOMA has notable benefits compared to classic orthogonal multiple access (OMA) schemes, its performance is greatly affected by variables such as the accuracy of channel estimates and the mitigation of interference. This study examines the efficiency of a NOMA system using Gold coding, a method that enhances user isolation and provides supplementary variety. The assumption of a common pilot channel (H_p) for all users is adopted in this chapter to analyze the fundamental challenges of channel estimation in NOMA systems, where superimposed signals inherently cause pilot contamination. While real-world scenarios involve distinct channel responses (h_n) for each user, this initial abstraction demonstrates why traditional pilot-based estimation fails under NOMA's interference-heavy regime. Dedicated pilots consume orthogonal resources (time/frequency slots), wasting resource consumption, which eventually conflicts with the massive connectivity characteristics of NOMA. The use of dedicated pilot signals exacerbates the near-far effect in NOMA systems by causing inaccurate channel estimation for distant users due to power disparity. Gold sequences mitigate user interference through their low cross-correlation properties, while the CPF leverages power allocation and partially decoded data to refine estimates dynamically. This phased approach—first exposing the problem via simplification, then resolving it with advanced techniques—aligns with methodological best practices in NOMA research. Moreover, the paper investigates

the use of deep learning for channel prediction in NOMA systems. A deep learning model is trained on a dataset to properly predict channel behavior, resulting in enhanced channel estimation and overall system performance. The proposed channel estimate approach integrates received pilot signals, power allocation vectors, and data symbols, showcasing its superiority over conventional pilot-based algorithms. This discovery has the potential to be used in different fields, such as 5G and future wireless networks. To guarantee effective and dependable NOMA communication, network operators may improve resource allocation, power control, and interference management by comprehending the influence of various noise components and channel circumstances on system performance.

6.2 System Model

We consider a downlink NOMA network where a transmitter transmits signals to multiple receivers. We focus on a single-antenna per-user decoding approach and a N number of users. The wireless channel between the transmitter and a receiver is modeled as a frequency-flat Rayleigh fading channel denoted by $H = [h_1, h_2, \dots, h_N] \in \mathbb{C}^N$. We assume a block-fading channel where the elements of H remain constant during a transmission frame.

A transmission block consists of a pilot subcarrier and data subcarriers. The transmitter sends a known pilot symbol x_p on the pilot subcarrier during the pilot transmission. All users experience the same pilot channel H_p . The received pilot signal at time slot t is:

$$y_p(t) = H_p x_p + z_p(t) \quad (6.1)$$

Where $z_p(t)$ is the additive white Gaussian noise at the receiver. During data transmission, user data symbols $x_n^k(t)$ are transmitted on specific subcarriers k within the block for user n . Vector power allocation $\phi_n = [\phi_n^1, \phi_n^2, \dots, \phi_n^K]$ assigns power to each subcarrier k for user n . The received signal for user n at time slot t is:

$$y_n(t) = \sum_{k=1}^K \sqrt{\phi_n^k} H_n^k x_n^k(t) + \sum_{(i \neq n)} \sum_{k=1}^K \sqrt{\phi_i^k} H_i^k x_i^k(t) + z(t) \quad (6.2)$$

where,

H_n^k : Channel gain for user n on subcarrier k , $x_n^k(t)$: Data symbol for user n on subcarrier

k at time slot t , $z(t)$: Additive white Gaussian noise. Here, we consider a system with a total of K subcarriers. While a portion p of these subcarriers is dedicated to pilot signals. The remaining subcarriers are dynamically assigned to user data. A block diagram of subcarrier allocation is illustrated in Fig 6.1.

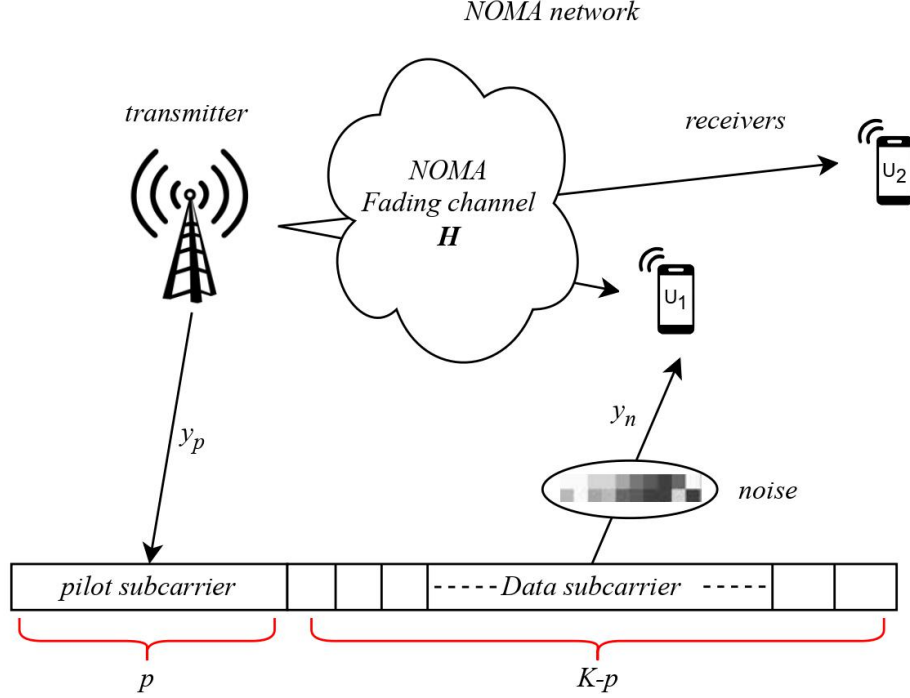


Figure 6.1: Transmission block structure at the BS in NOMA network.

In this work, we propose a CPF that incorporates not only the received pilot signal $y_p(t)$ and the allocated power vector $\phi_n^k(t)$, reliable partially decoded data symbols $\hat{x}_n^k(t)$ for user n on subcarrier k . Here, \hat{x} denotes the estimated symbol value based on the initial decoding attempt.

$$H_n^k \text{ (predicted)} = \text{CPF} \left(\hat{h}_n^{\text{raw}}, \phi_n^k(t), \hat{x}_n^k(t) \right) \quad (6.3)$$

We consider a downlink NOMA system with a single-antenna base station serving N users over frequency-flat Rayleigh fading channels (h_1, \dots, h_N) with block fading. The transmission comprises: (1) a common pilot phase where all users share pilot x_p , resulting in contaminated reception $y_p(t) = \sum_{n=1}^N h_n x_p + z_p(t)$ (Eq.1), and (2) a data phase with

superimposed user signals $y_n(t) = \sum_{k=1}^K \sqrt{\phi_n^k} h_n x_n^k(t) + \sum_{i \neq n} \sqrt{\phi_i^k} h_i x_i^k(t) + z(t)$ (Eq.2). To address pilot contamination and interference, we propose a Gold-CP framework where: (i) each user is assigned a unique Gold code C_n (lengths $L = 31, 63, 127$) for spreading ($x = \sqrt{P} \sum_{n=1}^N S_n C_n$, Eq.4), leveraging low cross-correlation ($|\rho_{ij}| \leq 1/\sqrt{L}$) for initial channel estimation via despreading ($\hat{h}_n^{raw} = y_p \star C_n^H$); and (ii) a Channel Prediction Function (CPF) refines estimates using power allocation weights ϕ_n^k (prioritizing far users via $w_{far} > w_{near}$) and partially decoded data \hat{x}_n^k , yielding final estimates $\hat{h}_n^{final} = CPF(\hat{h}_n^{raw}, \phi_n^k, \hat{x}_n^k)$ (Eq.3).

6.3 Channel Estimation Problem in NOMA Network

Building upon the well-established data-aided channel estimation technique, this work proposes a novel approach tailored explicitly for downlink NOMA networks with a single pilot for two users. Here, the data blocks containing superimposed symbols from both users are utilized. A "semi-data-aided" approach [54] is used in the MIMO system to improve the channel estimation accuracy. Reliable data symbols are crucial for accurate channel estimation. However, the number of reliably decoded symbols might be limited in NOMA with solid interference, even with advanced decoding techniques. This scarcity of reliable data can make it challenging to obtain accurate channel estimates, especially for the user experiencing more substantial interference. Instead of blindly using all reliable information symbols that can be contaminated by residual interference, our work involves selecting subcarriers with a higher power allocation (fractional power) from the superimposed data blocks. These subcarriers are likely to carry stronger signals for a particular user. Additionally, reliable data symbols detected before reaching this point in the decoding process are also incorporated. This combined information set, including the pilot signal, highly reliable data symbols, and high power-allocated subcarriers, empowers the channel estimation process, leading to more accurate channel knowledge for improved NOMA system performance.

In NOMA, the transmission frame contains superimposed symbols from multiple users, making reliable channel estimation using only detected data symbols (even reliable ones) insufficient. Reliable data symbols for one user might still be corrupted by interference from the other user's superimposed signal. This residual interference can lead to inaccurate channel estimates. In contrast, MIMO systems benefit significantly from data-aided channel

estimation using reliable detected symbol vectors. MIMO channels typically experience independent fading for each path. Reliable data from one path can provide accurate channel information for that specific path, aiding overall channel estimation. It exploits multiple antennas to achieve spatial diversity. Reliable data from different antennas can offer valuable insights into the channel response. Therefore, while data-aided channel estimation is effective in MIMO, the superimposed nature of NOMA signals necessitates a more sophisticated approach.

In a NOMA network with a single pilot for two users and superimposed data blocks, selecting the "best" fractional power allocation for channel estimation depends on balancing reliable data for user estimation and information gain for both users. In the first scenario, We want to leverage data symbols with a high probability of correct decoding for channel estimation. In the second one, the chosen subcarriers should provide valuable information for estimating channels of both the near user (good channel) and the far user (challenging channel).

In Algorithm 8, we calculate a weighted average for each subcarrier. The weights of w_{near} and w_{far} determine the relative contribution of power allocation from each user. Sorting the weighted average ensures subcarriers with a more robust combined power allocation based on their weights appear at the beginning of the list. Finally, the algorithm selects the top K subcarriers based on their weighted average for channel estimation. This approach prioritizes subcarriers with potentially stronger signals for either user while incorporating information from both users.

In our work, we adjust the weighting factors w_{near} and w_{far} to prioritize the far user's contribution (higher w_{far} compared to w_{near}). This will include subcarriers with a stronger power allocation from the far user in the weighted average calculation for selecting subcarriers for channel estimation.

ALGORITHM 8: Channel Estimation using Weighted Power Allocation in NOMA

Input: ϕ_{near} : Vector of fractional power allocation for near user (length: number of subcarriers)
 ϕ_{far} : Vector of fractional power allocation for far user (length: number of subcarriers)
 w_{near} : Weighting factor for the near user ($0 \leq w_{near} \leq 1$)
 w_{far} : Weighting factor for far user ($0 \leq w_{far} \leq 1$)
 K : Number of subcarriers to select for channel estimation

- 1 **Initialization:** *Selected subcarriers: List of K subcarrier indices chosen for channel estimation*
- 2 *Calculate Weighted Average:*
- 3 *Initialize an empty list $weighted_{average}$ to store the weighted average for each subcarrier.*
- 4 **for** $k \leftarrow 0$ **to** number of subcarriers -1 **do**
- 5 Calculate the weighted average:

$$weighted_{average}[k] = (\phi_{near}[k] \times w_{near}) + (\phi_{far}[k] \times w_{far}) \quad (6.4)$$
- 6 **Sort Subcarriers:** Sort the weighted average list in descending order. This ensures subcarriers with the highest weighted average appear first. **Select Subcarriers:** Initialize an empty list of selected subcarriers.
- 7 **for** $i \leftarrow 0$ **to** $K - 1$ **do**
- 8 **Add the corresponding subcarrier index from the sorted $weighted_{average}$ list to selected subcarriers.**

ALGORITHM 9: Channel Estimation using a two-step process in NOMA

Input: User set $U = \{1, \dots, N\}$, Gold code length $L_c \in \{31, 63, 127\}$, Subcarriers K

Output: Refined channel estimates \hat{h}_n^{final}

- 1 **Common Pilot Transmission:**
- 2 4. Broadcast x_p : $y_p(t) = \sum_{n=1}^N h_n x_p + z_p(t)$ //Contaminated pilot
- 3 **Phase 2: Gold Code Processing**
- 4 **for** $i \leftarrow 1$ **to** N **do**
- 5 5. Correlate: $\hat{h}_n^{raw} = y_p * C_n^H$ //Despreading
- 6 6. Apply cross-correlation bound: $|\rho_{ij}| \leq 1/\sqrt{L_c}$
- 7 7. Weighted subcarrier (w_n) selection (from Algorithm 2)
- 8 **Phase 3: Data Transmission**
- 9 8. Allocate power: $\phi_n^k = P \cdot d_n^{-\alpha} / K$ //Fractional allocation
- 10 9. Transmit superimposed signal: $x = \sqrt{P} \sum_{n=1}^N S_n C_n$
- 11 10. Receive: $y_n(t) = \sum_{k=1}^K \sqrt{\phi_n^k} h_n x_n^k(t) + \sum_{i \neq n} \sqrt{\phi_i^k} h_i x_i^k(t) + z(t)$
- 12 **Phase 4: CPF Refinement**
- 13 **for** $i \leftarrow 1$ **to** N **do**
- 14 11. Perform SIC to obtain \hat{x}_n^k
- 15 12. LSTM Processing: $\hat{h}_n^{final} = CPF(\hat{h}_n^{raw}, \phi_n^k, \hat{x}_n^k)$
- 16 13. Update via MSE: $L = \|h_n - \hat{h}_n^{final}\|^2$

6.4 Gold Sequences for NOMA Channel Estimation

Unlike MIMO systems, NOMA networks cannot directly exploit the spatial correlation between subcarriers for user separation. Identifying which subcarriers reliably carry data for a specific user is challenging, especially when multiple users' data is superimposed on the same subcarriers. However, Gold sequences offer a solution. The system can differentiate between the users' data by applying a Gold sequence to a transmission frame containing one pilot and two superimposed data blocks. The key lies in finding reliable data symbols. Gold sequences' properties allow the system to distinguish between different users' data, even when occupying overlapping subcarriers. This enables the NOMA network to separate and decode data intended for each user effectively.

Our work builds upon the concept of NOMA downlink channel estimation with Gold codes, where we have a single transmit antenna at the BS and a total of N number of UEs with a single antenna each. Data symbol vector $S = (S_1, S_2, \dots, S_N)$ where S_n represents information intended for user n where $n = (1, 2, \dots, N)$. The channel between the BS and each UE is represented by a vector $H = (H_1, H_2, \dots, H_N)$, where H_n represents the channel for user n . A unique code C_n of size L_c is assigned to user n from a spreading code vector $C = (C_1, C_2, \dots, C_N)$. L_c represents the Spreading code length. P represents the total transmit power at the BS. The transmitted signal x is a vector of size $L_c \times N$ and is formed as follows:

$$x = \sqrt{P} * \sum_{n=1}^N S_n * C_n \quad (6.5)$$

Gold codes have specific Autocorrelation Function (ACF) and Cross-correlation Function (CCF) properties. These properties are crucial for user separation in NOMA. Low out-of-phase ACF and CCF values allow the NOMA system to differentiate between users' data encoded with different Gold codes. The analysis of user separation and identification of reliable data symbols remains similar to the uplink case. In this scenario, UEs can potentially identify reliable data symbols \hat{S}_n from their received signals y_n . At the BS, we can exploit the uplink channel reciprocity (assuming a quasi-static channel) to estimate the downlink channel for each user. Each UE transmits a pilot signal encoded with its assigned Gold code C_n during a designated channel estimation phase. The BS receives the pilot signals from all UEs and can leverage the reliable data symbols \hat{S}_n for user n to estimate the

channel (h_n). We can estimate the downlink channel \hat{h}_n of user n by utilizing the received pilot signal y_n^{pilot} :

$$\hat{h}_n = \left(y_n^{pilot} * C_n^H \right) * \text{diag} \left(\hat{S}_n \right) * \text{inv} \left(P * H * C_n * C_n^H + N \right) \quad (6.6)$$

where y_n^{pilot} is the pilot signal received from user n . C_n^H represents the hermitian transpose of user n 's spreading code. $\text{diag}(\hat{S}_n)$ represents the diagonal matrix with reliable data symbols of user n on the diagonal. $\text{inv}()$ represents the matrix inversion and N is the noise vector.

We can evaluate the effectiveness of using Gold codes by analyzing metrics like Mean Squared Error (MSE) between the estimated channel (\hat{h}_n) and the actual channel (h_n) for each user. Symbol Error Rate (SER) of each user's data after channel estimation and data decoding at the UEs. By incorporating Gold codes in a NOMA downlink network with a single transmit antenna, we can improve user separation during decoding at the UEs. This allows for identifying reliable data symbols, which the BS can then use to estimate downlink channels for each user. This approach can lead to more accurate channel estimation and improved system performance. Further analysis in the next section involving simulations on real-world data can provide more concrete performance evaluations.

Building upon the initial approach from Section III of using reliable data and power allocation for channel estimation in NOMA, further improvements can be achieved through techniques like Gold sequences in Section IV through an iterative technique. Traditional methods struggle to differentiate between users' data on the same subcarriers. However, with their specific correlation properties, Gold sequences allow the system to distinguish between users' data even when occupying the same subcarriers. The iterative channel estimation method enables more accurate channel estimation and improved system performance in NOMA networks.

6.5 Results and Discussion

6.5.1 Simulation Setup

A single-cell network with 43 dBm transmission power and 5 MHz bandwidth at 2 GHz is simulated. Path loss is modeled using a 3.76 exponent and 10 dB shadowing standard

deviation. Noise has a spectral density of -174 dBm/Hz and a figure of 7 dB. The simulation assumes a minimum 10 meters between the base station and users, with near and distant users at 20 and 50 meters. The simulation lasts 10,000 attempts at -15 to 25 dB SNR.

Parameter	Value
Number of Cells	1
Max Transmission Power	43 dBm
Bandwidth	5 MHz
Carrier Frequency	2 GHz
Path Loss Exponent	3.76
Shadowing Standard Deviation	10 dB
Noise Spectral Density	-174 dBm/Hz
Noise Figure	7 dB
Min Distance BS to User	10 meters
Number of Simulation Trials	10,000
Signal-to-Noise Ratio (SNR) Range	-15 dB to 25 dB
Distance from BS to near user	20
Distance from BS to far user	50

Table 6.1: Simulation Setup.

Model Parameter	values
Total Time Steps	10000
Phased Time Steps	120
Prediction Steps	20
LSTM Layers	128, 64
GRU Layer	32
Dropout Rate	0.2, 0.3
Batch Normalization	After each layer
Dense Layer	50
Output Layer	20, Linear Activation
Optimizer	Adam
Learning rate	0.0008
Loss Function	Mean Squared Error
Batch Size	32
Epochs	15

Table 6.2: Model Parameters for LSTM-based Prediction Model

6.5.2 Performance Comparison of NOMA with Gold Coding and C-V-BLAST

Fig 6.2 presents the symbol error rate (SER) performance of a two-user NOMA system equipped with single antennas, utilizing Gold sequences of lengths 31, 63, and 127. The plot illustrates the SER as a function of signal-to-noise ratio (SNR) for both the near and far users. Ideally, the SER curves for both users should exhibit a downward trend with increasing SNR. However, a significant disparity in SER is expected between the near and far users due to the inherent path loss advantage of the former. While the impact of code length on the near user's SER might be less pronounced, it could potentially offer improvements for the far user, especially in challenging propagation conditions.

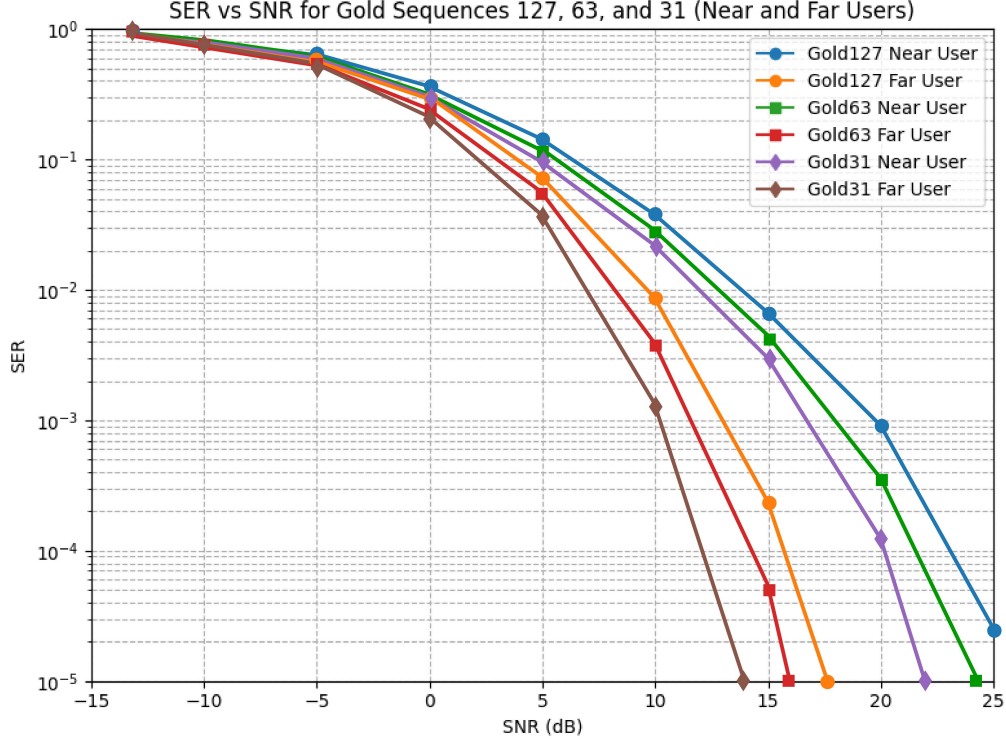


Figure 6.2: SER performance comparison of a two-user NOMA system employing Gold sequence lengths 31, 63, and 127.

Fig 6.3 contrasts the SER performance of a two-user NOMA system utilizing C-V-BLAST [54] and Gold sequences of lengths 31, 63, and 127. Due to the constrained spatial degrees of freedom in our single-antenna system, the potential benefits of C-V-BLAST, which relies on spatial processing for interference mitigation, are limited. Consequently,

the figure demonstrates that gold-coded NOMA outperforms C-V-BLAST across a range of SNR values, typically spanning from -20 dB to 0 dB. The diversity inherent in Gold sequences proves to be particularly advantageous in overcoming the challenges posed by the limited spatial dimensions.

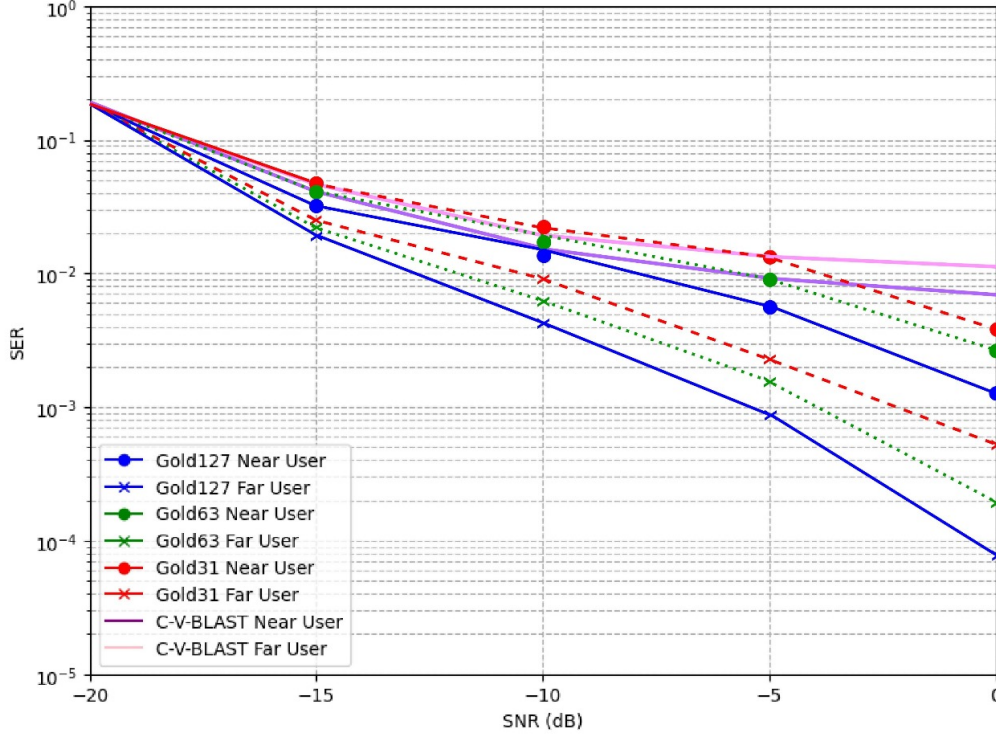


Figure 6.3: SER performance comparison of Gold coding and C-V BLAST for a two-user NOMA system.

6.5.3 Performance Evaluation Via Deep Learning Model

To generate a realistic simulation environment for a 5G NOMA network, we constructed a noisy dataset of 11000 data points using the latitude and longitude data from [51]. We introduced a combination of noise sources relevant to 5G networks to mimic real-world propagation conditions. This includes additive white Gaussian noise (AWGN) with a standard deviation of 0.001 to represent thermal noise in the system. Additionally, we incorporated Rayleigh fading, characterized by a scale factor of 1.0, to simulate the multipath propagation effects prevalent in urban environments. A shadowing component modeled as a log-normal distribution with a mean of 0.0 dB and a standard deviation of 8.0 dB

was added to capture large-scale path loss. This comprehensive noise model, incorporating AWGN, Rayleigh fading, and shadowing, provides a robust foundation for evaluating the performance of our proposed NOMA system under realistic channel conditions.

To capture the dynamic nature of 5G wireless channels, we employed a rolling window approach with a window size of 2 minutes on the generated 10-minute dataset in Fig 6.4. This method effectively balances the need for capturing rapid channel fluctuations, essential for 5G systems, with maintaining sufficient data points for statistically reliable analysis. By analyzing data within this window, we can effectively evaluate the impact of different noise components on system performance, identify channel dynamics, and develop robust channel estimation and decoding algorithms tailored for the 5G environment. Moreover, the rolling window approach allows for the analysis of time-varying channel conditions, enabling the study of channel coherence time and Doppler spread, crucial parameters for 5G system design.

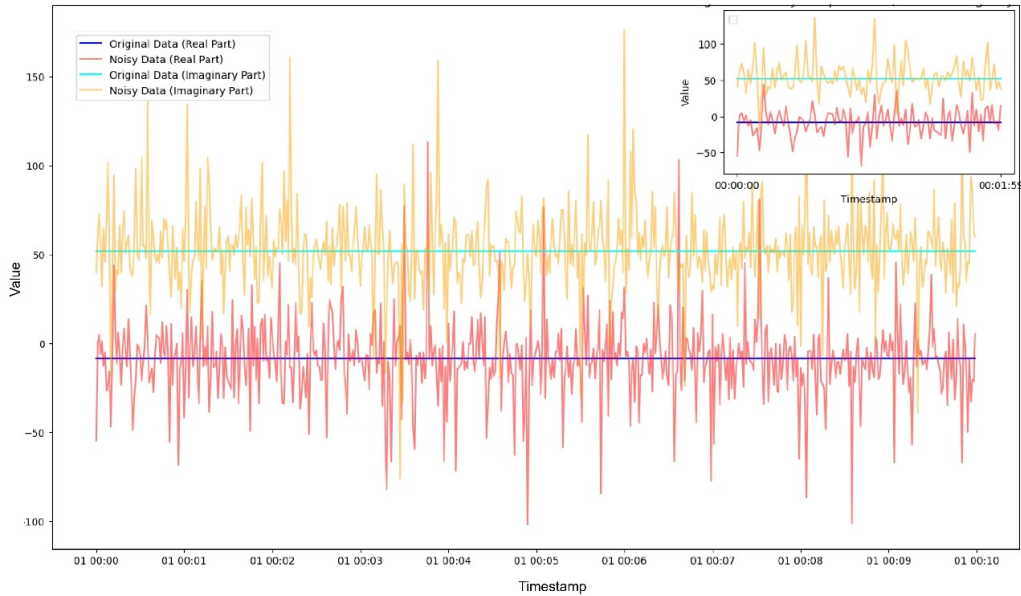


Figure 6.4: A rolling window approach with a 2-minute window size was applied to the 10-minute dataset.

To balance computational efficiency and model effectiveness, a subset of 3000 data points was meticulously selected for training the LSTM model, as shown in Fig 6.5. This approach allowed for a focused exploration of the dataset's key characteristics while preventing overfitting issues arising from excessively large datasets. By training on this

representative subset, the model was able to learn essential patterns and dependencies within the data, leading to improved generalization capabilities and accurate channel predictions.

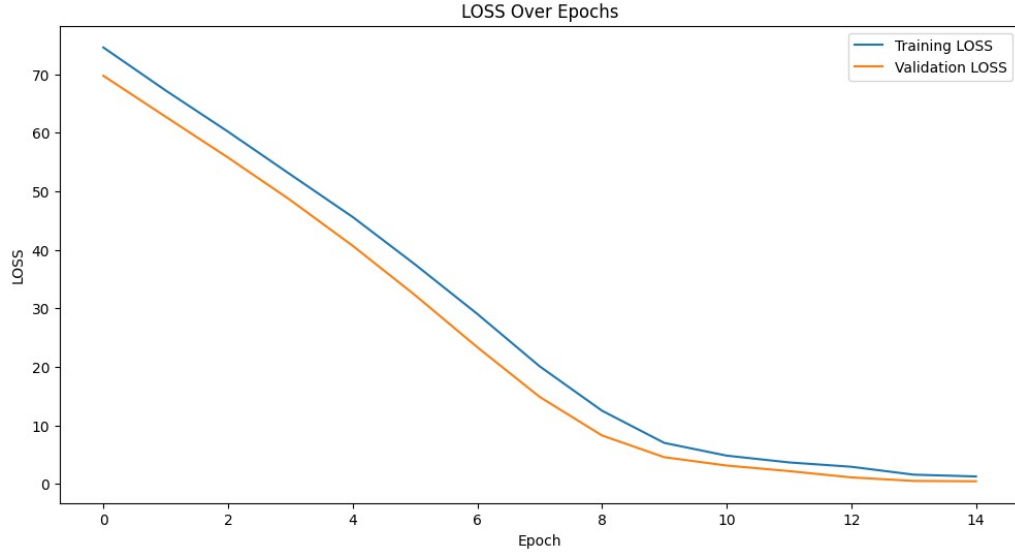


Figure 6.5: Loss function of training and validation dataset.

Our proposed CPF incorporating received pilot signals, power allocation vectors, and partially decoded data symbols significantly enhances channel estimation accuracy compared to a CPF relying solely on received pilot signals in NOMA networks. By leveraging additional information about the fractional power allocation to the subcarrier, the CPF can more effectively capture the dynamic channel variations and interference characteristics inherent in NOMA systems. This refined CPF translates to superior SNR performance compared to traditional methods that rely solely on pilot-based estimation, as shown in Fig 6.6.

6.5.4 Addressing Scalability Challenges for Larger Networks

In Fig 6.7, simulates and evaluates the performance of channel estimation in the NOMA network using Gold sequences, which are ideal for multi-user environments due to their excellent correlation properties and low cross-correlation. The process begins with generating Gold sequences by combining two preferred pairs of maximum-length sequences (m-sequences) using linear feedback shift registers (LFSRs) with specific polynomial coefficients. The simulation models a NOMA network with varying numbers of users, incorporating sequence reuse to accommodate larger networks, which introduces interference, a realistic challenge in

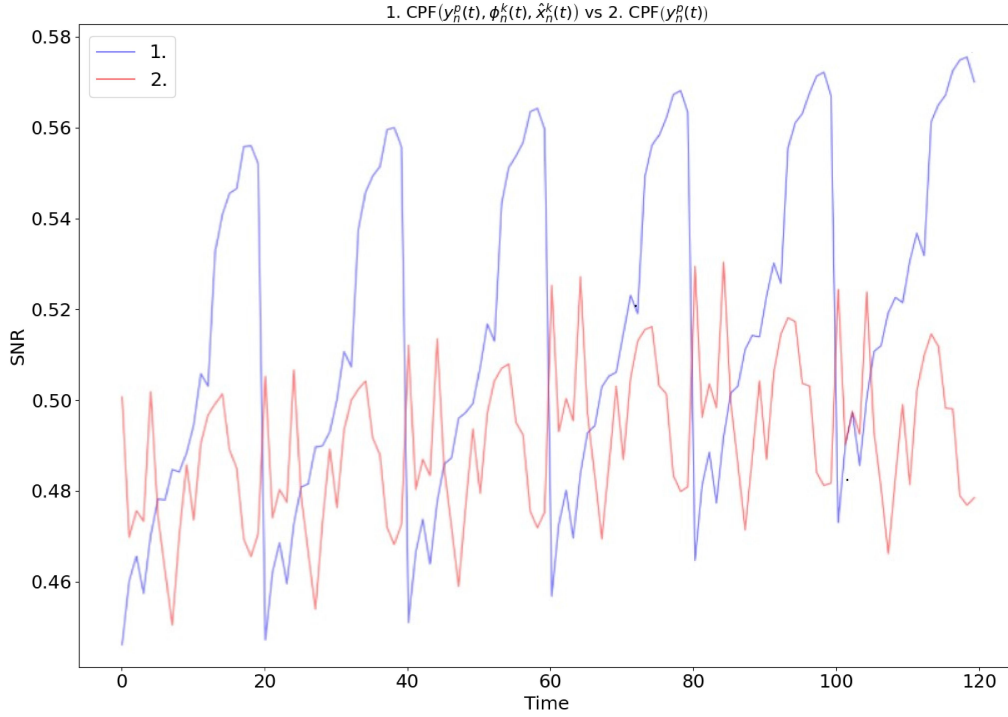


Figure 6.6: Enhanced channel estimation in NOMA via CPF with fractional power allocation.

large-scale systems. Channel estimation is performed using matched filtering, where received signals are correlated with the transmitted Gold sequences to estimate channel coefficients. The performance is evaluated using the Mean Squared Error (MSE) metric, with results showing that as for the larger network of size 40 to 100 UEs sequences are reused, and interference grows, leading to higher MSE values. Despite this, Gold sequences maintain relatively low MSE values, demonstrating their robustness in multi-user environments. However, the simulation reveals scalability limitations, as performance degrades in very large networks (> 60 UEs) due to increased interference. The findings emphasize the importance of sequence design and interference management in NOMA systems, highlighting the need for advanced techniques like interference cancellation or adaptive sequence allocation to improve scalability. Limitations include the use of a fixed Gold sequence length (31), a simplified interference model, suggesting future work should explore adaptive sequence lengths, more realistic interference models.

Gold sequences are widely used in communication systems, including NOMA, due to their good correlation properties and low cross-correlation values, making them suitable for user separation and interference mitigation in multi-user environments. However, their

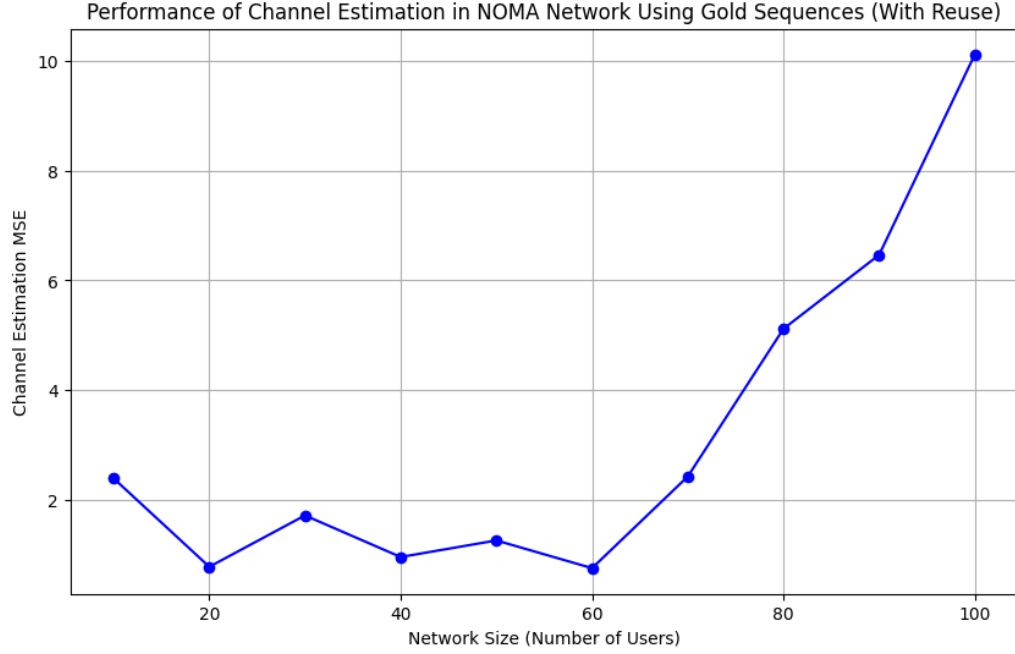


Figure 6.7: Channel Estimation in NOMA Networks Using Gold Sequences: Evaluating Scalability, Interference, and MSE.

scalability for larger networks in NOMA systems depends on several factors. First, Gold sequences are generated using preferred pairs of m-sequences with a length of $2^n - 1$, where n is the degree of the polynomial used to generate the m-sequences. As the network size grows, the number of required sequences increases, and if the number of users exceeds the available Gold sequences, sequences must be reused, leading to increased interference. To support larger networks, the sequence length must be increased, which raises the complexity of sequence generation and processing. Second, Gold sequences have bounded cross-correlation values, which are crucial for minimizing interference between users, but as the network size grows, cross-correlation may become a limiting factor, especially with sequence reuse, degrading system performance through increased multi-user interference (MUI). Third, generating and processing longer Gold sequences requires more computational resources, posing challenges for larger networks, particularly in real-time systems, while the complexity of detecting and decoding signals in NOMA systems also increases with the number of users and sequence length. Fourth, NOMA relies on superposition coding and successive interference cancellation (SIC) to achieve high spectral efficiency, and Gold sequences must be designed to ensure that the SIC process is not overly complicated by high cross-correlation

or interference, with the trade-off between sequence length, correlation properties, and spectral efficiency becoming critical for larger networks. Fifth, if Gold sequences are not scalable for very large networks, alternative sequence designs or multiple access techniques, such as Zadoff-Chu sequences, random sequences, or hybrid approaches combining Gold sequences with power-domain or spatial-domain NOMA, may be considered. Finally, in practice, the scalability of Gold sequences for NOMA systems depends on the specific application, channel conditions, and hardware limitations, with simulation and testing essential to evaluate their performance in larger networks and determine whether they meet the required quality of service (QoS) metrics. In conclusion, Gold sequences are effective for small to medium-sized NOMA networks due to their excellent correlation properties, but for larger networks, their scalability is limited by sequence length, cross-correlation, and computational complexity, necessitating alternative sequences or hybrid approaches to ensure efficient and reliable communication in large-scale NOMA systems.

6.6 Summary

The presented research investigates the performance of a NOMA system utilizing Gold coding and compares its efficacy to traditional C-V-BLAST techniques. The results demonstrate the superiority of gold-coded NOMA in terms of SER across a range of SNR values. This advantage is attributed to the inherent diversity offered by Gold sequences, which mitigates the challenges posed by limited spatial dimensions in single-antenna systems. A deep learning model network was trained on a dataset to predict channel behavior and lead to accurate channel predictions. The proposed channel estimation method, incorporating received pilot signals, power allocation vectors, and data symbols, significantly outperforms traditional pilot-based methods. The proposed methodology and findings have potential applications in various domains. Identifying the impact of different noise components and channel conditions on system performance can guide network operators in optimizing resource allocation, power control, and interference management.



Conclusions and Future Works

7.1 Conclusions

NOMA has lately been recognized as a viable multiple access approach for 5G and beyond wireless networks owing to its potential advantages, such as greater spectral efficiency and user fairness. In contrast to traditional OMA systems like TDMA and OFDMA, NOMA-based DL transmission allows many users to share the same orthogonal radio resources, such as time and frequency, by using power-domain multiplexing at the transmitter. This kind of multiplexing is known as Space Division Multiple Access (SDMA), where signals destined for various users are encoded with varying power levels that are inversely proportionate to the users' channel strengths. Specifically, enabling the simultaneous service of several users inside the same resource block using NOMA facilitates the widespread adoption of IoTs by providing extensive connection. The receiver uses the SIC approach to decipher the signals meant for weaker users before decoding their own signals. In addition, NOMA has recently been integrated with other multiple-access approaches. These approaches include NOMA with multiple antennae. These strategic pairings provide extra opportunities for flexibility, allowing for the development of its inherent advantages. Resource allocation and interference management are essential in the design of wireless systems and networks as they facilitate the optimal use of resources. Thus, this thesis concentrated on various resource allocation and interference management strategies for distinct kinds of NOMA systems.

Chapter 3 discusses how the aim of maximizing the total sum rate of the network

and decreasing power consumption may be expressed as a Multi-objective optimization (MOO) problem in this study. The issue is resolved by seeking the most favorable collection of solutions. Integrating reinforcement learning into multi-objective optimization enables automated parameter tuning, minimizing the need for human intervention. The method described offers a Pareto optimum solution for competing goals in a dynamic setting.

Chapter 4 discusses the use of the MIC method in MIMO-NOMA wireless cellular systems as a practical approach to enhance spectrum and energy efficiency. This study specifically examined the downlink multiuser MIMO-NOMA, where the number of devices with receiving antennas in a cell is much more than the number of broadcast antennas at the base station. Each MIMO-NOMA cluster is equipped with a distinct MIMO beam that is perpendicular to the beams of the other clusters. Additionally, all users within a cluster are scheduled based on NOMA. The majority of MIMO-NOMA solutions discussed in existing literature focus on mitigating inter-cluster interference, whereas there is a limited amount of research dedicated to tackling intra-cluster interference. The use of the MIC approach in the MIMO-NOMA network leads to a substantial improvement in both spectrum and energy efficiency. In addition, we have used the correlation coefficient to establish the NOMA network inside each cluster, resulting in a substantial improvement in the system's spectral efficiency (SE) and energy efficiency (EE) performance. Algorithm 1 utilizes the channel status information of the device to identify the relay nodes and operates on two time stamps. Potential future research might focus on enhancing the study by using imperfect channel state information.

Chapter 5 provides an explanation of... This work proposed a unique approach for predicting NOMA channels, using a wider range of CSI characteristics including RSRP, RSRQ, CQI, SNR, and particularly PDD. System-level simulations demonstrated that a low Channel State Information (CSI) significantly impacts the occurrence of radio connection failures and handover failures. The findings of our study clearly illustrate the advantages of PDD as an additional measure for measuring CSI. PDD reduces signaling overhead and improves the representation of channel dynamics compared to traditional methods by eliminating the need for specific pilot signals. Moreover, this approach is flexible in accommodating changing user traffic patterns. Our proposed technique outperformed a deterministic model in terms of Mean Squared Error (MSE) and Bit Error Rate (BER).

This research is the first to examine the use of PDD in NOMA networks for predicting handover and radio link failures. Recognizing that machine learning may be used for channel estimation due to its ability to operate without the need for several stringent assumptions. Furthermore, we used a transfer learning approach to circumvent limitations imposed by the size of the dataset. Moreover, we demonstrated the competitive efficacy of our model in contrast to previous studies and explored the use of scale-free and scale-dependent metrics. This research distinguishes itself by using PDD as a valuable source of channel information to predict channel activity in NOMA networks. In future deployments, this method has the potential to improve network performance and the process of determining handover decisions. Future goals for the project include investigating the impact of PDD on network performance in various traffic situations and further exploring the integration of machine learning methods for channel estimation.

Chapter 6 discusses a research study that examines the performance of a NOMA system using Gold coding and compares it to classic C-V-BLAST methodologies. The findings indicate that gold-coded NOMA outperforms other methods in terms of Symbol Error Rate (SER) across various Signal-to-Noise Ratio (SNR) levels. The benefit is due to the intrinsic variety provided by Gold sequences, which helps to overcome the limitations caused by restricted spatial dimensions in single-antenna systems. A deep learning model was developed on a dataset to accurately anticipate channel activity. The suggested channel estimation technique, which includes received pilot signals, power allocation vectors, and data symbols, exhibits superior performance compared to conventional pilot-based approaches. The suggested approach and discoveries have the capacity to be used in diverse fields. Analyzing the influence of various noise components and channel conditions on system performance may assist network operators in improving resource allocation, power control, and interference management.

7.2 Future Works

The current research in this thesis on NOMA has mainly used conventional genetic and reinforcement learning (RL) algorithms. Future researchers may look into other RL methods to make the proposed multi-objective optimization framework for NOMA networks work better and be more adaptable. Deep Reinforcement Learning (DRL) uses deep and reinforcement

learning methods to help agents learn and make choices in complicated settings. Using neural networks involves DRL combining reinforcement learning with deep neural networks to describe states and make more complex decisions. NOMA networks with high-dimensional state spaces benefit from this. DRL's flexibility to learn from prior experiences may lead to more effective methods in shifting environments, making it ideal for NOMA systems that operate in different environments. Reinforcement learning techniques with actor and critic components are called actor-critical methods. Actor-critic methods can learn policies (actors) that can make decisions in a more stable environment faster than standard policy gradient methods. Actor-critic algorithms may perform better in complex NOMA settings, especially when opposing objectives are present. Combination approaches include integrating DRL with traditional RL, which may improve performance and adaptability by combining DRL and RL algorithms. DRL may be used for specific optimization problem components and RL for others. Alternatively, these two strategies may be hierarchically mixed.

This thesis' NOMA study largely uses Successive interference cancellation (SIC). Further research will examine various multiple interference cancellation (MIC) methods. By eliminating user interference, MIC improves NOMA system performance. The present research focused on one MIC approach, but future studies may analyze others to determine their pros and cons. SIC decodes user signals one after another, treating them as interference. SIC is computationally efficient but prone to error propagation, where early decoding errors might impair later decoding accuracy. Joint detection methods decode all users' signals simultaneously, considering interference. Joint detection may perform better in interference-filled environments but requires more processing power. Using SIC and joint detection, hybrid methods may sacrifice performance and computational complexity. Adapting between SIC and joint detection depending on channel or other criteria might improve performance. Finding the optimum MIC strategy for diverse NOMA conditions may need further investigation. This evaluation will include computer complexity, performance improvements, and channel resilience.

The current research in this thesis mostly focuses on small-scale NOMA networks. Addressing challenges in large-scale NOMA networks will be the focus of future research. In order to address the difficulties presented by extensive NOMA networks, future studies should investigate methods to improve scalability and computing efficiency. Distributed processing

approaches enable the distribution of computing tasks across numerous nodes, therefore alleviating the workload on individual systems. Dimensionality reduction strategies may reduce the effect of huge datasets, hence enhancing computing performance. Furthermore, the usage of lightweight or compact machine learning models may enhance the efficiency of resource allocation in situations with limited resources. This makes the suggested channel prediction technique more appropriate for practical implementation in large-scale NOMA networks.

The current research in this thesis on NOMA has mostly depended on using conventional Gold coding. To enhance the performance of NOMA systems, optimizing both power allocation and Gold code selection using a combined optimization framework is crucial. Researchers may determine the most advantageous combination that optimizes system performance by meticulously examining the trade-offs involving these two characteristics, such as user fairness, computing complexity, and implementation limitations. By investigating various optimization strategies, such as evolutionary algorithms or particle swarm optimization, it is possible to discover effective solutions to this intricate optimization issue. This may enhance spectral efficiency, user fairness, and overall system performance.



Bibliography

- [1] Quy Vu Khanh et al. “Wireless communication technologies for IoT in 5G: Vision, applications, and challenges”. In: *Wireless Communications and Mobile Computing* 2022.1 (2022), p. 3229294.
- [2] AFM Shahen Shah. “A survey from 1G to 5G including the advent of 6G: Architectures, multiple access techniques, and emerging technologies”. In: *2022 IEEE 12th Annual Computing and Communication Workshop and Conference (CCWC)*. IEEE. 2022, pp. 1117–1123.
- [3] Behrooz Makki et al. “A survey of NOMA: Current status and open research challenges”. In: *IEEE Open Journal of the Communications Society* 1 (2020), pp. 179–189.
- [4] Zhiqiang Wei et al. “On the performance gain of NOMA over OMA in uplink communication systems”. In: *IEEE Transactions on Communications* 68.1 (2019), pp. 536–568.
- [5] Yongming Huang et al. “Signal processing for MIMO-NOMA: Present and future challenges”. In: *IEEE Wireless Communications* 25.2 (2018), pp. 32–38.
- [6] Lina Liu et al. “Latency optimization for computation offloading with hybrid NOMA–OMA transmission”. In: *IEEE Internet of Things Journal* 8.8 (2021), pp. 6677–6691.
- [7] Maraj Uddin Ahmed Siddiqui et al. “Interference Management in 5G and Beyond Network: Requirements, Challenges and Future Directions”. In: *IEEE Access* 9 (2021), pp. 68932–68965. DOI: 10.1109/ACCESS.2021.3073543.
- [8] Yatong Wang et al. “Decentralized Learning Based Indoor Interference Mitigation for 5G-and-Beyond Systems”. In: *IEEE Transactions on Vehicular Technology* 69.10 (2020), pp. 12124–12135. DOI: 10.1109/TVT.2020.3012311.
- [9] Mohammad Abrar Shakil Sejan et al. “Interference Management for a Wireless Communication Network Using a Recurrent Neural Network Approach”. In: *Mathematics* 12.11 (2024), p. 1755.

- [10] Dimitrios Sifarakis, Elias A. Alwan, and John L. Volakis. “Interference Mitigation for 5G Millimeter-Wave Communications”. In: *IEEE Access* 7 (2019), pp. 7448–7455. DOI: 10.1109/ACCESS.2018.2889620.
- [11] Pimmy Gandotra, Rakesh Kumar Jha, and Sanjeev Jain. “Green NOMA With Multiple Interference Cancellation (MIC) Using Sector-Based Resource Allocation”. In: *IEEE Transactions on Network and Service Management* 15.3 (2018), pp. 1006–1017. DOI: 10.1109/TNSM.2018.2848595.
- [12] Ayesha Jehan and Muhammad Zeeshan. “Comparative performance analysis of code-domain noma and power-domain noma”. In: *2022 16th International Conference on Ubiquitous Information Management and Communication (IMCOM)*. IEEE, 2022, pp. 1–6.
- [13] Jie Zeng. “Candidate NMA Technologies in 5G”. In: *Multiple Access Technologies for 5G: New Approaches and Insight* (2021), p. 43.
- [14] Bo Zhang et al. “ECG data compression using a neural network model based on multi-objective optimization”. In: *PloS one* 12.10 (2017), e0182500.
- [15] Sumita Majhi and Pinaki Mitra. “Multi-objective Optimization in NOMA-IoT Networks”. In: *North-East Research Conclave*. Springer, 2022, pp. 75–88.
- [16] Zahra Ghaemi, Thomas TD Tran, and Amanda D Smith. “Comparing classical and metaheuristic methods to optimize multi-objective operation planning of district energy systems considering uncertainties”. In: *Applied Energy* 321 (2022), p. 119400.
- [17] Gang Kou et al. “Optimal computing budget allocation for the vector evaluated genetic algorithm in multi-objective simulation optimization”. In: *Automatica* 129 (2021), p. 109599.
- [18] Yu Zhou et al. “A problem-specific non-dominated sorting genetic algorithm for supervised feature selection”. In: *Information Sciences* 547 (2021), pp. 841–859.
- [19] Hu Wu, Xinning Li, and Xianhai Yang. “Dimensional synthesis for multi-linkage robots based on a niched Pareto genetic algorithm”. In: *Algorithms* 13.9 (2020), p. 203.
- [20] Pawan Kumar Mandal. “A review of classical methods and Nature-Inspired Algorithms (NIAs) for optimization problems”. In: *Results in Control and Optimization* (2023), p. 100315.

- [21] Robin Chataut and Robert Akl. “Massive MIMO systems for 5G and beyond networks—overview, recent trends, challenges, and future research direction”. In: *Sensors* 20.10 (2020), p. 2753.
- [22] Mohamed Hassan et al. “Modeling of NOMA-MIMO-Based Power Domain for 5G Network under Selective Rayleigh Fading Channels”. In: *Energies* 15.15 (2022), p. 5668.
- [23] Dinh-Thuan Do et al. “Joint impacts of imperfect CSI and imperfect SIC in cognitive radio-assisted NOMA-V2X communications”. In: *IEEE Access* 8 (2020), pp. 128629–128645.
- [24] Xiaoliang Wang et al. “Joint user association and power allocation in heterogeneous NOMA networks with imperfect CSI”. In: *IEEE Access* 8 (2020), pp. 47607–47618.
- [25] Kaiqiang Liu et al. “Large Sets of Binary Spreading Sequences with Low Correlation and Low PAPR via Gold Functions”. In: *IEEE Transactions on Information Theory* (2024).
- [26] Chen Quan et al. “A novel spectrally-efficient uplink hybrid-domain NOMA system”. In: *IEEE Communications Letters* 24.11 (2020), pp. 2609–2613.
- [27] SM Riazul Islam et al. “Power-domain non-orthogonal multiple access (NOMA) in 5G systems: Potentials and challenges”. In: *IEEE Communications Surveys & Tutorials* 19.2 (2016), pp. 721–742.
- [28] Peng Xu et al. “NOMA: An information theoretic perspective”. In: *arXiv preprint arXiv:1504.07751* (2015).
- [29] Mojtaba Vaezi and H Vincent Poor. “NOMA: An information-theoretic perspective”. In: *Multiple access techniques for 5G wireless networks and beyond* (2019), pp. 167–193.
- [30] Hongyun Xiao et al. “An improved PSO-based power allocation algorithm for the optimal EE and SE tradeoff in downlink NOMA systems”. In: *2018 IEEE 29th Annual International Symposium on Personal, Indoor and Mobile Radio Communications (PIMRC)*. IEEE. 2018, pp. 1–5.
- [31] Dadong Ni et al. “Energy-spectral efficiency tradeoff of downlink NOMA system with fairness consideration”. In: *2018 IEEE 87th vehicular technology conference (VTC Spring)*. IEEE. 2018, pp. 1–5.

- [32] Il Yong Kim and Olivier L. de Weck. “Adaptive weighted sum method for multiobjective optimization: a new method for Pareto front generation”. In: *Structural and Multidisciplinary Optimization* 31 (2006), pp. 105–116.
- [33] Abdullah Konak, David W. Coit, and Alice E. Smith. “Multi-objective optimization using genetic algorithms: A tutorial”. In: *Reliability Engineering & System Safety* 91.9 (2006). Special Issue - Genetic Algorithms and Reliability, pp. 992–1007. ISSN: 0951-8320. DOI: <https://doi.org/10.1016/j.ress.2005.11.018>. URL: <https://www.sciencedirect.com/science/article/pii/S0951832005002012>.
- [34] Lam Thu Bui and Sameer Alam. *Multi-Objective Optimization in Computational Intelligence: Theory and Practice: Theory and Practice*. IGI global, 2008.
- [35] JiGuan G Lin. “On min-norm and min-max methods of multi-objective optimization”. In: *Mathematical programming* 103.1 (2005), pp. 1–33.
- [36] Jiuting Yang and Amin Mohajer. “Multi objective constellation optimization and dynamic link utilization for sustainable information delivery using PD-NOMA deep reinforcement learning”. In: *Wireless Networks* 31.2 (2025), pp. 1839–1859.
- [37] Thuc Kieu-Xuan, Hong Nguyen-Thi, and Anh Le-Thi. “Multi-objective optimization-based GA in PLS of IRS-assisted PDNOMA communication”. In: *IEEE Access* 12 (2024), pp. 87361–87383.
- [38] Kefeng Guo et al. “NOMA-Enabled RIS-Assisted SATINs Under Multi-objective Optimization: A Deep Reinforcement Learning Approach”. In: *Integrated Terrestrial and Non-Terrestrial Networks*. Springer, 2024, pp. 129–163.
- [39] Oscar Brito Augusto et al. “Multi-objective genetic algorithms: A way to improve the convergence rate”. In: *Engineering Applications of Artificial Intelligence* 19.5 (2006), pp. 501–510.
- [40] Kalyanmoy Deb et al. “A fast and elitist multiobjective genetic algorithm: NSGA-II”. In: *IEEE transactions on evolutionary computation* 6.2 (2002), pp. 182–197.
- [41] Samir W Mahfoud. “Genetic drift in sharing methods”. In: *Proceedings of the First IEEE Conference on Evolutionary Computation. IEEE World Congress on Computational Intelligence*. IEEE. 1994, pp. 67–72.

- [42] Richard S Sutton and Andrew G Barto. *Reinforcement learning: An introduction*. MIT press, 2018.
- [43] Martin Mandischer. “A comparison of evolution strategies and backpropagation for neural network training”. In: *Neurocomputing* 42.1-4 (2002), pp. 87–117.
- [44] Nitchakun Kantasewi et al. “Multi Q-table Q-learning”. In: *2019 10th International Conference of Information and Communication Technology for Embedded Systems (IC-ICTES)*. IEEE. 2019, pp. 1–7.
- [45] Xinan Wang, Jianhui Wang, and Jianzhe Liu. “Vehicle to grid frequency regulation capacity optimal scheduling for battery swapping station using deep Q-network”. In: *IEEE Transactions on Industrial Informatics* 17.2 (2020), pp. 1342–1351.
- [46] Wali Ullah Khan et al. “Multiobjective optimization of uplink NOMA-enabled vehicle-to-infrastructure communication”. In: *IEEE Access* 8 (2020), pp. 84467–84478.
- [47] Chunlin Yan et al. “Receiver design for downlink non-orthogonal multiple access (NOMA)”. In: *2015 IEEE 81st vehicular technology conference (VTC Spring)*. IEEE. 2015, pp. 1–6.
- [48] Huiyi Ding and Ka-Cheong Leung. “Cross-layer resource allocation in NOMA systems with dynamic traffic arrivals”. In: *2020 IEEE Wireless Communications and Networking Conference (WCNC)*. IEEE. 2020, pp. 1–6.
- [49] Hyun-Ho Choi et al. “Non-orthogonal multiple access-based handover for throughput enhancement”. In: *IEEE Transactions on Vehicular Technology* 70.11 (2021), pp. 12278–12282.
- [50] Inhoo Hur and Sungjin Lee. “Handover and Radio Link Performance Analysis on Standalone Non-Orthogonal Multiple Access (NOMA) Environment”. In: *2024 IEEE International Conference on Consumer Electronics (ICCE)*. IEEE. 2024, pp. 1–5.
- [51] <https://github.com/uccmisl/5Gdataset>.
- [52] <https://github.com/sumita06/Python>.
- [53] David Lopez-Perez, Ismail Guvenc, and Xiaoli Chu. “Mobility management challenges in 3GPP heterogeneous networks”. In: *IEEE Communications Magazine* 50.12 (2012), pp. 70–78.

- [54] Tae-Kyoung Kim et al. “Semi-data-aided channel estimation for MIMO systems via reinforcement learning”. In: *IEEE Transactions on Wireless Communications* 22.7 (2022), pp. 4565–4579.

LIST OF PUBLICATIONS

PUBLICATIONS FROM THESIS WORK:

Refereed Journals

1. **Sumita Majhi**, and Pinaki Mitra, “Multiple Interference Cancellation in MIMO-NOMA-D2D Network”, *CURRENT TRENDS IN COMPUTER SCIENCES and APPLICATIONS*, Volume 2, Issue 5, pp. 11, July 2023.
DOI: <https://10.32474/CTCSA.2023.02.000149>

Refereed Conferences

2. **Sumita Majhi**, and Pinaki Mitra, “Multi-objective Optimization in NOMA-IoT Networks”, *North-East Research Conclave, Singapore: Springer Nature Singapore*, IIT Guwahati, India, May 2022.

Journal Submitted

3. **Sumita Majhi**, and Pinaki Mitra, “A PDD-Inspired Channel Estimation Scheme in NOMA Network”, *IEEE Transactions on Systems, Man and Cybernetics: Systems*.

Conference Submitted

4. **Sumita Majhi**, Kaushal Shelke, Pinaki Mitra, and Ujjwal Biswas “Data-Aware Channel Estimation for NOMA Network”, *2025 IEEE International Conference on Acoustics, Speech, and Signal Processing*.

PUBLICATIONS OTHER THAN THESIS WORK:

1. **Sumita Majhi**, and Pinaki Mitra, “Lightweight Cryptographic Techniques in 5G Software-Defined Internet of Things Networking”, *Lightweight Cryptographic Techniques and Cybersecurity Approaches*, 2022, *intechopen.com*
DOI: [https://10.5772/intechopen.102984](https://doi.org/10.5772/intechopen.102984)

DOCTORAL COMMITTEE

- Chairperson:** Prof. Pradip K. Das
Professor
Department of Computer Science and Engineering
Indian Institute of Technology Guwahati
- Research Advisor:** Dr. Pinaki Mitra
Associate Professor
Department of Computer Science and Engineering
Indian Institute of Technology Guwahati
- Members:** Dr. Hanumant Singh Shekhawat
Assistant Professor
Department of Electronics and Electrical Engineering
Indian Institute of Technology Guwahati
- Dr. Moumita Patra
Assistant Professor
Department of Computer Science and Engineering
Indian Institute of Technology Guwahati

